Fall 12-3-2010

Development of an Integrated Soil Properties Mapping System

Rajveer S. Dhillon
University of Nebraska - Lincoln, rajdhillon85@gmail.com

DEVELOPMENT OF AN INTEGRATED SOIL PROPERTIES MAPPING SYSTEM

By

Rajveer S. Dhillon

A THESIS

Presented to the Faculty of

The Graduate College at the University of Nebraska

In Partial Fulfillment of Requirements

For the Degree of Master of Science

Major: Agricultural and Biological Systems Engineering

Under the Supervision of Professor Viacheslav I. Adamchuk

Lincoln, Nebraska

December, 2010

Development of an Integrated Soil Properties Mapping System

Rajveer S. Dhillon, M.S.

University of Nebraska, 2010

Advisor: Viacheslav I. Adamchuk

One of the main goals of precision agriculture (PA) is to define spatial variability in soil properties within an agricultural field to make decisions that can maximize profitability and reduce negative environmental impact. Various soil sensor systems have been developed over the years to map soil properties on-the-go. In this study, an Integrated Soil Mapping System (ISMS) was developed to predict soil water content, soil organic matter, and soil mechanical resistance on-the-go using a capacitance moisture sensor, an optical sensor, and a load cell sensor respectively. These sensors were mounted on the ISMS for acquiring three different data layers at the same time. Each sensor was calibrated under laboratory conditions and the ISMS was also tested in fields. For example, volumetric soil water content estimated from the two-sided capacitance moisture sensor was compared with volumetric water content measured by the oven-drying method which produced $R^2 = 0.94$ in laboratory conditions with a standard error of 0.017 cm^3/cm^3. Soil index calculated as the sum of individual soil reflectance measurements by the optical sensor in red (660 nm) and blue (480 nm) parts of the spectrum predicted soil organic matter with $R^2 = 0.73$ and with standard error of 0.47 OM%. The load cell sensor was tested by applying different loads on the hitch for simulating field conditions and measuring value of known weights with an $R^2 = 0.99$ and standard error of 0.032 kN. Then ISMS was tested in field conditions for mapping the three data layers simultaneously. High sampling density data collected by the ISMS was

compared with data collected at the same time using conventional laboratory methods by developing the maps of soil properties and R^2 of 0.74, 0.67 and 0.28 were obtained for the moisture, optical and load cell sensors, respectively when regressed with standard laboratory methods.

ACKNOWLWDGEMENTS

I would like to express my sincere appreciation and gratitude to my advisor Dr. Viacheslav Adamchuk for his guidance, continuous encouragement during my studies, for his support and guidance in field experiments, and finally for introducing me to the world of precision agriculture.

I am very thankful to Dr. Richard Ferguson who guided me throughout my degree and also helped me in field data collection. I am also thankful to Dr. Roger Hoy, and Dr. Michael Kocher for serving on my graduate committee and for their valuable support and guidance during my research.

I am grateful to all faculty and staff members in the Department of Biological Systems Engineering, especially to Scott Minchow for his help in manufacturing the ISMS components. I am also thankful to fellow students Colin Lutz, Ahmad Mat Su, Allison Jonjak, Luan Pan, Brian Krienke, Luciano Shiratsuchi, and Andrew Landgraf for their help with the project. I am very thankful to faculty and staff members at the Agricultural Research and Development Center (ARDC) and the South Central Agricultural Laboratory (SCAL) for their help during field testing.

I would like to extend my thanks to my parents, friends, family members and specially my brother-in-law and sister for their never-ending support and encouragement throughout my student career.

Above all, I thank the God for His blessings and providing me with the ability and motivation to achieve my goals throughout my life.

TABLE OF CONTENTS

Page

LIST OF FIGURES

Page

LIST OF TABLES

Page

1. INTRODUCTION

Precision agriculture (PA) involves information-based agricultural production management to obtain economic, agronomic, and environmental benefits. Maximum returns to growers are provided with optimum inputs for each specific location by studying in-field variability of soil and crop properties. PA can have a vital role in resource conservation and in reducing the harmful effects of conventional agricultural methods on the environment. For example, over application of fertilizers is responsible for polluting underground water, which can be significantly reduced by employing site-specific application of inputs. By using geo-referenced information of variability of soil and crop parameters, controllers for fertilizers, pesticides and herbicides can be employed to adjust input rates as required for each individual location in the field (Bongiovanni and Lowenberg-DeBoer, 2004). This process is called site-specific crop management (SSCM), which can be divided into the following components illustrated in Figure 1-1: 1) geo-referenced collection of data for soil or crop parameters; 2) analysis of data statistically and using geographic information systems (GIS) to provide thematic soil maps derived from maps of different soil-related parameters; 3) decision-making process to identify optimal treatments; 4) yield mapping to allow for comparison of the results of SSCM with those of traditional techniques of agriculture.

Collection of data from agricultural fields is a primary requirement of SSCM and many research groups throughout the world focus on development of new techniques for data acquisition (Adamchuk et al., 2004a). This research was based on on-the-go mapping of soil properties by integrating several sensors in a one mobile unit.

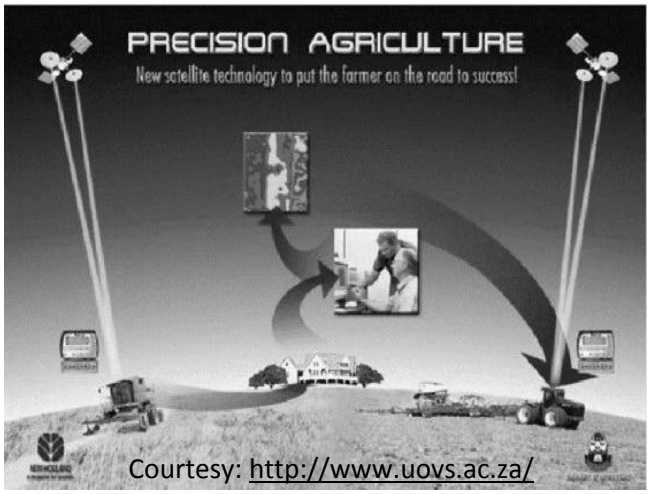

Figure 1-1: Precision Agriculture basic processes.

1.1. Problem statement

Data collection in PA is a crucial step, because the quality of the data collected is a necessary step toward successful adoption of SSCM. The conventional method of data collection for soil properties consists of taking soil cores from the field and sending the cores for lab analysis. Besides being very time consuming, labor demanding and expensive, this method does not produce true maps of soil properties, because sparsely populated sample points are not sufficient to identify the significant part of spatial variability in the field. As properties of soil can influence plant growth, it is helpful to map them with high resolution. The introduction of different types of on-the-go soil sensors in recent years combined with global navigation satellite system (GNSS) receivers allow fields to be mapped with high density of measurements. Although on-the-go mapping of soil properties can reduce the resources employed in conventional methods of sampling the soils, it is still expensive for a grower to map all influential soil properties in the field because of high initial cost of the sensor systems and software. In

addition to the added expense, other negative impacts are the intensive use of heavy machinery and more passes through agricultural land that causes soil structure degradation and an eventual increase of soil compaction. A promising solution for all these problems is to combine several sensors simultaneously into one system/platform (Swinton and Lowenberg-DeBoer, 1998). In this study, an Integrated Soil Mapping System (ISMS) was developed to combine three different soil sensors together to measure soil moisture content, soil organic matter and soil mechanical resistance in a single pass through the field. A capacitance-based soil water content sensor was used to detect the dielectric constant of the soil, and that data was used to predict the volumetric and gravimetric water content of soil. To predict soil organic matter content two optical sensors were used which measured the soil reflectance at two different wavelengths i.e. visible (Amber, 505±10 nm) and near-infrared (880±15 nm). Another similar sensor had both wavelengths in visible region, red (660±10 nm) and blue (480±10 nm). A capacitance-type load cell was developed to measure the force on a chisel driven through the soil while traveling in field as an indicator of soil mechanical resistance.

1.2. Objectives

The objectives of this study were to develop and evaluate an Integrated Soil Measuring System (ISMS) to simultaneously map soil water content, soil organic matter content, and soil mechanical resistance. In particular, the tasks were: 1) to design and test a load cell sensor to measure an implement pull force, 2) to adopt an optical sensor for mapping subsurface soil reflectance, and 3) to optimize capacitance-type sensor design to measure dielectric soil properties.

2. LITERATURE REVIEW

2.1. Sensor systems

Soils are very complex systems due to the significant temporal and spatial variability of physical, chemical and biological properties within a production field (McBratney and Pringle, 1997). Soils influence the growth of plants by providing nutrients, water and physical support. Spatial variability of soil properties is measured to optimize the use of agricultural chemicals, water and energy. Characterization of the spatial variability is highly influenced by the density of sampling. Traditional, grid-based sampling is expensive and time consuming limiting the collection of a high density of measurements which makes it difficult to accurately determine the within field variability of influential soil properties. On-the-go soil sensors have been developed in recent years (Adamchuk et al., 2004a) as an alternative to improve sampling density as compared to grid sampling (Adamchuk et al., 2004b).

Economic feasibility of site-specific-crop-management based on on-the-go data has been demonstrated. For example, a $15 to $35 per hectare economic advantage was recorded by variable rate management of nitrogen following management zones (Ostergaard, 1997). Although economic benefits can be seen, still on-the-go mapping of soil properties is expensive to adopt by most farmers, resulting in slow adoption due to high initial cost (Kitchen et al., 2002). Sensor integration is one of the methods recommended to lower the expense of data collection (Swinton et al., 1998). Integrating several soil sensors on one platform to measure the most important soil properties simultaneously can help in

lowering the cost by saving energy, time and labor. More significantly, the complex behavior of soil can be better studied by getting different signals from different sensors in soil at the same time (Yurui et al., 2008).

2.2. Soil organic matter (SOM)

Soil organic matter is considered an important indicator of soil quality (Reeves, 1997). Information about the spatial variability of SOM within a field is required for site-specific management of fertilizers and herbicides (Roberts et al., 2010). Surface soil color can be used to predict SOM content (Schulze et al., 1993). Previously, SOM was predicted using soil color based on Munsell color charts (Alexander, 1969). Remote sensing is a technique used to correlate SOM with soil color data obtained by aerial and satellite imagery (Frazier et al., 1997), which has limitations due to crop residue and weather interference.

Diffuse reflectance spectroscopy (DRS) provides an alternative to conventional methods and bare soil imagery to predict SOM. Light of certain wavelengths is used to illuminate the soil to be tested, and the amount of energy absorbed depends on soil attributes, while the reflected energy is used to measure the constituents of the soil responsible for absorption of energy. Soil organic matter is one of the important attributes which affects the soil color and further its spectral reflectance properties (Krishnan et al., 1980). Diffuse reflectance spectroscopy is a rapid, non-destructive, less expensive method as compared to conventional laboratory methods of predicting SOM. Quite a few studies have been completed to develop on-the-go spectrophotometers for the prediction of SOM.

Shonk et al. (1991) developed a real-time shank-mounted sensor emitting light in the range of 560 nm to 700 nm with a peak value at 660 nm and used it to map fields for SOM. Sudduth and Hummel (1993) tested a NIR portable spectrophotometer with a sensing range from 1650 nm to 2650 nm with the bandwidth of 55 nm in the laboratory and field on Illinois soils which yielded r^2 values of 0.89 with standard error of prediction (SEP) of 0.40% in lab with large errors during field tests. Shibusawa et al. (1999) also developed an on-line spectrophotometer for sensing soil moisture, pH, apparent electrical conductivity (EC_a) and SOM of soils with wavelengths in the range of 400-1700 nm and obtained an r^2 value of 0.87 for a linear regression between a predicted and actual SOM. Christy (2008) tested the feasibility of near-infrared spectroscopy (NIRS) and presented an on-the-go spectrophotometer for in-situ measurement of reflectance spectra. Spectrophotometer data and soil samples from eight fields in central Kansas were used. The best validation results were obtained for SOM, with a root-mean-square error (RMSE) of 0.52% and a coefficient of determination (R^2) of 0.67.

2.3. Soil water content

Knowledge of the spatial variability of surface and sub-surface water content is essential in agricultural, environmental, soil physics, and ground water hydrology studies especially while studying infiltration, runoff and evapotranspiration (Weihermüller et al., 2007). Information on the spatial variability of soil water content can provide important knowledge in the prediction of infiltration and surface runoff (Merz and Bárdossy, 1998; Pauwels et al., 2001), crop yield and flood control (Schlesinger et al., 1990), and meso-scale transpiration loss (Wood,1997)**.** Vehicle traffic and tillage in the presence of the

high soil moisture contents can produce undesirable effects such as high compaction levels and degradation of soil structure (Hamza and Anderson, 2005; Topp, 1993).

Soil water content (SWC) can be measured using three different methods: 1) laboratory analysis of soil cores taken from field; 2) point measurements in situ; and 2) on-the-go sensing. Laboratory analysis involves the determination of the soil sample weight before and after water evaporation through the oven drying method (Topp, 1993), which is time consuming and labor intensive. Time-domain reflectrometry (TDR), neutron probes, gypsum blocks and gamma-ray attenuation are all examples of sensing techniques adopted for point methods (Topp, 1993). Point-based measurements become expensive when the SWC of a large number of locations must be monitored.

The most promising method to map large fields for SWC is on-the-go sensing in which geo-referenced data are collected while moving across a landscape (Adamchuk et al., 2004b). Several on-the-go soil moisture sensors have been developed based either on radiometric or electrical principles. Near infrared absorbance spectroscopy is based on the capacity of water to absorb light energy at certain bands of the spectrum (Norris, 1964). A VIS/NIR spectrophotometer was tested by Mouazen et al. (2005) to develop a sensor for on-the- go measurement of soil water content by detecting light reflectance. The spectrophotometer was calibrated by comparing NIR spectra with gravimetric moisture, and acceptable results were obtained. Nuclear magnetic resonance is a technique which depends on the interaction between hydrogen nuclear magnetic moments and a magnetic field. It has been used to develop an instrument that can be mounted on a tractor (Paetzold et al., 1985), which had a relatively high power requirement.

A promising technique of capacitance-based sensors was explored by some researchers. Dean et al. (1987) developed a capacitance-based sensor operating at 150 MHz. A similar sensor was evaluated dynamically by Whalley et al. (1992) using speeds typical of those found during seed planting, which was found to be sensitive to fluctuations in soil bulk density as well as SWC. Lui et al. (1996) and later Andrade-Sanchez et al. (2007) evaluated a dielectric-based moisture sensor under dynamic conditions by incorporating it into a nylon block that was attached to an instrumented tine. A series of studies demonstrated that salinity, texture, and temperature also affected sensor measurements. A similar capacitance-type sensor was evaluated more recently by Adamchuk et al. (2009), who concluded that their sensor was able to produce high resolution SWC data with relatively low standard error (0.027 g/g or 0.039 ml/ml). Soil bulk density was also predicted in that study by measuring resistance of soil to penetration simultaneously with moisture content data.

2.4. Soil compaction

Soil compaction is defined as "the process by which the soil grains are rearranged to decrease void space, bringing particles into closer contact with one another hence increasing bulk density"(SSSA,1996). Heavy agricultural farm machinery used in modern farm operations, working with soil at excessive soil moisture content and, animal trampling have been considered the main factors responsible for soil compaction (Hamza and Anderson 2005). The primary effect of high soil compaction is hindrance to plant root growth. Soil compaction can lead to poor soil structure; a decrease in water holding capacity, and a poor supply of nutrients to plants which results in a decreased crop yield.

Increased soil compaction can also cause soil erosion and surface runoff of soil (Fleige and Horn, 2000). Measurement of soil compaction levels in agricultural fields has been performed to aid in avoiding these harmful effects, preserving soil structure in field areas without compaction related limitations. Also, soil compaction data have been used to determine variable-depth tillage, which could successfully save fuel while fracturing soil layers compacted sufficiently to not impede plant root penetration. Using soil compaction data Gorucu et al. (2001) found that 75% of tested fields required shallower depth tillage than the recommended uniform tillage depth and also achieved 42.8% energy savings and 28.4% fuel savings with variable depth tillage as compared to uniform-depth tillage.

Measuring soil cone indexs with a cone penetrometer (ASAE, 2004) at different points throughout a field is considered a standard method to estimate spatial variability of soil compaction in the field. However, using a cone penetrometer is an expensive and time consuming method to get an accurate representation of soil compaction of the field due to poor sampling density. Automation of a cone penetrometer has been explored to reduce cost while achieving higher sampling density. A tractor-mounted, automated soil penetrometer–shearometer unit was designed and developed for the purpose of obtaining simultaneous in-situ measurements of soil penetration resistance and shear stress (Boon et al., 2005). They found significant correlations of soil moisture content with soil penetration resistance and shear stress.

On-the-go soil sensors for measuring soil compaction indirectly by measuring other behavioral soil properties have been explored. Mechanical, pneumatic and acoustic methods have been used to measure soil compaction on-the-go (Adamchuk et al., 2004a).

Several researchers have tested mechanical sensors which measure soil compaction indirectly by through the soil resistance to the penetration of a mechanical sensor. Hemmat et al. (2008) reviewed the studies on the use of mechanical sensors in measuring soil compaction and classified them on the basis of their measurement concepts.

2.5. Sensor fusion

As the three soil properties reviewed above have been mapped using one of the sensor approaches described, it was noted that virtually none of existent sensor systems could become a universal predictor for that particular soil property. Thus, it was noted that soil series and water content have a significant effect on the relationship between soil reflectance and SOM. On the other hand, the relationship between capacitor sensor voltage output and soil water content was not the same for different soil types and for soils with different SOM. Finally, the cone index or any other measures of soil mechanical resistance have been drastically affected by SWC as moist soils significantly reduce soil strength.

Therefore, an idea of merging three instruments (e.g., optical reflectance, capacitance and mechanical resistance sensors) in a single unit for on-the-go mapping has an appeal to be applicable in a wider range of soil conditions than any of the components independently. With an adequate calibration process such a tool could be used to construct high-density thematic soil maps that reveal spatial distribution of critical soil characteristics.

3. MATERIAL AND METHODS

3.1. Sensors system development

The Integrated Soil Mapping System (ISMS) (Figure 3-1) was constructed as a pull-type platform, which can be attached to a pickup truck. A linear hydraulic actuator (Veris Inc., Salina, KS) was installed to raise and lower the system which was operated by the driver. The hydraulic pump for the linear actuator was driven by a DC motor powered by the electrical system of the pickup.

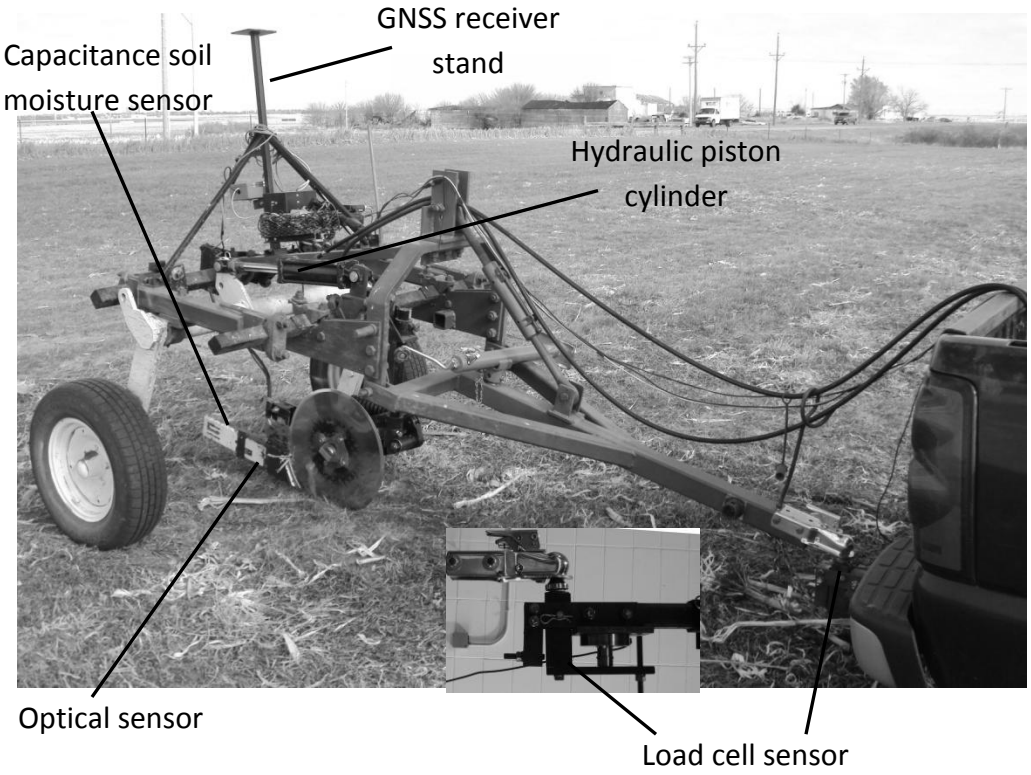

Figure 3-1: ISMS components

A coulter-knife assembly (Model no. 2995, Yetter Manufacturing Co., Colchester, IL), shown in Figures 3-2 and 3-3, was mounted on the ISMS to hold the optical and moisture

sensors and to drive them through the soil at adjustable depths. A bracket was designed and welded behind the anhydrous knife to hold both sensors in place. The function of the 50.8 cm diameter coulter was to cut crop residues left on field surface.

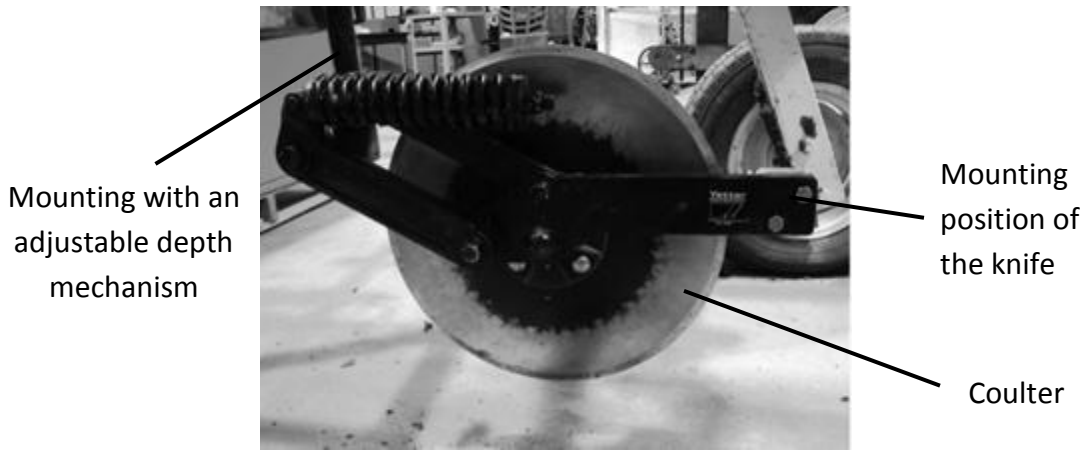

Figure 3-2: Coulter-knife assembly used to hold sensors.

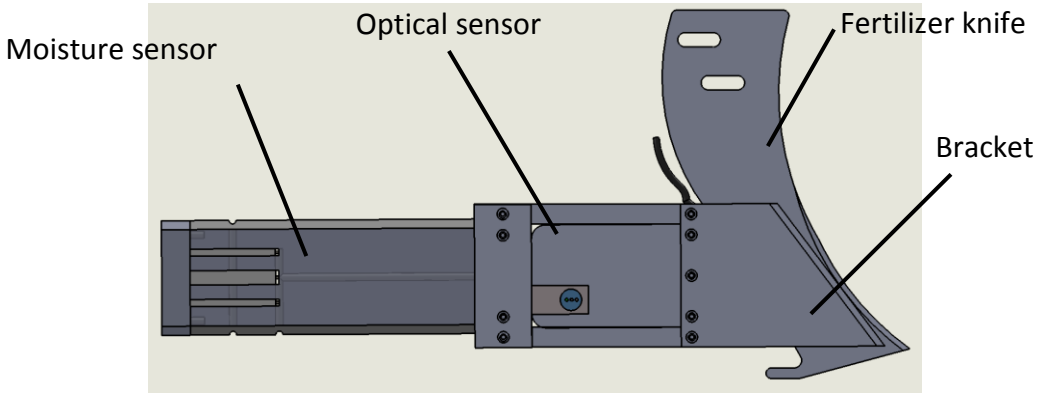

Figure 3-3: Bracket welded to fertilizer knife with the optical sensor and moisture sensor bolted to the bracket.

The overall width of the knife and bracket, 21 mm (about 13/16 in.) which was kept as small as possible to minimize soil disturbance. The knife with both sensors was mounted

immediately behind the coulter. A portable 12 VDC rechargeable battery was used to supply power to the optical sensor and the moisture sensor which required regulated voltages of 12 V DC and 5V DC respectively. A voltage regulator (Model no. QA1107518, Semiconductor Circuits, Inc., Atkinson, NH) was used to convert 12 V DC to 5 V DC for the moisture sensor. The analog signal from the capacitance moisture sensor was converted into a digital signal by an A/D convertor (ADI XL-05 8100-0121, Crossbow Technology Inc., Milpitas, CA). A baud rate convertor (232BRC, B&B Electronics Mfg. Co., Inc. Ottawa, IL) was used to convert the baud rate of the optical sensor into a conventional rate acceptable by a typical PC interface. All the components of the electrical circuit of the ISMS are shown in Figure 3-4.

3.1.1. Capacitance based sensor

The principle involved in capacitance sensors was based on measuring the dielectric constant of the medium present in an electric field produced by a capacitor consisting of two electrodes. Dielectric constants for dry soil, air and water are 3 to 5, 1, and 80, respectively. Therefore, the dielectric constant of mixture of soil, water and air was mostly dominated by SWC. The capacitance (C) can be estimated as:

$$C = \varepsilon_r \frac{A}{4\pi d} \tag{3.1}$$

where, A is the surface area of the metal electrodes, d is the distance of separation of the capacitor plates, and ε_r is the dielectric constant of soil. Because A and d were constant, C changes were proportional to the variation of the εr, which represented the variation of the SWC.

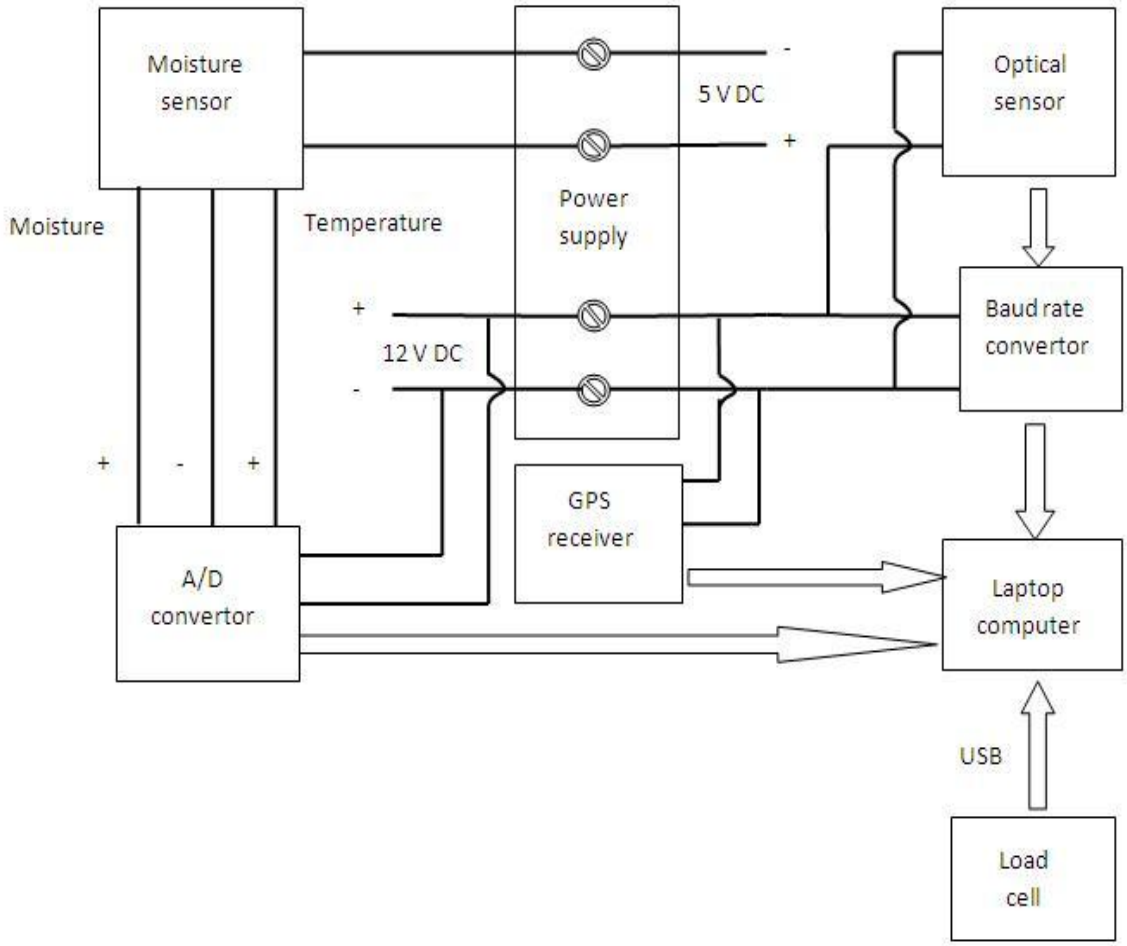

Figure 3-4: Components of the electric circuit of the ISMS.

Two designs of capacitance-based moisture sensors were used to predict the soil moisture content during laboratory test. The electronic components of both designs were built by Retrokool Inc. (Berkley, CA). The electrodes and their installations were different between the two sensors, but in both cases were inserted into a 19 mm (0.75 in.) thick Teflon plate (Figure 3.5). One of the designs had only one sensing surface while in the

second design, metal electrodes passed all the way through the Teflon plate making both surfaces sensitive to SWC.

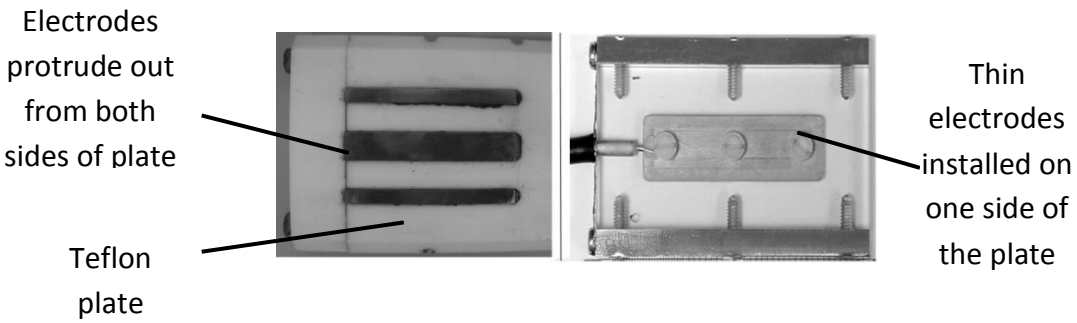

Figure 3-5: Two-sided and one-sided capacitance sensor design.

Both types of design were tested under similar laboratory conditions. Linear regression was used to determine calibration equations to predict volumetric and gravimetric water content:

$$w = a_1 + b_1 * \ln(V_{air} - V) \quad (3.2)$$

$$\theta = a_2 + b_2 * \ln(V_{air} - V) \quad (3.3)$$

where w is the gravimetric water content (g/g), θ is the volumetric water content (cm^3/cm^3), a_1, a_2 are intercepts and b_1, b_2 are slopes, V_{air} is the voltage output by the sensor while the sensor is in air, and V is the output when the sensor is in a measured soil.

3.1.2. Optical sensor

The optical sensor manufactured by Holland Scientific, Inc. (Lincoln, NE) was evaluated in this study to predict soil organic matter (SOM). The principle of this sensor was based on the fact that SOM can be predicted by calibrating the sensor with soil color. Soil reflectance measurements were taken by two different sensors, which differed only by the wavelengths at which they acquired soil reflectance; otherwise both sensors were similar with respect to design and dimensions. For the NIR/Amber sensor, wavelengths within the visible and NIR regions were 505±10 nm (amber) and 880±15 nm respectively. These two wavelengths were chosen to maximize the difference in the magnitudes at the wavelengths while both being wavelengths were mostly on linear portion of soil reflectance curve. The other sensor determined soil reflectance from two wavelengths in visible region (red at 660 nm and blue at 480 nm). The compact design of the optical sensor made it possible to move it through the groove made by a narrow knife assembly through the soil. The orientation of the sensor relative to the soil surface scene was vertical so the sapphire window used as an interface was perpendicular to the ground surface and parallel to the side walls of the groove in soil. By having the sensor in a vertical position in the soil there was no interference from crop residue on the soil surface and also this resulted in a relatively low soil disturbance. As the LEDs illuminated the soil surface, the reflected part of the energy was measured by a photodiode, and converted into soil reflectance values at both wavelengths separately (Figure 3-6). The supply voltage required for this sensor was 12 VDC and the sensor collected data at 1 Hz. The raw soil reflectance measurements were used to calculate several different indices that included their difference, sum, and ratio. Other indices calculated were the

Normalized Difference Soil Index (NDSI) and the inverse of NDSI, which represents the average soil reflectance normalized by the reflectance spectrum's slope.

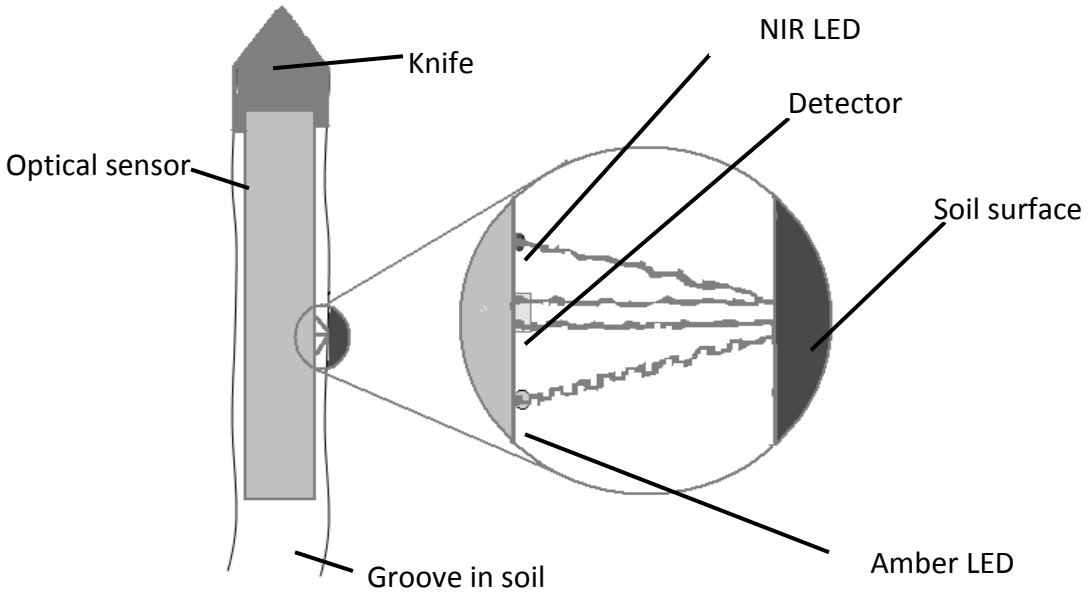

Figure 3-6: Top view of working process of optical sensor (NIR/Amber) moving through soil.

After acquiring the reflectance of soil samples in the laboratory or in the field, the different indices calculated to regress against measured SOM were: 1) difference (NIR-Amber or Red-Blue), 2) sum (NIR+Amber or Red+Blue), 3) ratio (NIR/Amber or Red/Blue), 4) NDSI [(NIR-Amber)/(NIR+Amber) or (Red-Blue)/(Red+Blue)], and 5) inverse NDSI. Sum of individual reflectance values was calculated to see how the average of individual values correlated with SOM. Difference was calculated to see the relation of slope of soil reflectance curve with the SOM. NDSI is a difference of individual values normalized by average of individual values which was calculated to look how the slope of curve was different when normalized by average. Similarly average of individual values normalized by slope was calculated by inverse of NDSI.

3.1.3. Load cell sensor

The load cell sensor (Figure 3-7) was designed to measure the mechanical resistance of the soil to horizontal penetration by a knife. As the knife was pulled through the soil, the resistance of the soil to penetration was measured by a capacitor-based compression-type USB load cell (PUF-10K-050-S, Loadstar sensors, Inc., Fremont, CA). Pull force was converted into compression force around the pivot point P (figure 3-8). One end of the load cell sensor was inserted in the standard receiver hitch (size 2 X 2 in.) found on most full-size pickup trucks and the ISMS was connected to the standard 2 in. hitch-ball.

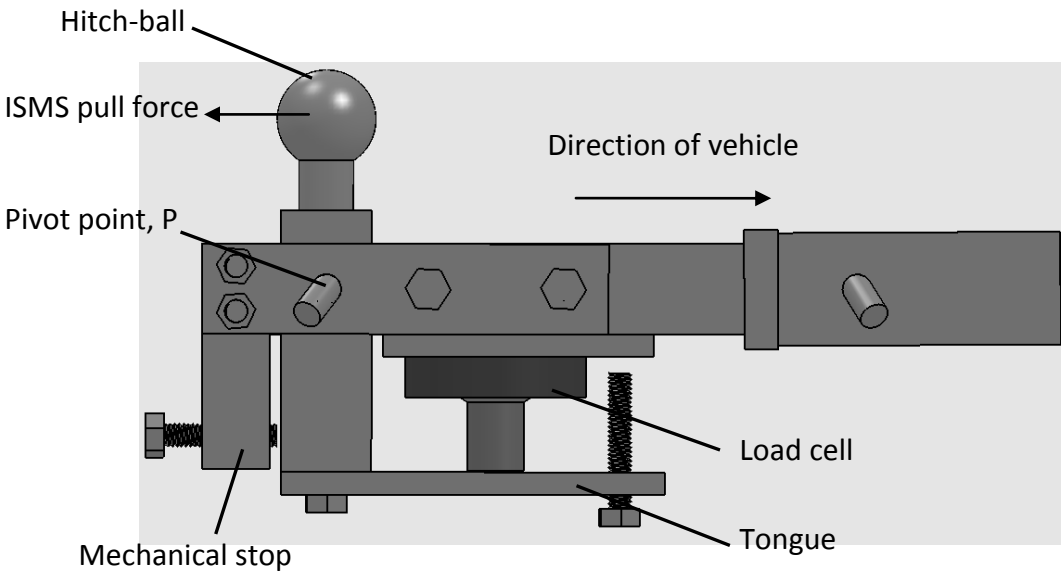

Figure 3-7: Pull sensor capable of measuring force required to pull any system behind the hitch.

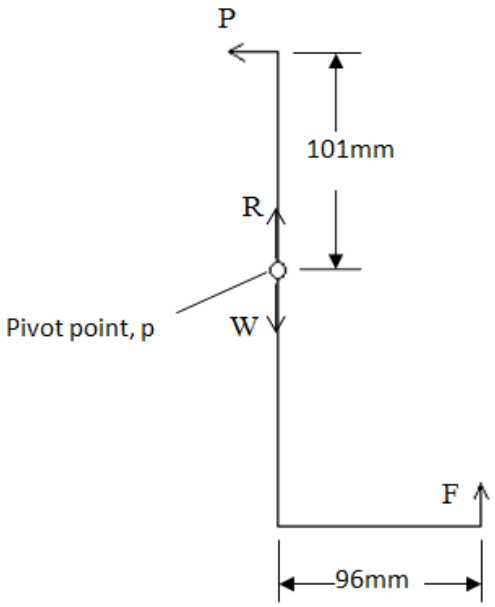

Figure 3-8: Free body diagram of Load cell sensor.

Based on the design, the tongue which is free to rotate around the pivot point, P (figure 3-8) pressed on the load cell button with the force, F produced and the magnitude of that force is measured by equation 3.6a and 3.6b.

$$R - W = 0 \tag{3.6 a}$$

$$96F - 101P = 0 \tag{3.6 b}$$

The load cell used in this design had capacity of 10,000 lbs, which was chosen by assuming that the maximum cutting force required per unit area of soil as 5 MN/m^2. The surface area of the front face of the cutting knife was measured as 0.0048 m^2, which produced a maximum force of 24,000 N (5,400 lbs) on the knife. Therefore, force F on

the load cell sensor as calculated by equation 3.6 was 25,250 N (5,681.2 lbs). To allow for a factor of safety and some dynamic effects, a load cell of 10K lbs capacity was chosen.

For this calculation, it was assumed that the pull force exerted by cart is acting at the center of hitch-ball in the horizontal direction, which was not always true in dynamic conditions. The point of application of the force determines the length of the lever arm (lever arm = 101 mm from the center of hitch-ball). Therefore the actual point at which the force is acting can increase or decrease the length of the lever arm. Variations of the length of the lever arm depended upon on the angle of tilt of the drawbar. Even though the angle of tilt is small in real situation, it can be a source of error, which was accounted for through laboratory calibration. For illustration of error due to angle of tilt, error was calculated when the force was acting at a 5° angle to the horizontal direction. Decrease/increase in length of arm, can be calculated using trigonometry. For an angle of 5°, decrease/increase was found out to be 2.21 mm, which causes error of 2.2% in force measurement and this error can be minimized by maximizing the length of arm while designing the load cell sensor.

3.1.4. Data acquisition system

The data acquisition software for the ISMS was developed using Lab-VIEW software (National Instruments Corporation, Austin, TX). The program was built to acquire geo-referenced data from the optical, moisture, and load cell sensors at the same time. As it stated earlier, moisture sensor analog voltage output was converted into digital data by an

A/D converter mounted on the system. Digital data output from the three sensors and geographic location were logged at 1 Hz in a tab delimited text file. The GNSS receiver, optical sensor, and A/D converter were connected to a USB serial port hub through RS-232 cables, which transmitted data to a laptop computer in the pickup. The load cell sensor included a digital USB load cell and was directly connected to the laptop through a separate USB cable. The maximum sampling frequencies of the A/D converter, optical sensor, and load cell sensor were approximately 20 Hz, 1 Hz and 80 Hz, respectively when data were acquired directly from these sensors without any filtering. Average values were calculated by the program for all three sensors to log data at the same frequency rate as the GNSS receiver (i.e. 1 Hz). The data flow implemented in the software is shown in Figure-3-9. After the start of the program, COM ports for all sensors were recognized by the program and then a dialog box appeared for selecting the file to which data was to be logged. After that continuous data acquisition was executed. Before the load cell virtual instrument (VI) started acquiring data, another dialogue box appeared with an option to tare the load cell. Geographic data and averaged data from the rest of the sensors were logged into a text file. This process continued until stopped by the user. Finally, when the program was stopped, the ports were closed and the log file was finalized. The front panel of the software developed is shown in Figure 3-10.

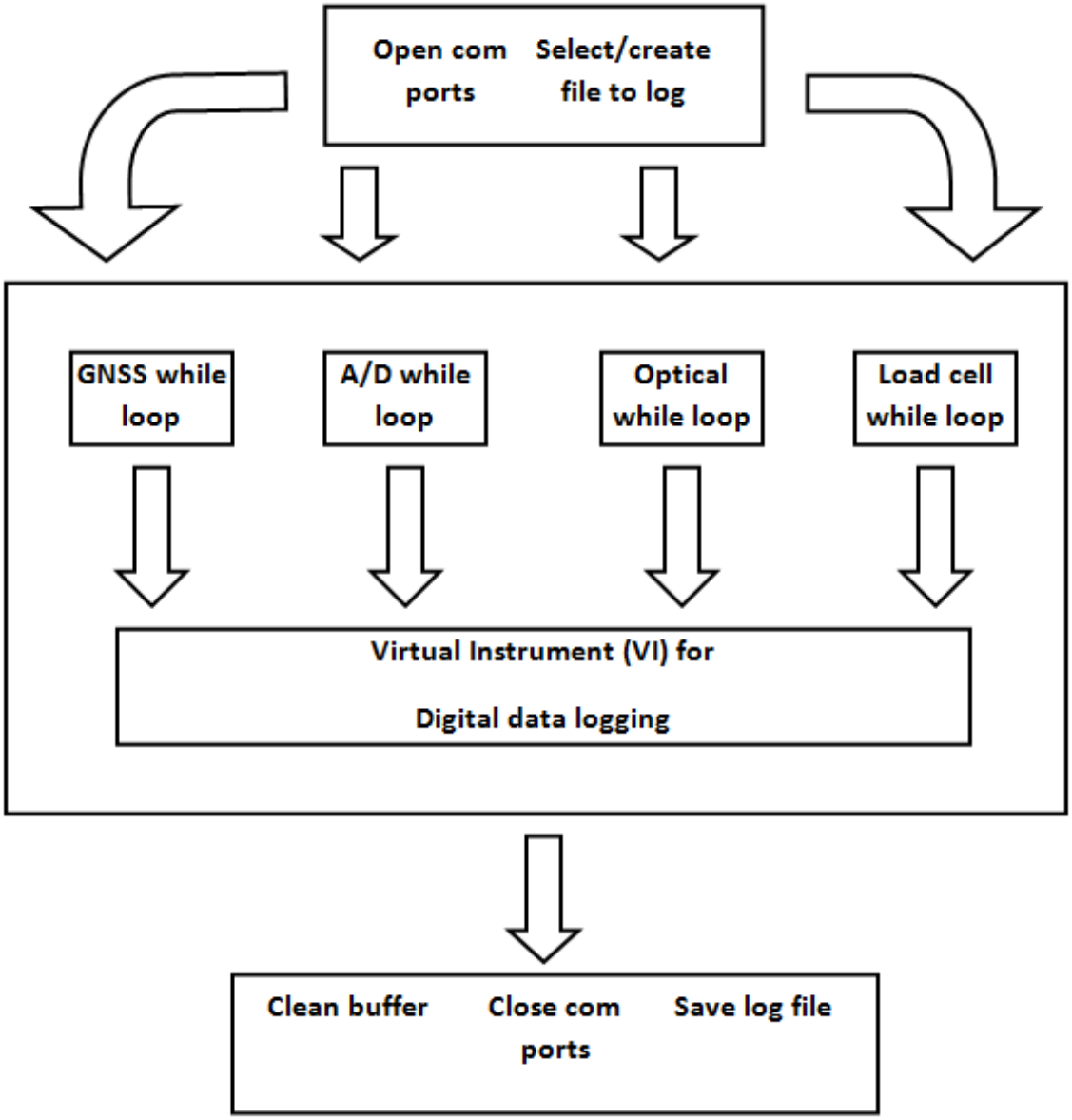

Figure 3-9: Flow of data in Lab VIEW program for the ISMS.

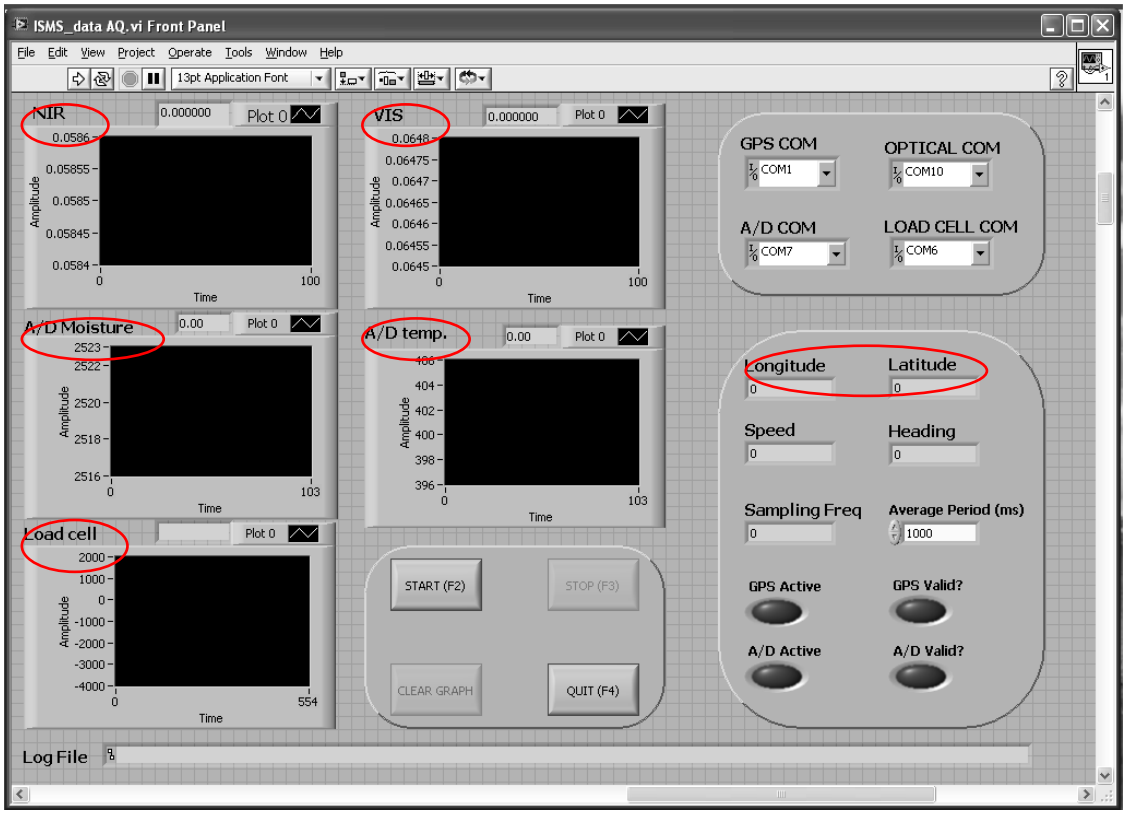

Figure 3-10: Front panel diagram of the ISMS data acquisition software.

3.2. Sensor system evaluation

3.2.1. Laboratory evaluation

3.2.1.1. Capacitance-based soil moisture sensor

Soil samples from 14 different fields were collected representing eastern Nebraska soils. The soil samples were analyzed in commercial laboratories, as shown in Table 3-1. The one-sided sensing and two-sided sensing capacitance-based moisture content sensors were used to acquire capacitance-related voltage values at different moisture contents in the range up to saturation for all samples. The moisture content sensor was placed on the

top of a 2-3 cm soil layer with defined moisture content and then a similar soil layer was added on the top of the sensor. The soil and the sensor combination were then compacted using a weight of 490 N every time, as shown in Figure 3-1.

Table 3-1: Soil organic matter and soil texture for 14 soils samples.

Soil ID	Measured OM (%)	Particle size distribution, %			Texture class
		Sand	Silt	Clay	
1	2.63	14	54	31	Silty Clay Loam
2	2.77	19	63	18	Silt Loam
3	3.07	16	58	25	Silt Loam
4	2.97	15	56	28	Silty Clay Loam
5	1.61	15	44	41	Silty Clay
6	2.61	13	51	36	Silty Clay Loam
7	3.83	15	61	24	Silt Loam
8	1.33	78	12	9	Loamy Sand
9	1.37	76	14	9	Sandy Loam
10	2.97	54	28	18	Sandy Loam
11	2.57	29	55	15	Loam
12	2.48	28	50	22	Silt Loam
13	1.46	72	21	8	Sandy Loam
14	0.99	87	7	6	Loamy sand

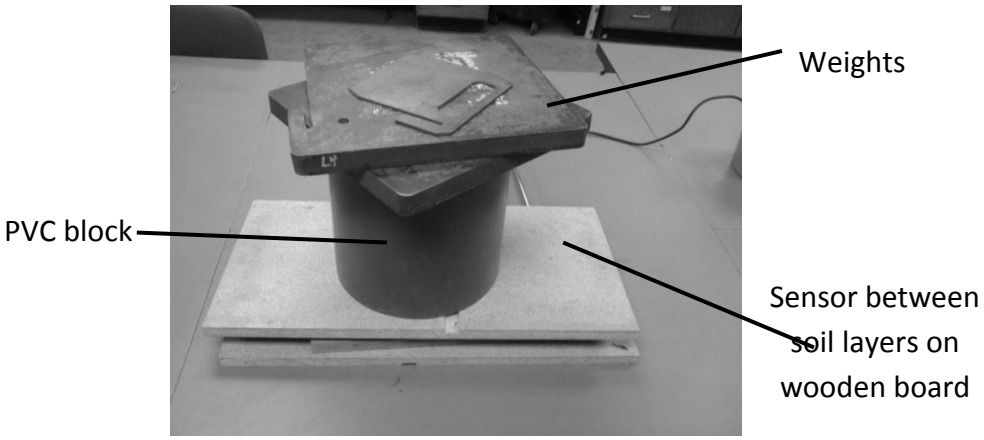

Figure 3-11: Laboratory setup for the moisture sensor calibration.

After acquiring the voltage signal from the capacitance-based sensor, a soil core of known total volume (v_b) was taken from the wooden board and was weighed before the core was dried in an oven for 24 h at 105˚ C. The mass of water evaporated (w_w) from soil core was calculated by again weighing the dried core. Then gravimetric (w) and volumetric (θ) water content were calculated as follows:

$$Gravimetric\ water\ content, w\ in\ g/g = \frac{w_t - w_s}{w_s} \qquad (3.7)$$

Where w_t is the mass of total soil core before drying and w_s is the mass of solids after it was dried in oven.

$$Volumetric\ water\ content, \theta\ in\ m^3/m^3 = \frac{v_w}{v_b} \qquad (3.8)$$

Where v_w is the volume of water present in soil and v_b is the bulk volume of soil after testing.

3.2.1.2. Optical sensor

A NIR/Amber optical sensor was used in preliminary tests run at an agricultural field near Mead, NE and another optical sensor (Red/Blue) was tested in laboratory conditions and in the rest of the experiments in this research. Thirteen samples shown in Table 3-1 (except Soil 1) were used for calibration of the second optical sensors. It was found from preliminary experiments that the optical sensor was very procedure sensitive, so the sensor was placed at a fixed position and three sub-samples from each soil were placed one-at-a-time on the sensor sapphire window. The sub-samples were prepared at three

different moisture contents. Three moisture contents chosen for these sub-samples were gravimetric water content of each soil at field capacity, half of value calculated at field capacity and air dried sample. The targeted and measured values of gravimetric water content are shown in table 3-2.

Table 3-2: Targeted and actuals moisture contents for all samples for 13 soils used for calibration of the Red/Blue optical sensor.

Soil id	Gravimetric water content, w (g/g)				
	Sub sample 1	Sub sample 2		Sub sample 3	
	measured	targeted	measured	targeted	measured
2	0.009	0.100	0.087	0.200	0.169
3	0.011	0.100	0.088	0.200	0.155
4	0.012	0.125	0.122	0.250	0.219
5	0.018	0.130	0.127	0.260	0.251
6	0.015	0.125	0.120	0.250	0.225
7	0.010	0.100	0.084	0.200	0.187
8	0.003	0.045	0.032	0.090	0.069
9	0.004	0.070	0.046	0.140	0.117
10	0.007	0.070	0.048	0.140	0.120
12	0.009	0.080	0.077	0.160	0.143
13	0.009	0.100	0.085	0.200	0.186
14	0.003	0.070	0.041	0.140	0.112
15	0.002	0.045	0.042	0.090	0.071

Gravimetric water content at field capacity for each soil was calculated by Adamchuk et al. (2005), using the following formula:

$$\theta g = \frac{\theta v field}{2.65(1-\theta v Saturated)} \tag{3.9}$$

where $\theta v field$ is the field capacity volumetric water content and $\theta v Saturated$ is the volumetric water content of saturated soil. Optical soil reflectance was logged averaging data every 10 s using a Lab-VIEW routine. Raw values were logged during the laboratory

test in the blue and red regions of the electromagnetic spectrum for all three sub samples from 13 different soils; and different soil indices were calculated to perform regression with measured SOM.

3.2.1.3. Load cell sensor

The load cell sensor was calibrated under laboratory conditions by applying known loads. Thus, when the sensor was mounted vertically, standard weights were hung from the hitch with increment of 0.22 kN (50 lbs) and the output value was logged. Three trials were run for this experiment. The calibration setup is shown in Figure 3-12. To simulate field conditions, weights were hung from the same hitch which was mounted on the ISMS to pull behind any pickup during field mapping.

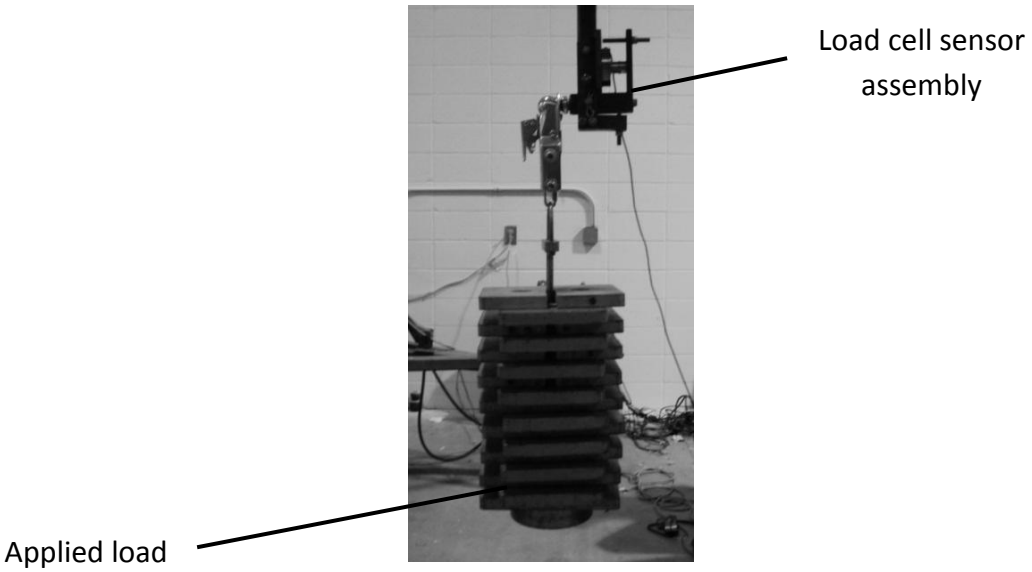

Figure 3-12: Load cell sensor calibration in laboratory.

3.2.2. Field test

The ISMS was tested in field conditions by pulling it behind a pickup truck (Figure 3-1). Preliminary tests were run at Field 1.10, Agricultural Research and Development Center (ARDC), University of Nebraska-Lincoln near Mead, Nebraska (study area 1). The soil series map and aerial image of the field are shown in Figure 3-13.

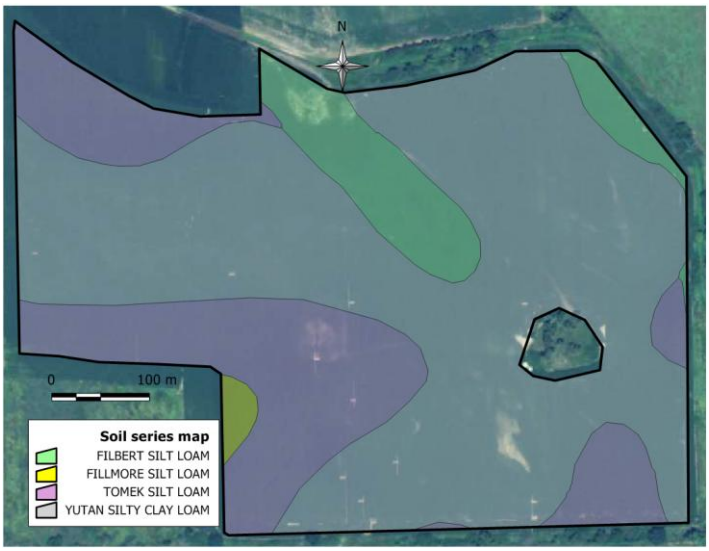

Figure 3-13: Soil series map and aerial imagery of Field 1.10 mapped by ISMS at study area 1. (Courtesy: NRCS Data Gateway).

The system was operated parallel to the established rows. It was observed that clay soils occasionally stuck on the sapphire window of the optical sensor (NIR & Amber) while mapping the field. Therefore to fully test the optical sensor again, three separate passes were made acquiring data for the optical sensor in Field 1.14. Parallel passes were made in such a way so that ISMS was exposed to maximum variability in organic matter. At same time, fifteen soil samples were collected along the three passes. Cores were collected within a 3 m radius of each sampling locations. Two sub samples were obtained from each of the fifteen sampling locations. One sub sample was used to obtain optical

reflectance values of the soil with the same optical sensor in laboratory and the other sub sample was sent to a commercial laboratory (Agsource Harris laboratories, Lincoln, NE) for determination of soil organic matter.

To further test the ISMS in field conditions, the system was run in another field in Merrick County near Clarks, Nebraska. The field was mapped with the ISMS operating all three sensors. Unfortunately, field conditions during this mapping operation were not suitable for ISMS evaluation. There was relatively low variation in SOM and absolutely no changes in SWC, which were required for the field test. Therefore variation in moisture content was created by irrigating the middle part of a site in another corn field at South Central Agricultural Laboratory (SCAL), Clay Center, Nebraska (study area 2).

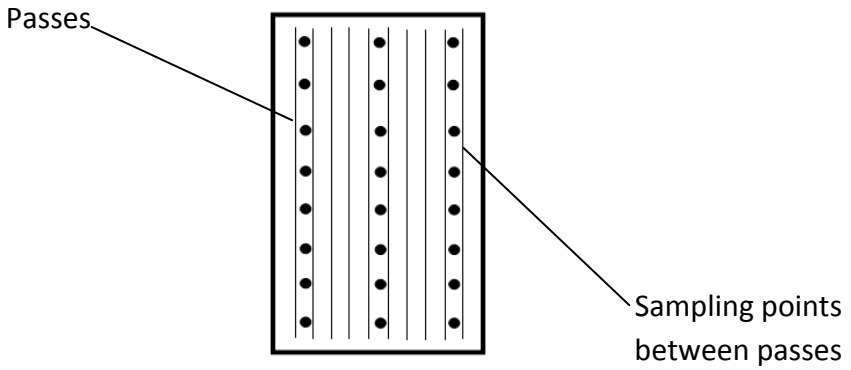

Figure 3-14: Mapping pattern of 10 passes and 24 sampling points at study area 2.

The ISMS was run in every row collecting data in ten different passes along the moisture variation (dry-wet-dry). Soil cores and cone index measurements using cone penetrometer (Spectrum Technologies., Inc. Plainfield, IL) were taken at the same time to compare sensor performance with laboratory results. Eight points were chosen along transects approximately 400 m long and three samples were taken at all eight points

between 1st & 2nd, 5th & 6th and 9th &10th passes (Figure 3-14). Three replications were measured of cone index at all twenty four sampling locations. The average speed at which the system was operated in the field was 7-10 km/h. Data were logged at a sampling rate of 1 Hz, travelling approximately 2-3 m for one sample. All laboratory and field experiment tests with information of the sensors tested in each test have been summarized in Table 3-3.

Table 3-3: Description of various laboratory and field experiments done in this research.

Test	Location	Date	Sensors tested	Comparison data	Conditions
1	Laboratory	02/06/2010	Both moisture sensors	Oven-dried w and θ	N/A
2	Laboratory	10/07/2010	Load cell sensor	Known weight	N/A
3	Laboratory	10/30/2010	Optical (Red & Blue)	SOM	N/A
4	ARDC 1.10	04/29/2010	Two-sided moisture sensor, optical (NIR & Red), load cell	N/A	Corn residue, entire field
5	ARDC 1.14	04/29/2010	Optical (NIR & Red)	SOM	Soybean residue, 3 transects, planted field
6	Merrick	10/19/2010	Two-sided moisture sensor, optical (Red & Blue), load cell	N/A	Corn residue, section of the field, low variation
7	SCAL	11/10/2010	Two-sided moisture sensor, optical (Red & Blue), load cell	Oven–dried w, Cone index	Corn residue, 10 transects

4. RESULTS AND DISCUSSION

4.1. Capacitance based sensor

Based on laboratory results, both types of capacitance based sensors predicted both gravimetric and volumetric water content reasonably well. The one-sided sensor showed linear response through the entire range of soil moisture, while the two-sided sensor had a non-linear response in the wet range. Linearization of the voltage values obtained from the sensor was conducted before running the linear regression with measured water content. Each voltage measurement was subtracted from the voltage output when the sensor was in air, and the natural logarithm was taken for each difference. Figures 4-1 and 4-2 show the response of both sensors to gravimetric and volumetric moisture contents measured by the oven-drying method. Prediction equations developed to predict water content corresponding to each sensor are also shown on the graphs. Non-linear regression was run for the two-sided sensor (Figure 4-2), since the sensor output was constant in wet soils. Thus, the two-sided sensor output in air was 2.53 V. The output decreased with an increase in moisture content until 1.60 V, which corresponded to 0.15 g/g gravimetric water content and 0.24 ml/ml volumetric water content. It was suspected that the electrodes of two-sided sensor when placed horizontally between soil layers could not be surrounded by a homogeneously wet soil. Thus, due to the load on the soil, water could be squeezed out of the soil on the upper sensing side of the metal electrodes which was a reason for the constant output of the two-side sensor in the wetter range but the sensitive side of the one sided sensor was facing downward and might not have been affected significantly by external load.

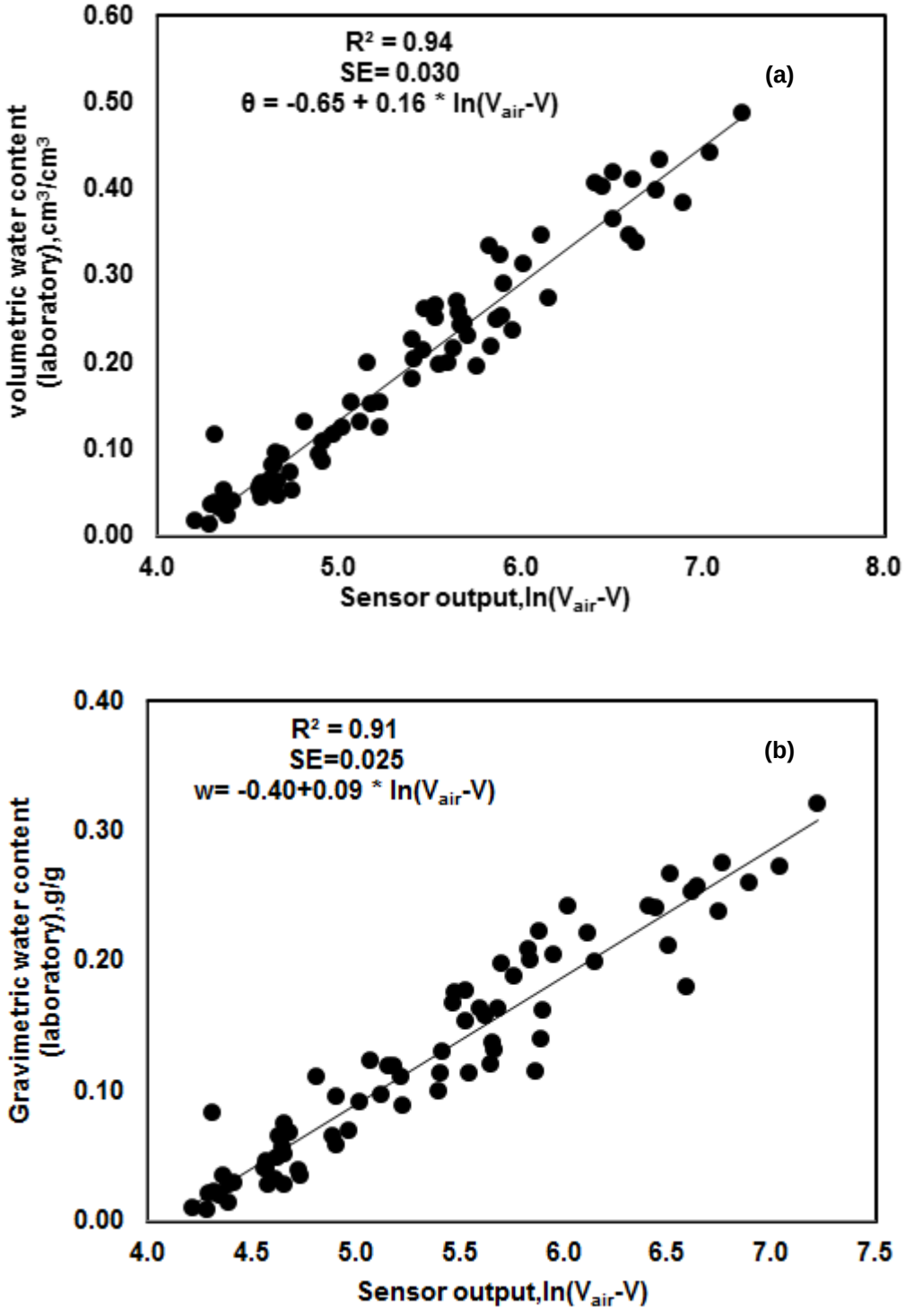

Figure 4-1: Comparisons of one-sided sensor output and oven drying measurements of (a) volumetric and (b) gravimetric water content

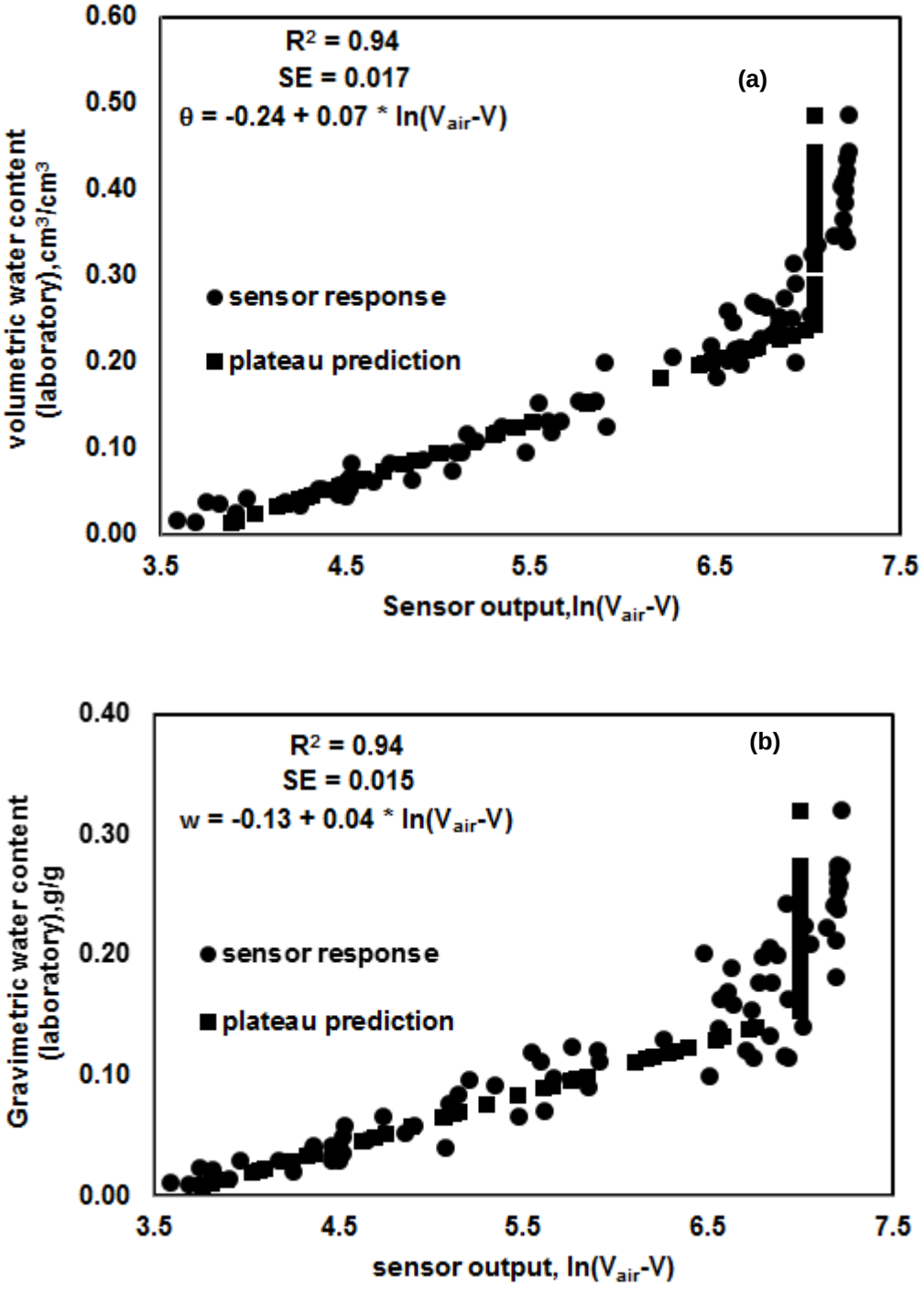

Figure 4-2: Comparisons of two-sided sensor output with oven drying measurements of (a) volumetric and (b) gravimetric water content.

During the SCAL field test, the ISMS was moved from the southern end to the northern end of the field through varying conditions of moisture content the sensor output responded in a similar trend, as shown in Figure 4-3. Three gravimetric water content measurements at eight sampling locations are also shown on the same graph. Figure 4-4 illustrates the linear regression between eight average laboratory measurements and 10-12 corresponding sensor outputs obtained from 20-30 m long sections of the transects corresponding to laboratory measurements. Average values at eight sampling locations of both methods resulted in a linear regression with $R^2 = 0.74$ and error bars in same graph shows that the standard deviation corresponding to both methods.

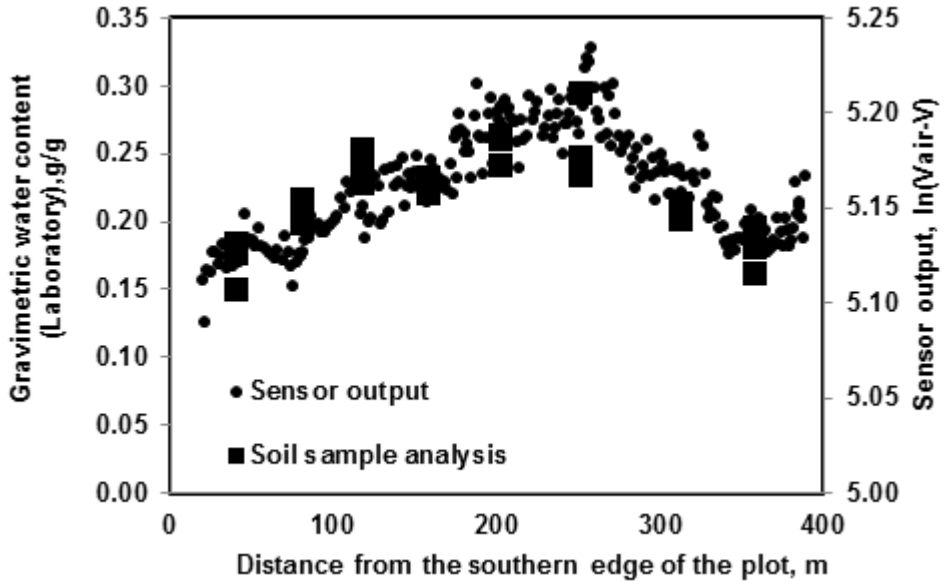

Figure 4-3: Two-sided capacitance sensor output at field SCAL, Clay Center, Nebraska compared with laboratory measurements.

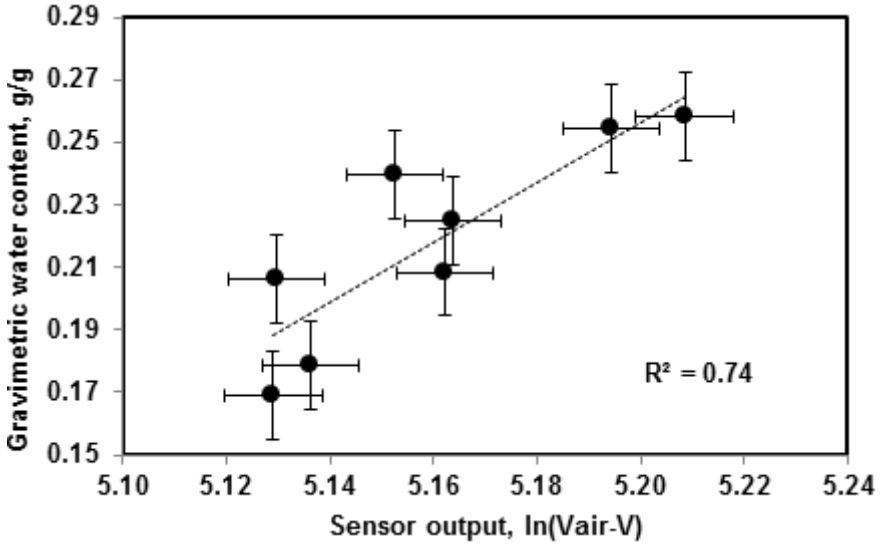

Figure 4-4: Linear regression between average sensor outputs and corresponding gravimetric water content measurements of data collected at SCAL. Error bars indicate standard deviation of each averaged value.

4.2. Optical sensor

Figure 4-5 and Table 4-1 show the results of linear regression of different soil index values with measured SOM. Based on results, it was found that the difference and the sum of individual soil reflectance and their difference predicted soil OM reasonably well with an R^2 of 0.77 and 0.75 respectively.

Table 4-1: Formulae and linear regression results of different soil indices against measured SOM for optical sensor (Red & Blue).

index	Red	blue	sum	difference	ratio	NDSI	ln. NDSI
Formula	R	B	(R + B)	(R – B)	(R/B)	(diff./sum)	(Sum/diff.)
R^2	0.75	0.69	0.73	0.77	0.39	0.39	0.39
SE (OM %)	0.45	0.5	0.47	0.43	0.70	0.70	0.70

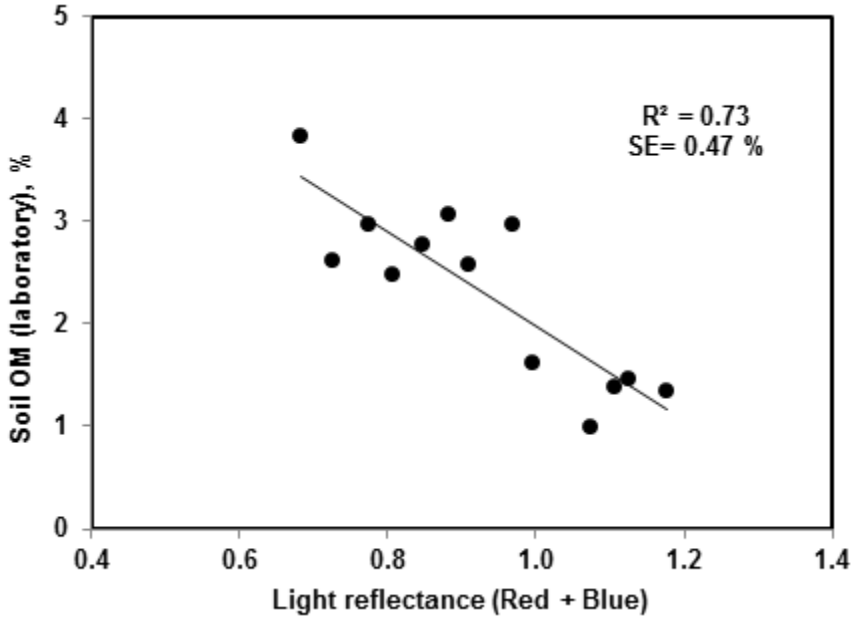

Figure 4-5: Laboratory calibration results for optical sensor (red & blue).

As listed in Table 3.3, during the ARDC 1.14 field test, three passes were made with the NIR/Amber sensor and 15 samples were taken between the three passes. The locations of three passes in the field and results are shown in Figure 4-6 and Figure 4-7. SOM at 15 sampling locations is also shown in Figure 4-7. During the passes, measured soil organic matter values tended to first decrease and then increase to the maximum value. A similar trend was found in the values of index sum (NIR + Amber) logged by the sensor. Linear regression was run between SOM and value of soil index sum (NIR + Amber) measured by the sensor for fifteen sampling locations. A comparison of both methods is shown in Figure 4-8.

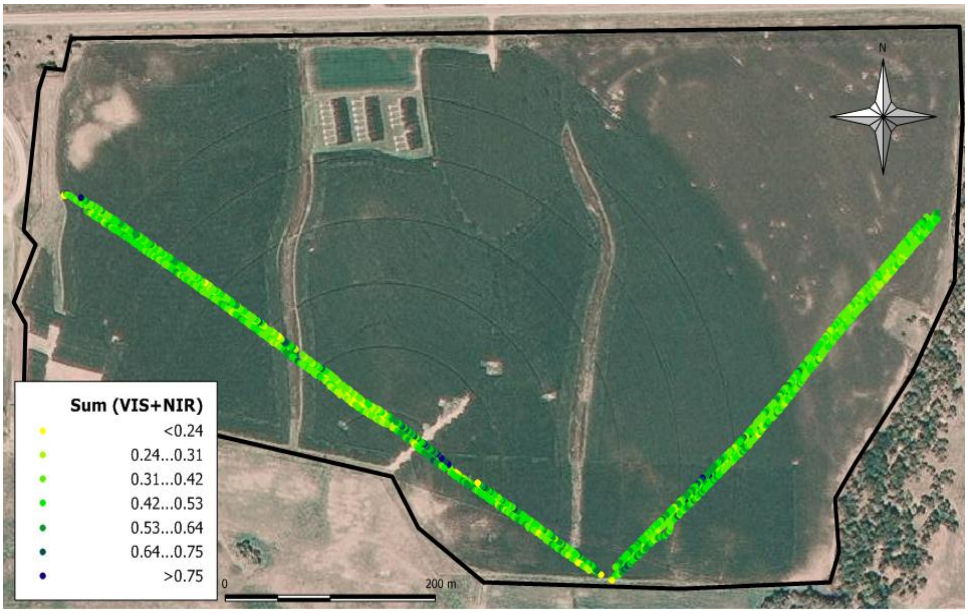

Figure 4-6: Three passes to compare soil organic matter with optical sensor (NIR/Amber) output at field ARDC 1.14.

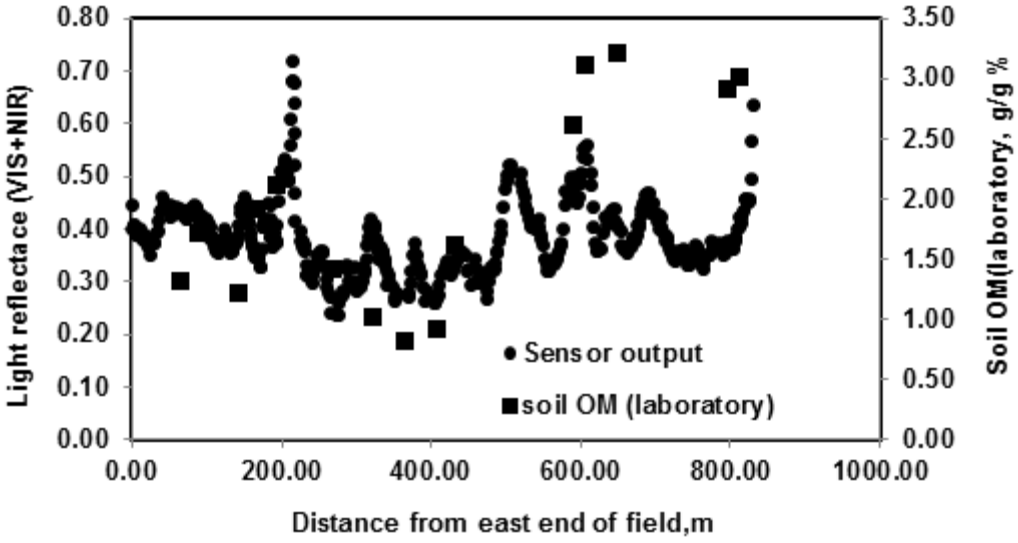

Figure 4-7: comparison of optical sensor (NIR+ Amber) output with measured soil organic matter at field ARDC 1.14, Mead, Nebraska.

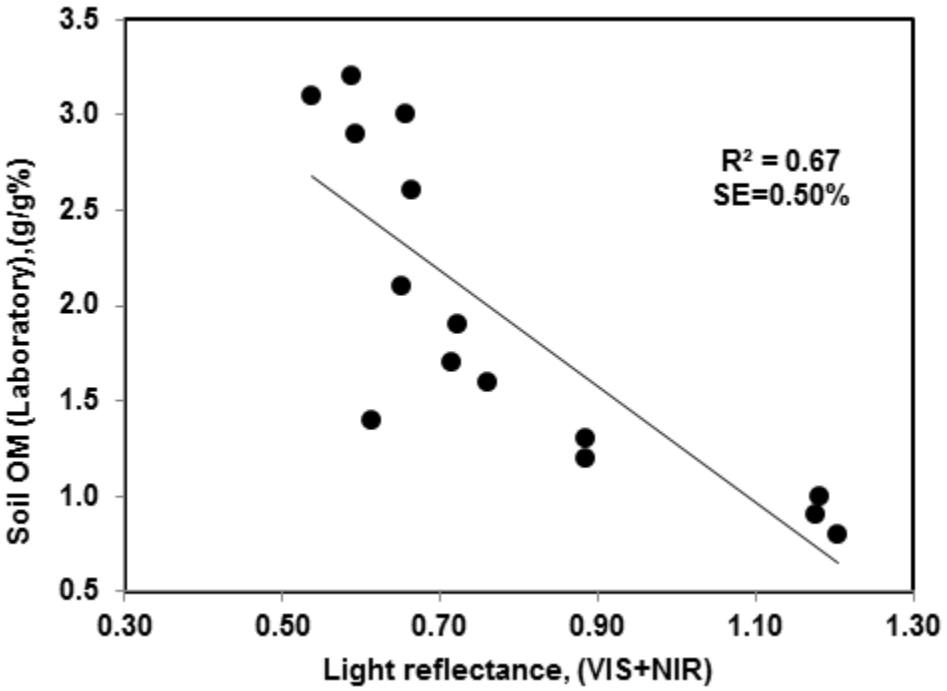

Figure 4-8: Comparison of optical sensor (NIR/Amber) output with soil organic matter (Laboratory) for 15 samples taken from field ARDC 1.14, Mead, Nebraska.

Table 4-2 summarized the performance of each index. Neither of the indices was superior to either of two individual wavelength reflectance measurements. The standard error of SOM measurements was once again about 0.5%.

Table 4-2: Formulae and Linear regression results of different soil indices for sensor (NIR/Amber) against measured SOM of 15 samples from field ARDC 1.14.

index	Amber	NIR	sum	difference	ratio	NDSI	in. NDSI
Formula	V	N	(V + N)	(V - N)	(V / N)	(diff./sum)	(sum/diff.)
R^2	0.68	0.61	0.67	0.68	0.59	0.59	0.57
Std. Error	0.50	0.55	0.50	0.50	0.56	0.56	0.58

4.3. Load cell sensor

Figure 4-9 illustrates the results of the load cell calibration test. With 0.031 kN standard error the regression equation produced 1.04 slope. The difference could originate from a small change of load application force placement on the ball. Laboratory results show that sensor was very accurate and sensor output was recorded as 96% of the input load.

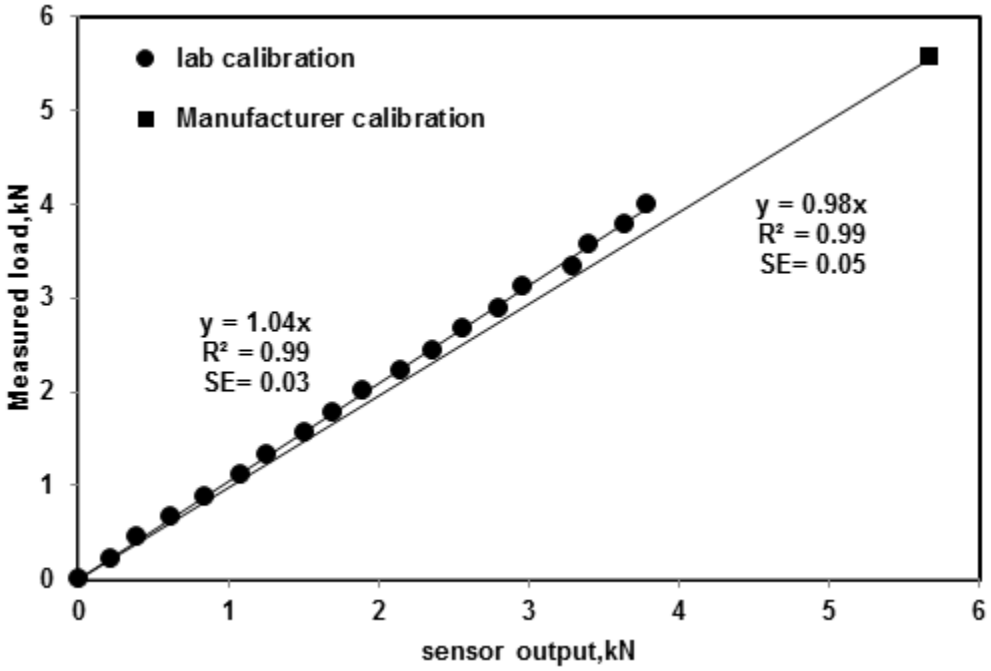

Figure 4-9 : Laboratory calibration results for load cell sensor assembly.

The possible sources of other 4% error could be change in length of lever arm with angle of tilt, for example decrease in arm length is calculated when force is acting at an angle of 5° to the horizontal in materials methods section. At an angle of 5° to horizontal, increase/decrease in arm length was found to be 2.21 mm which caused error of 2.2% in force measurement. The load cell itself was also calibrated by the manufacturer (Loadstar Sensors, Inc. Fremont, CA) with the input loads up to 45 kN, which suggest a slope of 0.99 at the lower end of their calibration curve. Average sensor output values of passes made during the SCAL field test and cone index values obtained are shown in Figure 4-

10. As many factors can affect highly variable soil mechanical resistance matched data did not always represent the same soil. That is why the relationship shown in Figure 4-11 between cone penetrometer index values and the closest load sensor measurements did not indicate a strong correlation. Another possible cause of the relatively weak correlation was that the ISMS did not have sufficient downward pressure when operated in dry conditions, which caused the moisture and optical sensor to rise slightly. This problem could have been easily overcome with a set of adds-on weights.

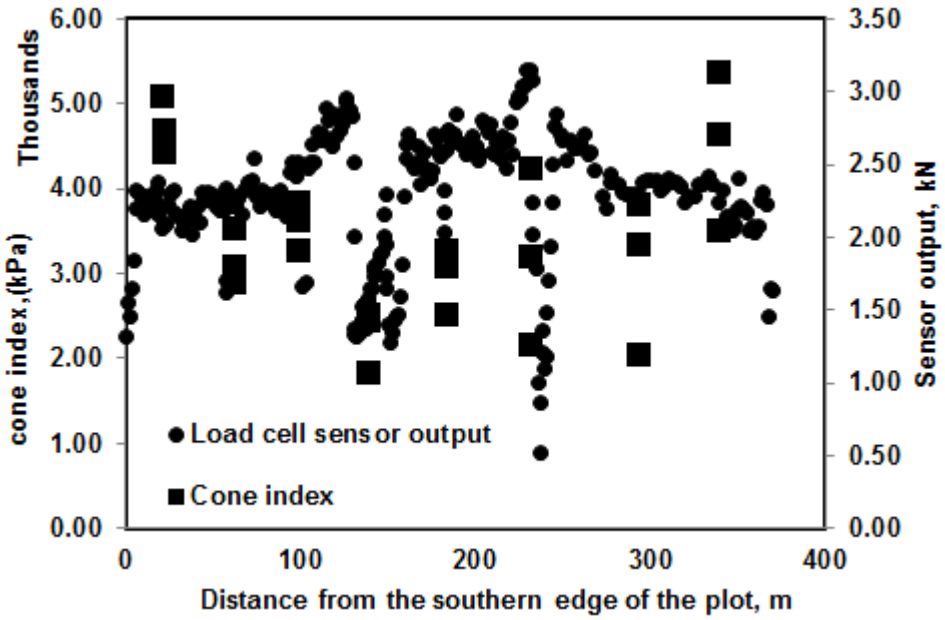

Figure 4-10 : comparison of cone index measurements and load cell sensor output at SCAL, Clay Center, Nebraska.

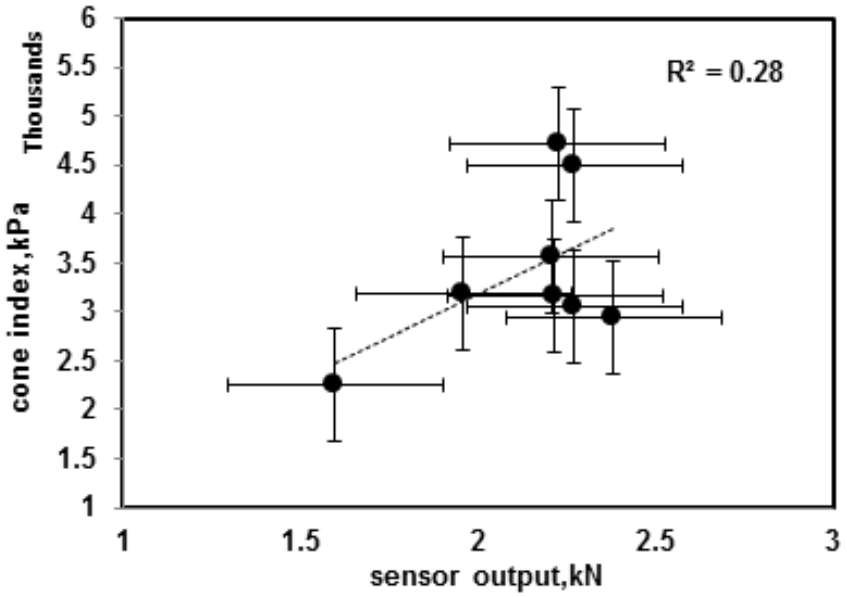

Figure 4-11 : Average and standard deviations for load cell sensor and cone index measurements.

4.4. Soil mapping and sensor fusion

To illustrate simultaneous operation of all sensor components, Figure 4-12 to 4-15 show thematic maps of individual sensor measurements. Since the accuracy of these maps was jeopardized by the relative position of the sensor in the row during mapping, no quantitative analysis among different data layers could be performed. However, it appears that there is a corresponding trend between soil mechanical resistance and soil water content, which also may relate to field elevation (Figure 4-14). Optical reflectance data (NIR + Amber, Figure 4-15) also reveals potential difference in SOM affiliated with different soil types (Figure 3-13).

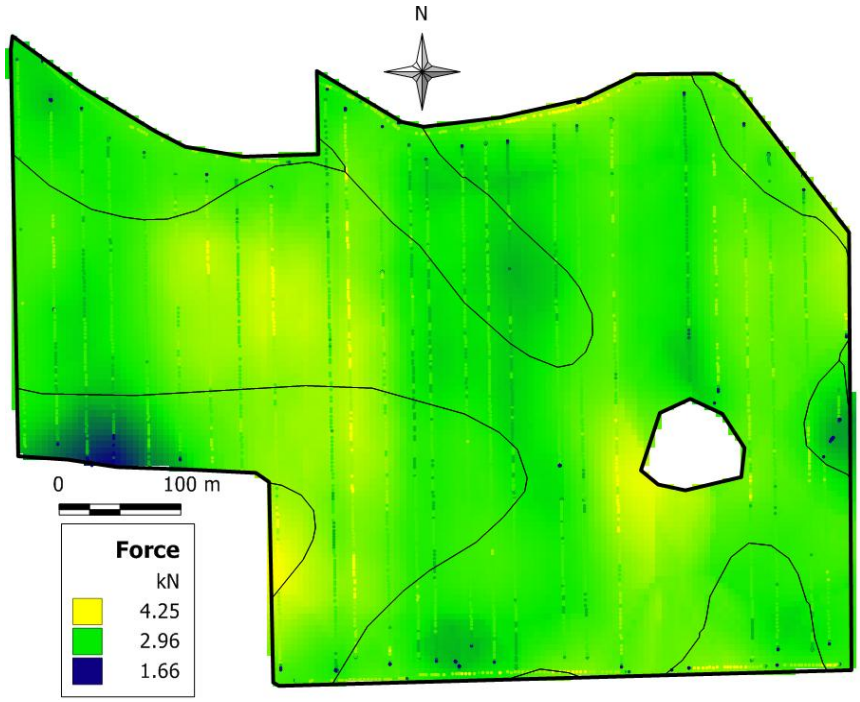

Figure 4-12 : Map of mechanical resistance of soil produced from data collected by the ISMS at Field 1.10, Mead, Nebraska.

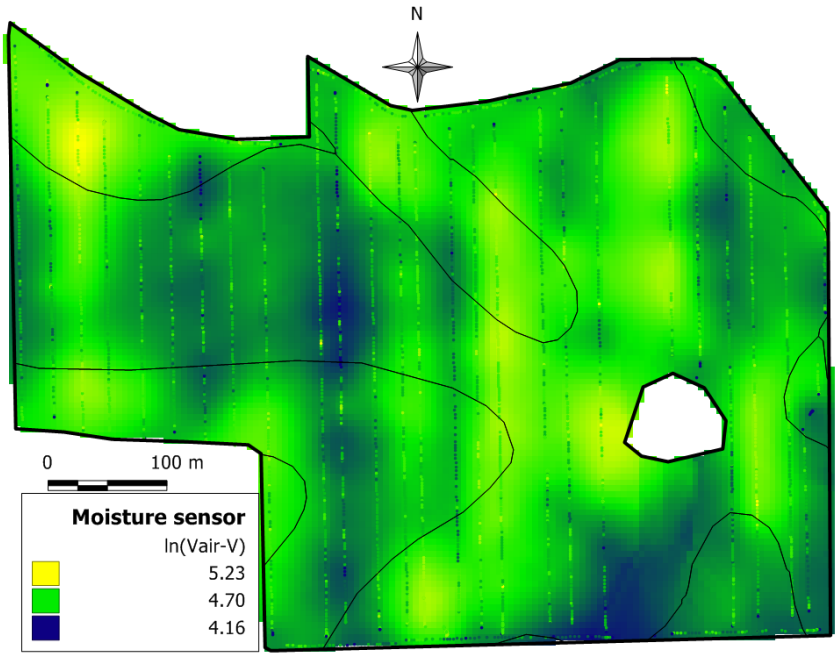

Figure 4-13 : Map of moisture content of soil produced from data collected by the ISMS at Field 1.10, Mead, Nebraska.

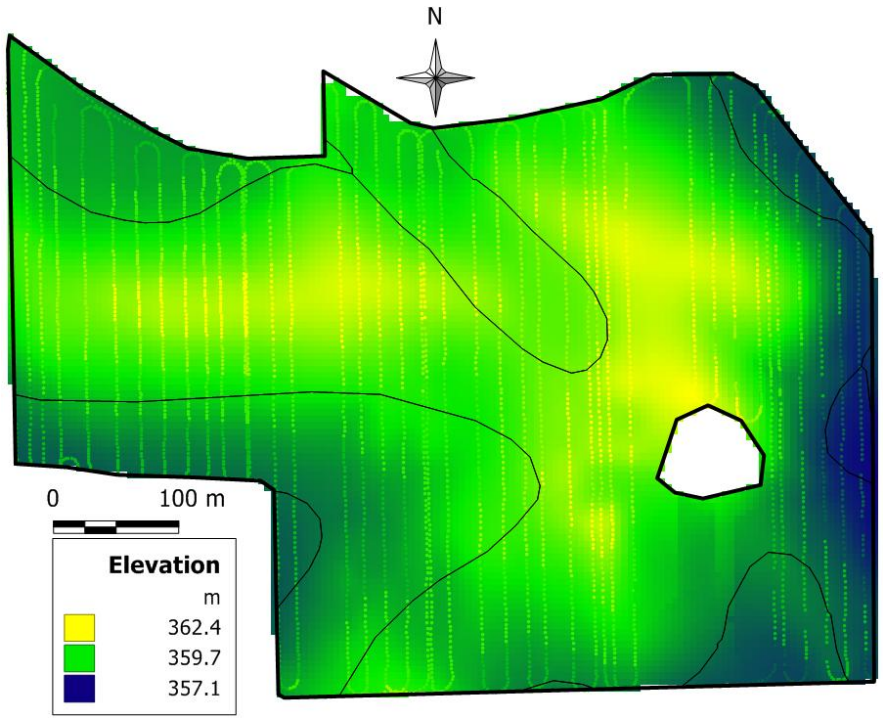

Figure 4-14 : Map of elevation of field at Field 1.10, Mead, Nebraska.

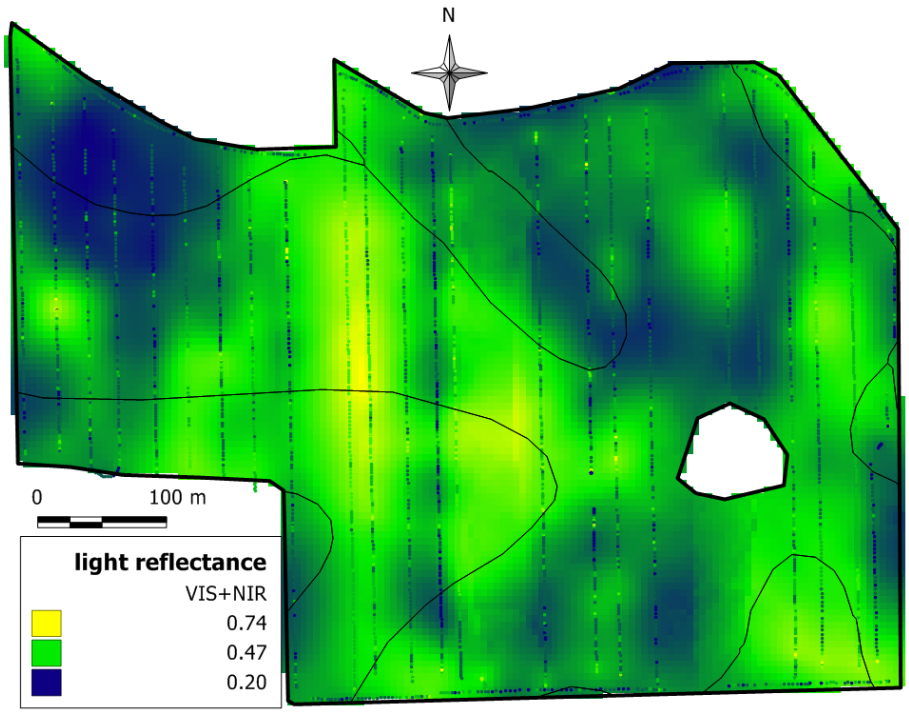

Figure 4-15 : Map of soil index sum produced from data collected by optical sensor (NIR/Amber) mounted on the ISMS at Field 1.10, Mead, Nebraska.

Theoretically, simultaneous data collected from different sensors can be used to predict soil properties with better precision. As soil bulk density can be influenced by soil water content and soil mechanical resistance to penetration, combining information from the capacitance-based moisture senor and the load cell should allow the prediction of soil compaction near the soil surface. Similarly, as soil reflectance can be affected by SOM as well as by SWC, combining the optical and capacitance-based moisture sensors should yield better prediction of SOM under variable moisture conditions. Therefore, the next step of this research is to conduct more comprehensive field studies with extensive spatial variability of soil compaction as well as water and organic matter contents.

5. CONCLUSIONS

An Integrated Soil mapping System (ISMS) was developed and tested to measure soil moisture content, soil organic matter, and soil mechanical resistance on-the-go. A capacitance moisture sensor, optical sensor, and load cell sensor were evaluated and mounted on a platform for acquiring three different data layers simultaneously. Each sensor was calibrated under laboratory conditions and the ISMS was also tested under field conditions. Both the one-sided and two-sided moisture content sensors could reasonable well predict volumetric and gravimetric soil moisture content. Volumetric water content estimated from the two-sided and one-sided sensors was compared with volumetric moisture content measured by the oven-drying method which resulted in an R^2 value of 0.94 for both sensors in laboratory conditions with a standard error of 0.017 cm^3/cm^3 and 0.030 cm^3/cm^3 respectively. Soil index was calculated as the plain sum of individual soil reflectance measurements by the optical sensor in red (660 nm) and blue (480 nm) regions predicted the soil organic matter with R^2 value of 0.73 with standard error of 0.47 OM%. Linear regression of sensor output values and known weights had an R^2 value of 0.99 and standard error of 0.032 kN. The load cell sensor was able to predict hard surfaces in a field with the same standard deviation as a cone penetrometer with R^2 of 0.28 between the average sensor readings and cone index measured by cone penetrometer. ISMS was also successfully tested in a field for mapping soil water content, soil optical reflectance and soil resistance to penetration simultaneously with high sampling density. Future work is needed to study add-on value of using multiple sensors on the same platform is needed. Based on the results of this research more

relatively accurate high-density thematic soil maps are feasible to characterize spatial variability in SWC, SOM and soil compaction. All these data layers can be used to improve the decision making process and enhance sustainability and profitability of a crop production system.

6. REFERENCES

Adamchuk, V.I., J.W. Hummel, M.T. Morgan, and S.K. Upadhyaya. 2004a. On-the-go soil sensors for precision agriculture. *Comp. and Elec. in Agric.* 44: 71-91.

Adamchuk, V. I., M. T. Morgan and J. Lowenberg-DeBoer. 2004b. A Model for Agro-Economic Analysis of Soil pH Mapping. *Precision agriculture* 5:111-129.

Adamchuk, V. I., E. D. Lund,B., Sethuramasamyraja,M.T. Morgan, A. Dobermann, and D.B.Marx. 2005. Direct measurement of soil chemical properties on-the-go using ion-selective electrodes.Computers and Electronics in Agriculture 48(3): 272-294

Adamchuk, V.I., C.R. Hempleman, and D.G. Jahraus. 2009. On-the-go capacitance sensing of soil water content. Paper No. MC09-201. St. Joseph, Michigan: ASABE.

Alexander, J. D. 1969. A color chart of organic matter. *Crops and soils* 21:15-17.

Andrade-Sanchez, P., S. K. Upadhyaya and B. M. Jenkins. 2007. Development, construction, and field evaluation of a soil compaction profile sensor. *Transactions of the ASABE* 50(3): 719-725.

ASAE standards, 2004. S313.3. Soil cone penetrometer. 50th ed., ASAE St. Joseph, MI

Bongiovanni, R., J. Lowenberg-Deboer. 2004. Precision agriculture and sustainability. *Precision agriculture* 5(4):359-387.

Boon, N. E., A. Yahya, A. F. Kheiralla, B. S. Wee and S. K. Gew. 2005. A Tractor-mounted, Automated Soil Penetrometer–shearometer Unit for Mapping Soil Mechanical Properties. *Biosystems Engineering* 90(4): 381-396.

Busscher, W., P. Bauer, C. Ramp, R. sojka. 1997. correction of soil index for soil water content in coastal plain soil. soil and tillage research 43: 205-217.

Christy, C. D. 2008. Real-time measurement of soil attributes using on-the-go near infrared reflectance spectroscopy. *Computers and Electronics in Agriculture* 61(1): 10-19.

Dean, T. J., J. P. Bell and A. J. B. Baty. 1987. Soil moisture measurement by an improved capacitance technique, Part I. Sensor design and performance. *Journal of Hydrology* 93(1-2): 67-78.

Fleige, H. and R. Horn, eds. 2000. *Field experiments of the effect of soil compaction on soil properties, runoff, interflow and erosion.* Reiskirchen, Germany: CATENA VERLAG.

Frazier, B. E., C. S. Walters, E. M. Perry, F. J. Pierce and E. J. Sadler. 1997. The state of Site-Specific Management for agriculture. Madison, Wisconsin: ASA-CSSA_SSSA.

Gorucu, S., A. Khalilian, Y. Han, R. Dodd, F. Wolak and M. Keskin. 2001. Variable depth tillage based on Geo-referenced soil compaction data in coastal plane region of south carolina. *ASAE* meeting presentation Paper Number: 01-1016.

Griffis, C. L. 1985. Electronic sensing of soil organic matter. *Transactions of ASAE* 28:703-705.

Hamza, M. A. and W. K. Anderson. 2005. Soil compaction in cropping systems - A review of nature, causes and possible solutions. *Soil & Tillage Research* 82(2): 121-145.

Hemmat, A., V. I. Adamchuk and P. Jasa. 2008. Use of an instrumented disc coulter for mapping soil mechanical resistance. *Soil & Tillage Research* 98(2): 150-163.

Kitchen, N. R., C. j. Snyder, D. W. Franzen and W. J. Wiebold. 2002. Educational needs of precision agriculture. *Precision agriculture* 3:341-351.

Krishnan, P., J. D. Alexander, B. J. Butler and J. W. Hummel. 1980. Reflectance technique for predicting soil organic matter. *soil science society of america journal* 44(6): 1282-1285.

Lui, W., S. K. Upadhyaya, T. Katakoa and S. Shibusawa. 1996. Development of a texture/soil compaction sensor. *In proceedings of the third international conference on precision agriculture*617-630.

McBratney, A. B. and M. J. Pringle. 1997. *Spatial Variability in soil- implications for precission agriculture.* Oxford, UK: BIOS Scientific publishing.

Merz, B. and A. Bárdossy. 1998. Effects of spatial variability on the rainfall runoff process in a small loess catchment. *Journal of Hydrology* 212-213304-317.

Mouazen, A. M., J. De Baerdemaeker and H. Ramon. 2005. Towards development of on-line soil moisture content sensor using a fibre-type NIR spectrophotometer. *Soil and Tillage Research* 80(1-2): 171-183.

Norris, k. H. 1964. Reports on design and development of a new moisture sensor. *Agriculture Engineering* 45(7): 370-372.

Ostergaard, H.G.S. 1997. Agronomic consequences of variable N fertilization. p. 315–320. *In* J.V. Stafford (ed.) *Precision agriculture* '97. Vol. 1. Spatial variability in soil and crop. Oxford, UK.

Paetzold, R. F., G. A. Matzkanin and A. De Los Santos. 1985. Surface Soil Water Content Measurement Using Pulsed Nuclear Magnetic Resonance Techniques. *soil science society of america journal* 49(3): 537-540.

Pauwels, V. R. N., R. Hoeben, N. E. C. Verhoest and F. P. De Troch. 2001. The importance of the spatial patterns of remotely sensed soil moisture in the improvement of discharge predictions for small-scale basins through data assimilation. *Journal of Hydrology* 251(1-2): 88-102.

Reeves, D. W. 1997. The role of soil organic matter in maintaining soil quality in continuous cropping systems. *Soil and Tillage Research* 43(1-2): 131-167.

Roberts, D. F., V. I. Adamchuk, J. F. Shanahan, R. B. Ferguson and J. S. Schepers. 2010. Estimation of surface soil organic matter using a ground-based active sensor and aerial imagery. *Precision agriculture*.

Schlesinger, W. H., J. F. Reynolds, G. L. Cunningham, L. F. Huenneke, W. M. Jarrell, R. A. Virginia and W. G. Whitford. 1990. Biological feed-backs in global desertification. *Science* 247:1043-1048.

Schulze, D. G., J. L. Nagel, G. E. Van Scoyvoc, T. L. Henderson, M. F. Baumgardner and D. E. Stott. 1993. Significance of organic matter in determining soil colors. *soil science society of america journal*.

Shibusawa, S., M. Z. Li, K. Sakai, A. Sasao, H. Sato, S. Hirako and A. Otomo. 1999. Spectrophotometer for real time Underground soil sensing. *ASAE meeting presentation* paper no. 993030.

Shonk, J. L., L. D. Gaultny, D. G. Schulze and G. E. Van Scoyvoc. 1991. Spectroscopic sensing of soil organic matter. *Transactions of ASAE* 34(5): 1978-1984.

Smith, D. L., C. R. Wormer and J. W. Hummel. 1987. Soil spectral refllectance relationship to organic matter content. *ASAE* paper no. 87-1608.(St. Joseph, MI, ASAE): .

SSSA (soil science society of America), 1996 Glossary of soil science terms. *SSSA*, Madison, WI, USA

Sudduth, K. A. and J. W. Hummel. 1993. Portable, Near-Infrared Spectrophotometer for rapid soil analysis. *ASAE* 36(1): 185-193.

Swinton, S. M. and J. Lowenberg-DeBoer. 1998. Evaluating the profitability of Site-Specific farming. *journal of production agriculture* 11(4): 439-446.

Topp, G. C. 1993. *soil water content.* Boca Raton,Florida: Lewis publishers.

Weihermüller, L., J. A. Huisman, S. Lambot, M. Herbst and H. Vereecken. 2007. Mapping the spatial variation of soil water content at the field scale with different ground penetrating radar techniques. *Journal of Hydrology* 340(3-4): 205-216.

Whalley, W. R., T. J. Dean and P. Izzard. 1992. Evaluation of the capacitance technique as a method for dynamically measuring soil water content. *Journal of Agricultural Engineering Research* 52:147-155.

Wood, E. F. 1997. Effects of soil moisture aggregation on surface evaporative fluxes. *Journal of Hydrology* 190(3-4): 397-412.

Yurui, S., P. S. Lammers, M. Daokun, L. Jianhui and Z. Qingmeng. 2008. Determining soil physical properties by multi-sensor technique. *Sensors and Actuators A: Physical* 147(1): 352-357.

APPENDIX A

Engineering Drawings of Load cell sensor assembly:

ITEM NO.	PART NUMBER	QTY.
1	2inch hollow bar	1
2	pickUp receiver	1
3	2-inch solid bar	1
4	tounge	1
5	loadcell plate	1
6	load cell	1
7	pin	2
8	threshold bolt	2
9	spacer	2
10	supporting plates	2
11	stopper	1
12	Hitch-ball	1
13	nut	4
14	stopper bolt	1
15	bolts	4

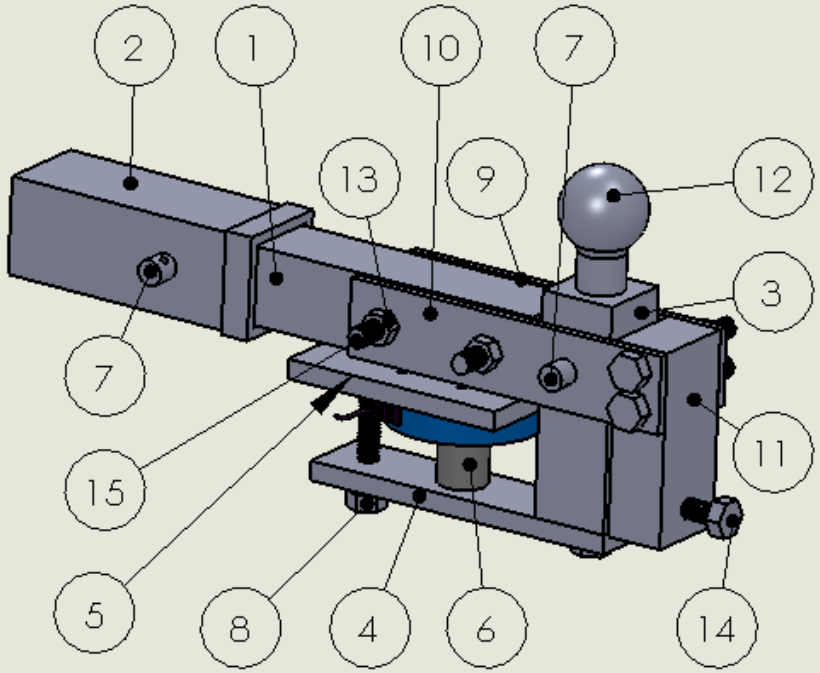

UNLESS OTHERWISE SPECIFIED: DIMENSIONS ARE IN MM TOLERANCES: ±0.001		NAME	DATE	TITLE Load cell sensor assembly
	DRAWN			
	CHECKED			
MATERIAL	SHEET 1 OF 1	SCALE: 1:10		DWG. NO.

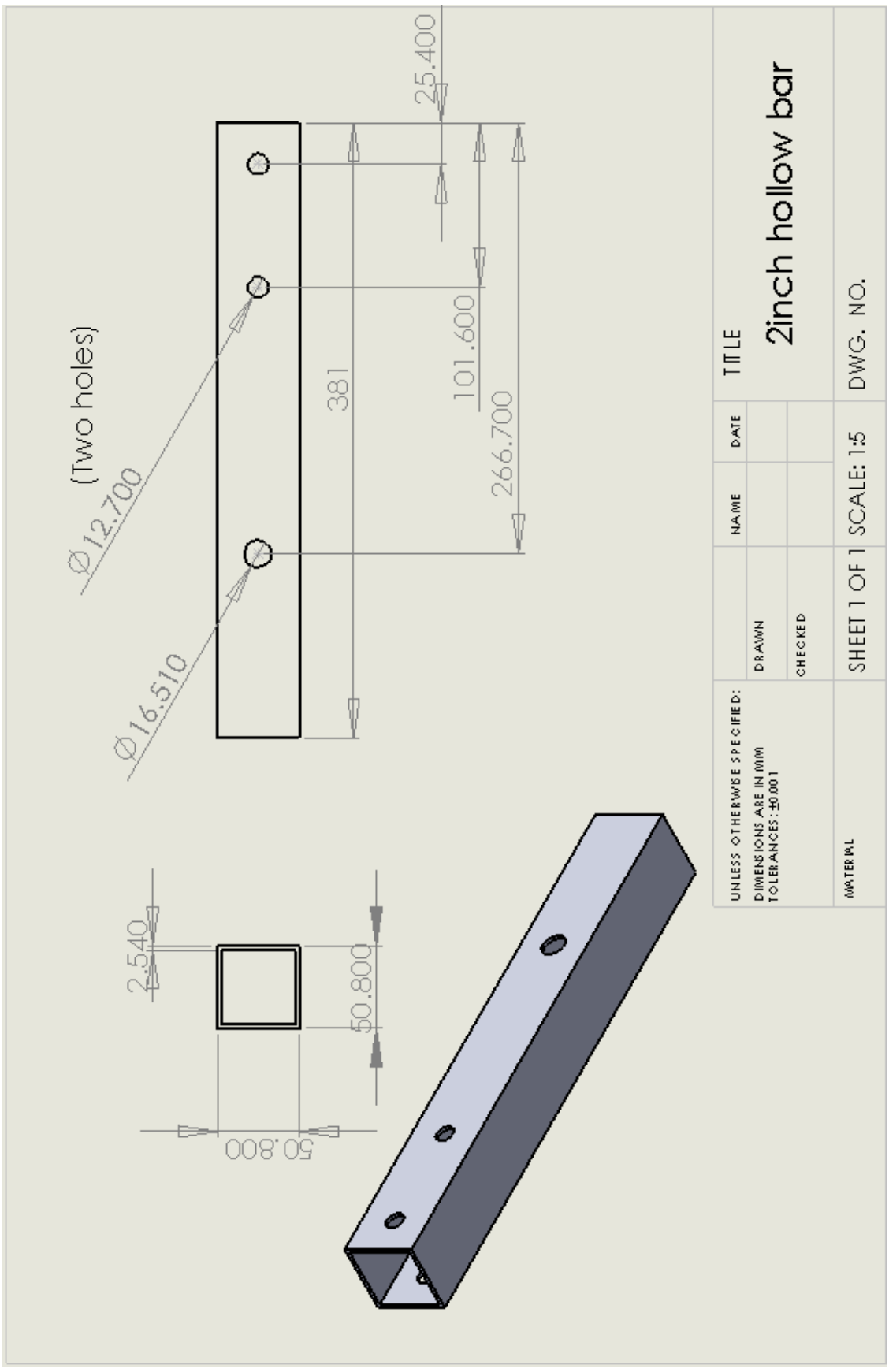
(Two holes)
Ø12.700
Ø16.510
25.400
381
101.600
266.700
2.540
50.800
50.800
UNLESS OTHERWISE SPECIFIED:
DIMENSIONS ARE IN MM
TOLERANCES: ±0.001
DRAWN
CHECKED
NAME
DATE
TITLE
2inch hollow bar
MATERIAL
SHEET 1 OF 1
SCALE: 1:5
DWG. NO.

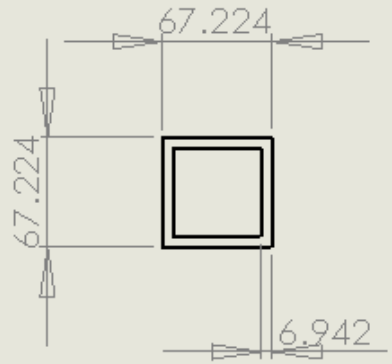

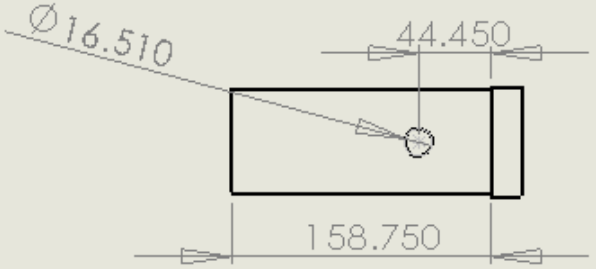

Sheet1

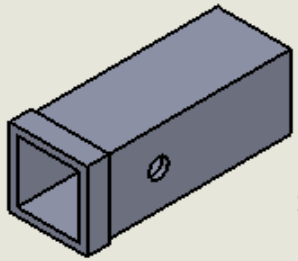

Standard pickUp receiver

UNLESS OTHERWISE SPECIFIED: DIMENSIONS ARE IN MM TOLERANCES: ±0.001		NAME	DATE	TITLE pickUp receiver
	DRAWN			
	CHECKED			
MATERIAL	SHEET 1 OF 1	SCALE: 1:5		DWG. NO.

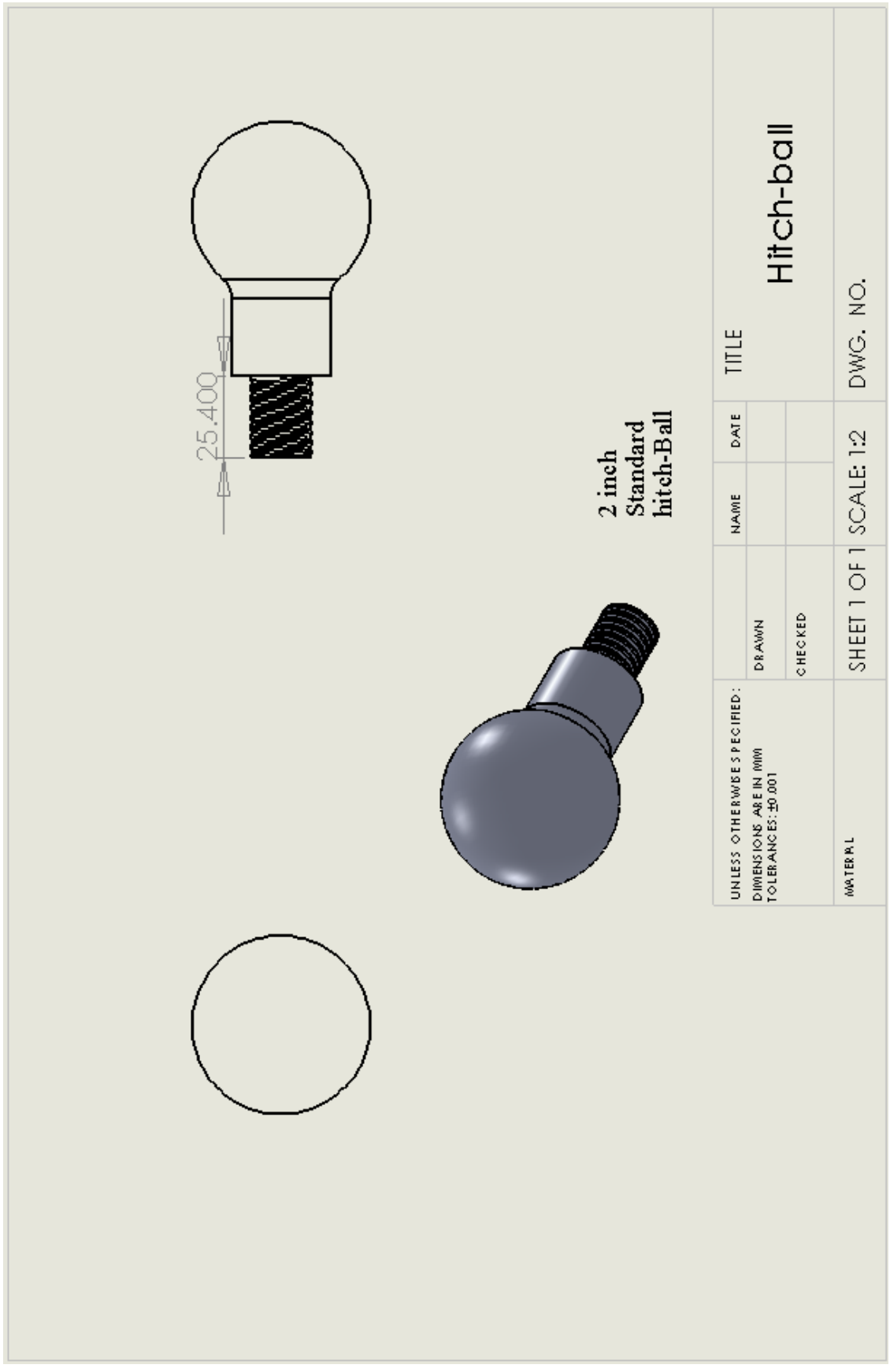
25.400
2 inch
Standard
hitch-Ball
UNLESS OTHERWISE SPECIFIED:
DIMENSIONS ARE IN MM
TOLERANCES: ±0.001
DRAWN
CHECKED
NAME
DATE
TITLE
Hitch-ball
MATERIAL
SHEET 1 OF 1
SCALE: 1:2
DWG. NO.

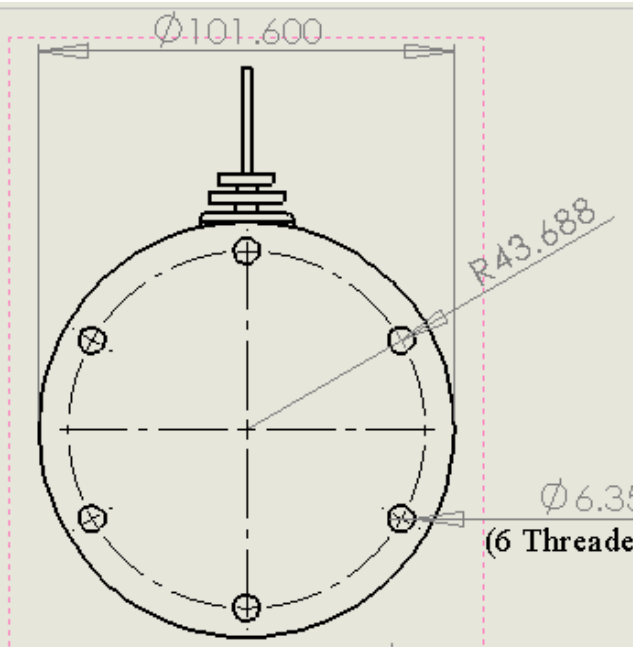

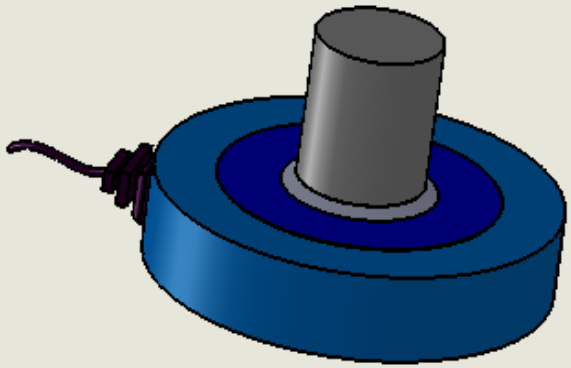

load cell model no. PUF-10K-050-S
(Loadstar sensors, inc. Fermont, CA)

UNLESS OTHERWISE SPECIFIED: DIMENSIONS ARE IN MM TOLERANCES: ±0.001		NAME	DATE	TITLE load cell
	DRAWN			
	CHECKED			
MATERIAL	SHEET 1 OF 1	SCALE: 1:2		DWG. NO.

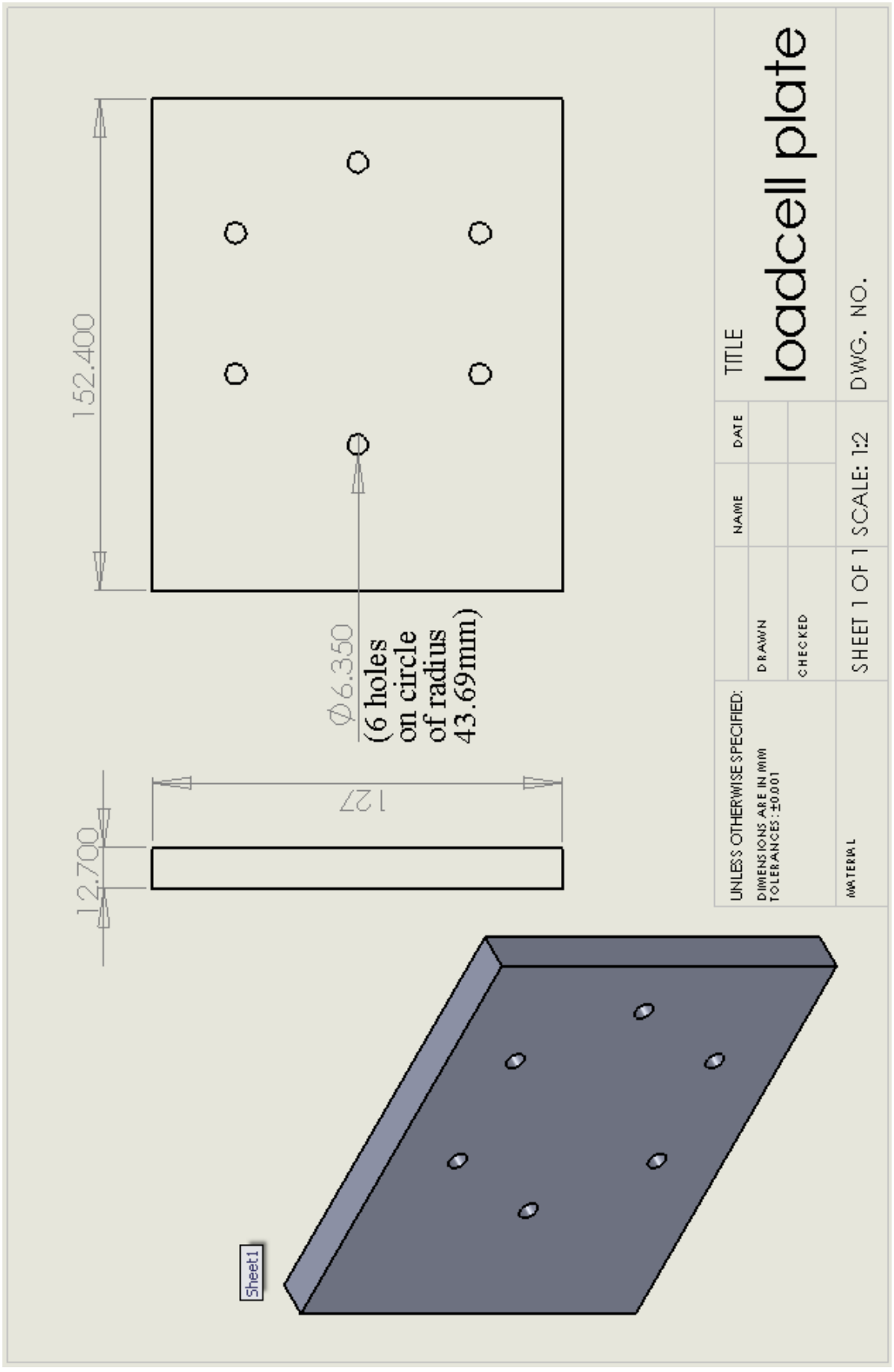
152.400
Ø6.350
(6 holes
on circle
of radius
43.69mm)
127
12.700
Sheet1
UNLESS OTHERWISE SPECIFIED:
DIMENSIONS ARE IN MM
TOLERANCES: ±0.001
DRAWN
CHECKED
NAME
DATE
TITLE
loadcell plate
MATERIAL
SHEET 1 OF 1
SCALE: 1:2
DWG. NO.

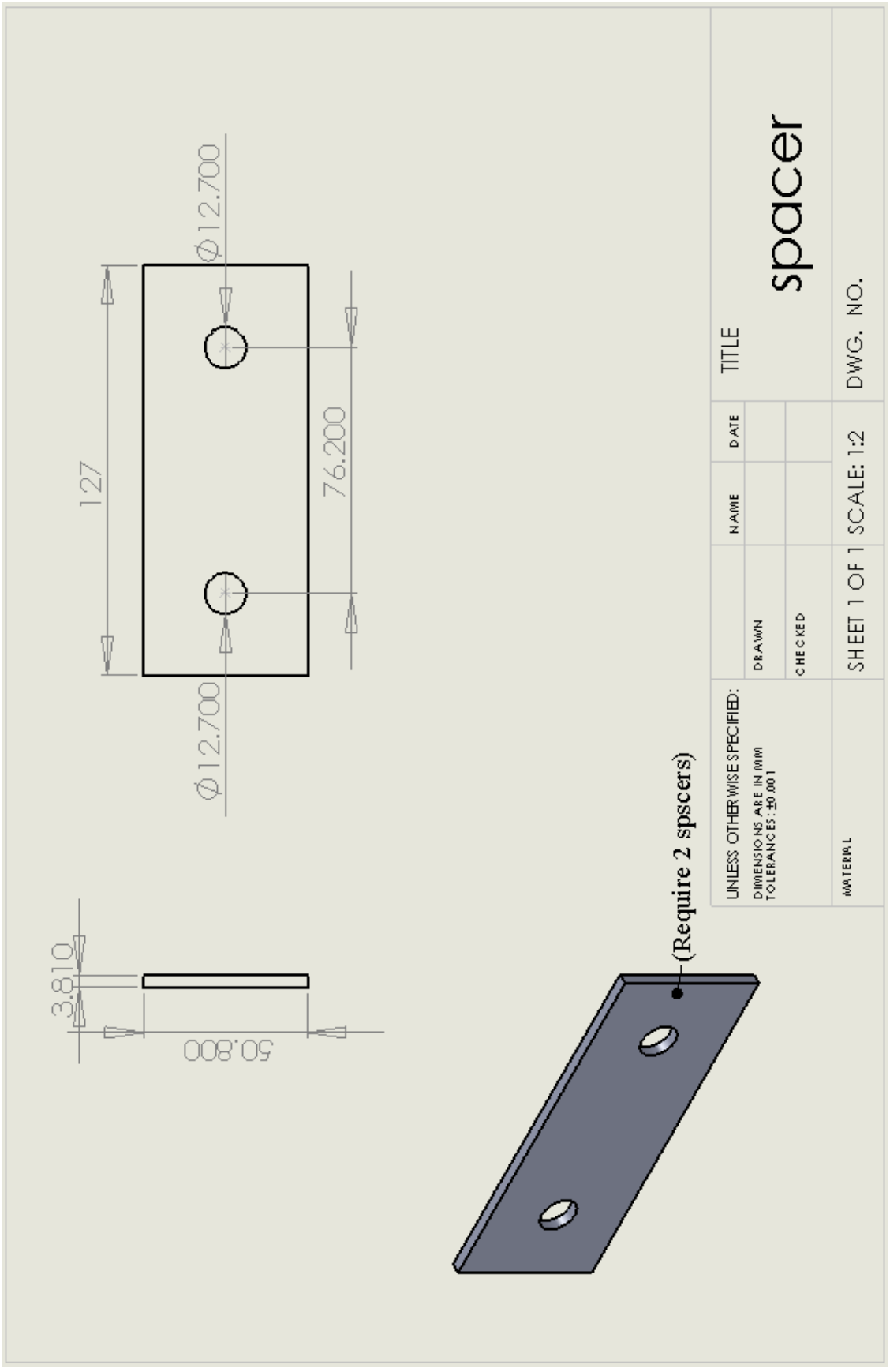
Ø12.700
127
76.200
Ø12.700
3.810
50.800
(Require 2 spscers)
UNLESS OTHERWISE SPECIFIED:
DIMENSIONS ARE IN MM
TOLERANCES: ±0.001
DRAWN
CHECKED
NAME
DATE
TITLE
spacer
MATERIAL
SHEET 1 OF 1
SCALE: 1:2
DWG. NO.

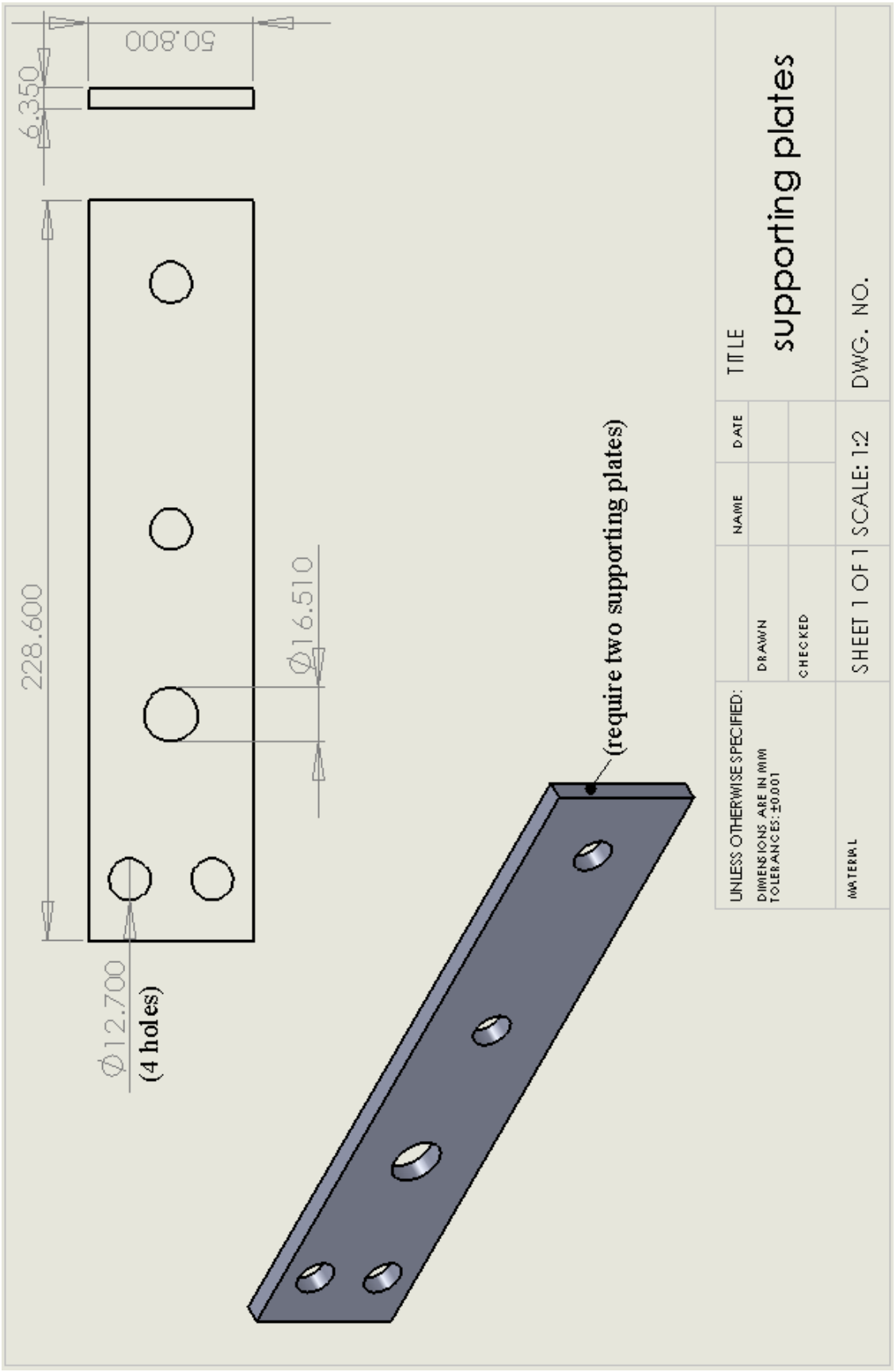
50.800
6.350
228.600
Ø16.510
Ø12.700
(4 holes)
(require two supporting plates)
UNLESS OTHERWISE SPECIFIED:
DIMENSIONS ARE IN MM
TOLERANCES: ±0.001
DRAWN
CHECKED
NAME
DATE
TITLE
supporting plates
MATERIAL
SHEET 1 OF 1
SCALE: 1:2
DWG. NO.

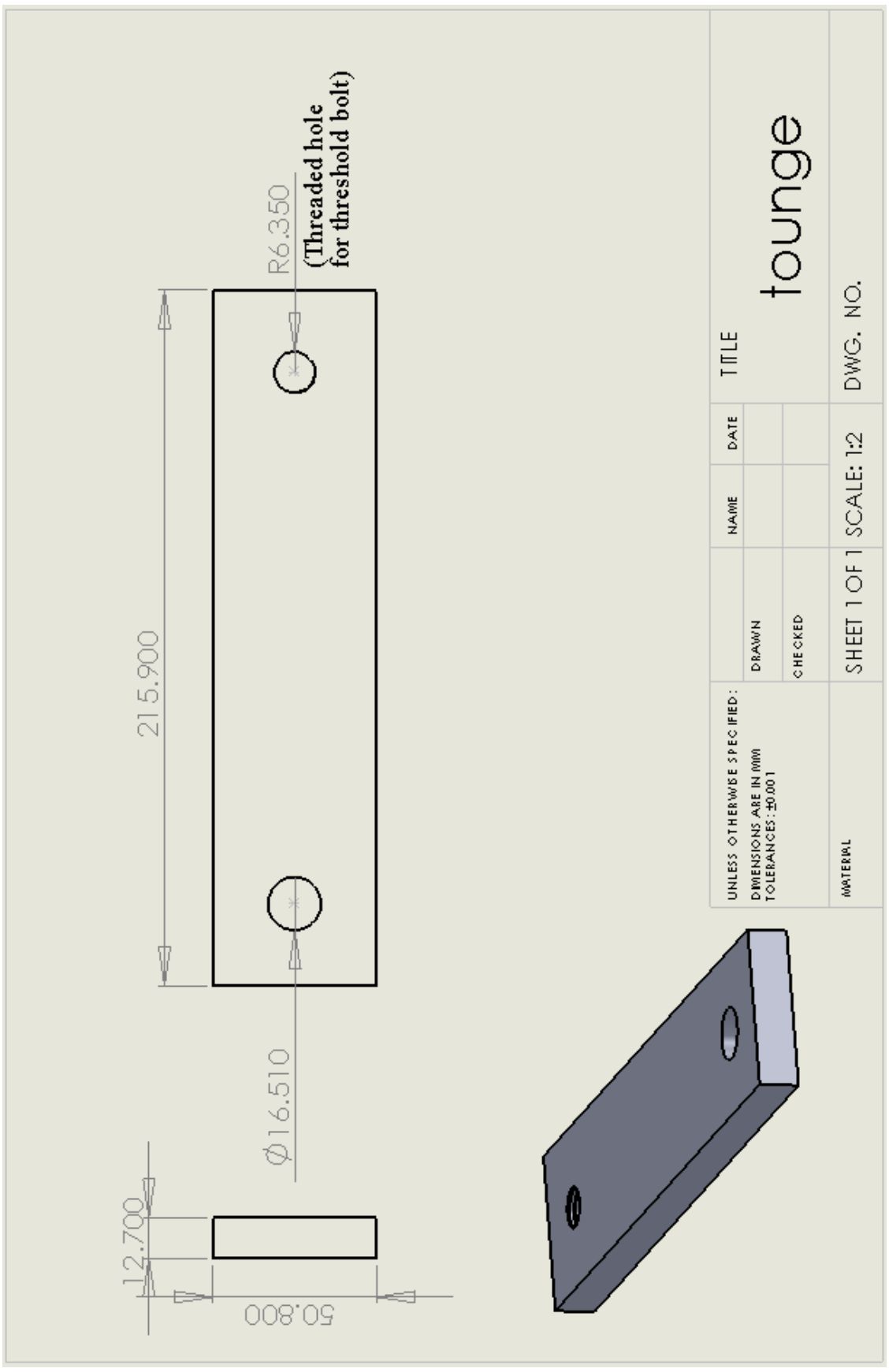
R6.350
(Threaded hole
for threshold bolt)
215.900
Ø16.510
12.700
50.800
UNLESS OTHERWISE SPECIFIED:
DIMENSIONS ARE IN mm
TOLERANCES: ±0.001
NAME
DATE
DRAWN
CHECKED
TITLE
tounge
MATERIAL
SHEET 1 OF 1
SCALE: 1:2
DWG. NO.

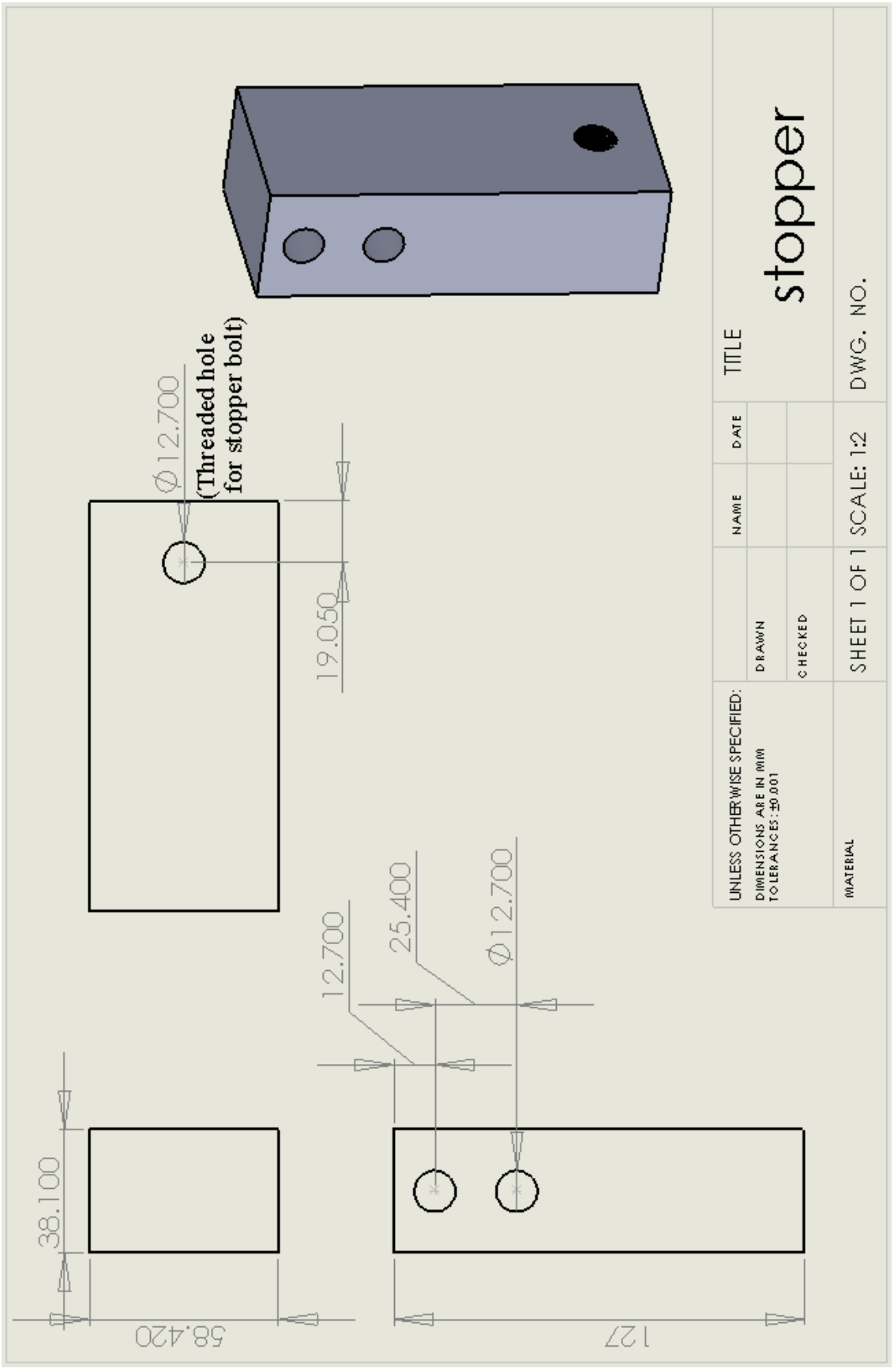
stopper
TITLE
DWG. NO.
SCALE: 1:2
SHEET 1 OF 1
MATERIAL
UNLESS OTHERWISE SPECIFIED:
DIMENSIONS ARE IN MM
TOLERANCES: ±0.001
DRAWN
CHECKED
NAME
DATE
Ø12.700
(Threaded hole
for stopper bolt)
19.050
12.700
25.400
Ø12.700
38.100
58.420
127

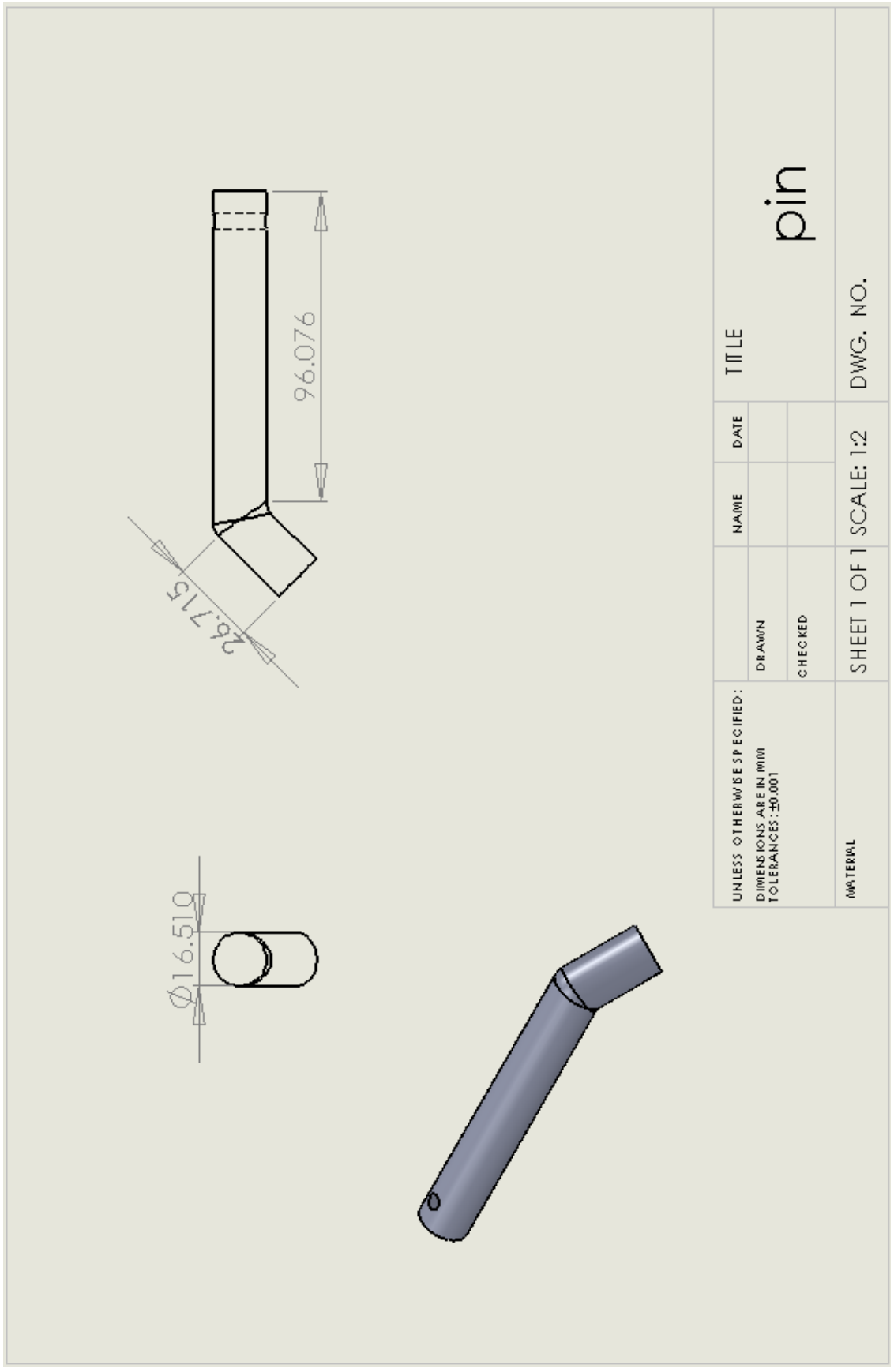
96.076
26.715
Ø16.510
UNLESS OTHERWISE SPECIFIED:
DIMENSIONS ARE IN MM
TOLERANCES: ±0.001
DRAWN
CHECKED
NAME
DATE
TITLE
pin
MATERIAL
SHEET 1 OF 1
SCALE: 1:2
DWG. NO.

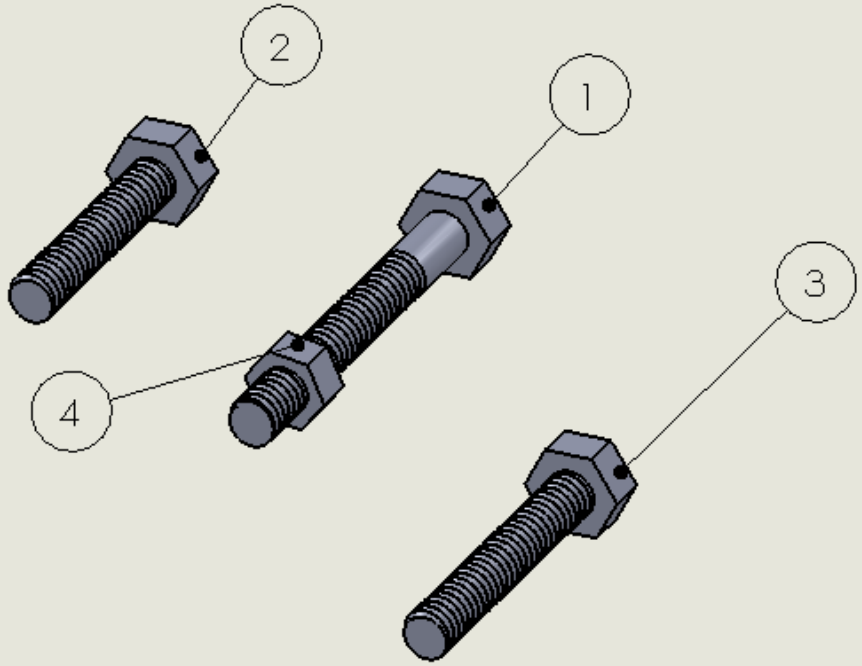

1. 4 bolts (dia. 12.7 mm)
2. stopper bolt (dia. 12.7 mm)
3. threshold bolt (dia. 12.7 mm)
4. 4 nuts

UNLESS OTHERWISE SPECIFIED: DIMENSIONS ARE IN MM TOLERANCES: ±0.001		NAME	DATE	TITLE nuts and bolts
	DRAWN			
	CHECKED			
MATERIAL	SHEET 1 OF 1	SCALE: 1:2		DWG. NO.

ITEM NO.	PART NUMBER	QTY.
1	fertilizer knife	1
2	bracket for optical sensor	1
3	Optical sensor base	1
4	moisture sensor	1
5	Bracket for moisture sensor	1
6	counter sunk screw	9

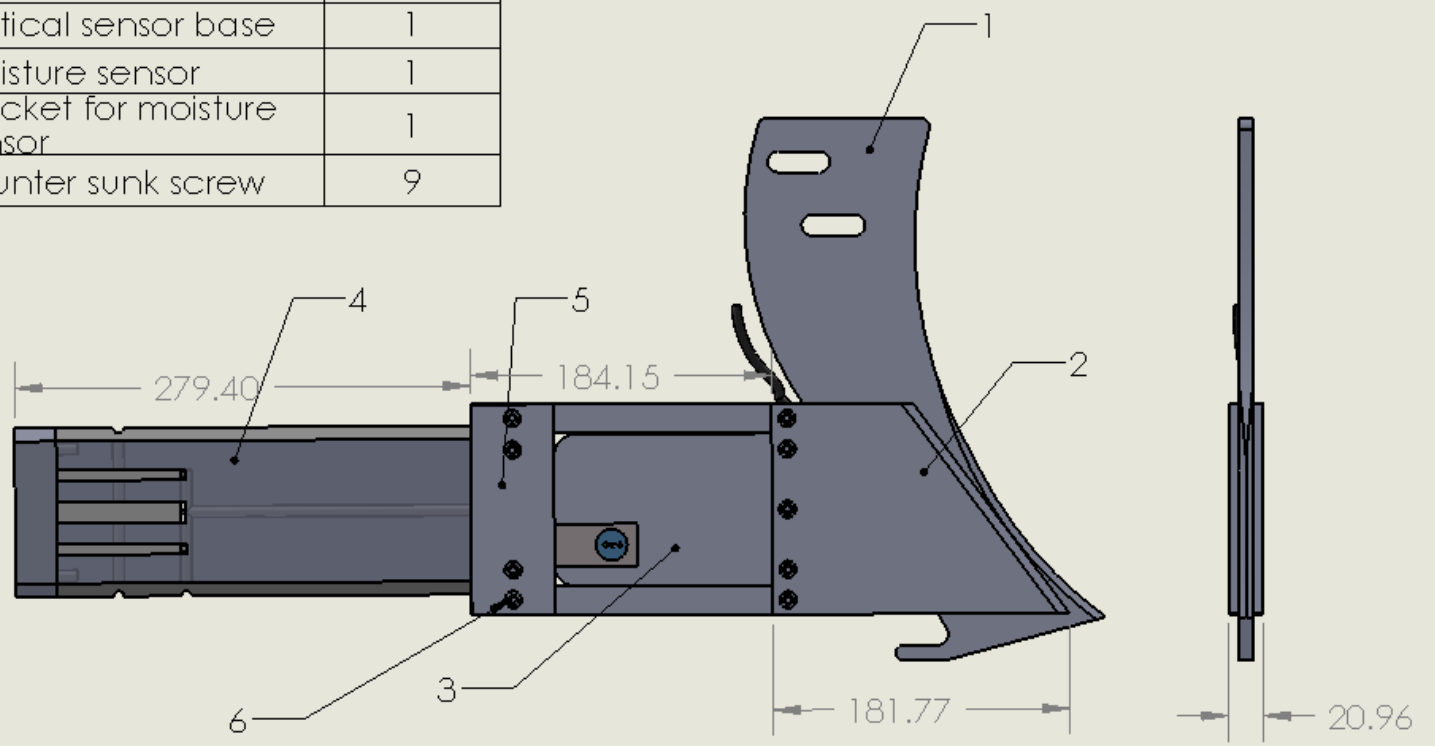

UNLESS OTHERWISE SPECIFIED:		NAME	DATE	TITLE
DIMENSIONS ARE IN INCHES TOLERANCES:	DRAWN			Bracket
	CHECKED			
MATERIAL	SHEET 1 OF 1	SCALE: 1:5		DWG. NO.

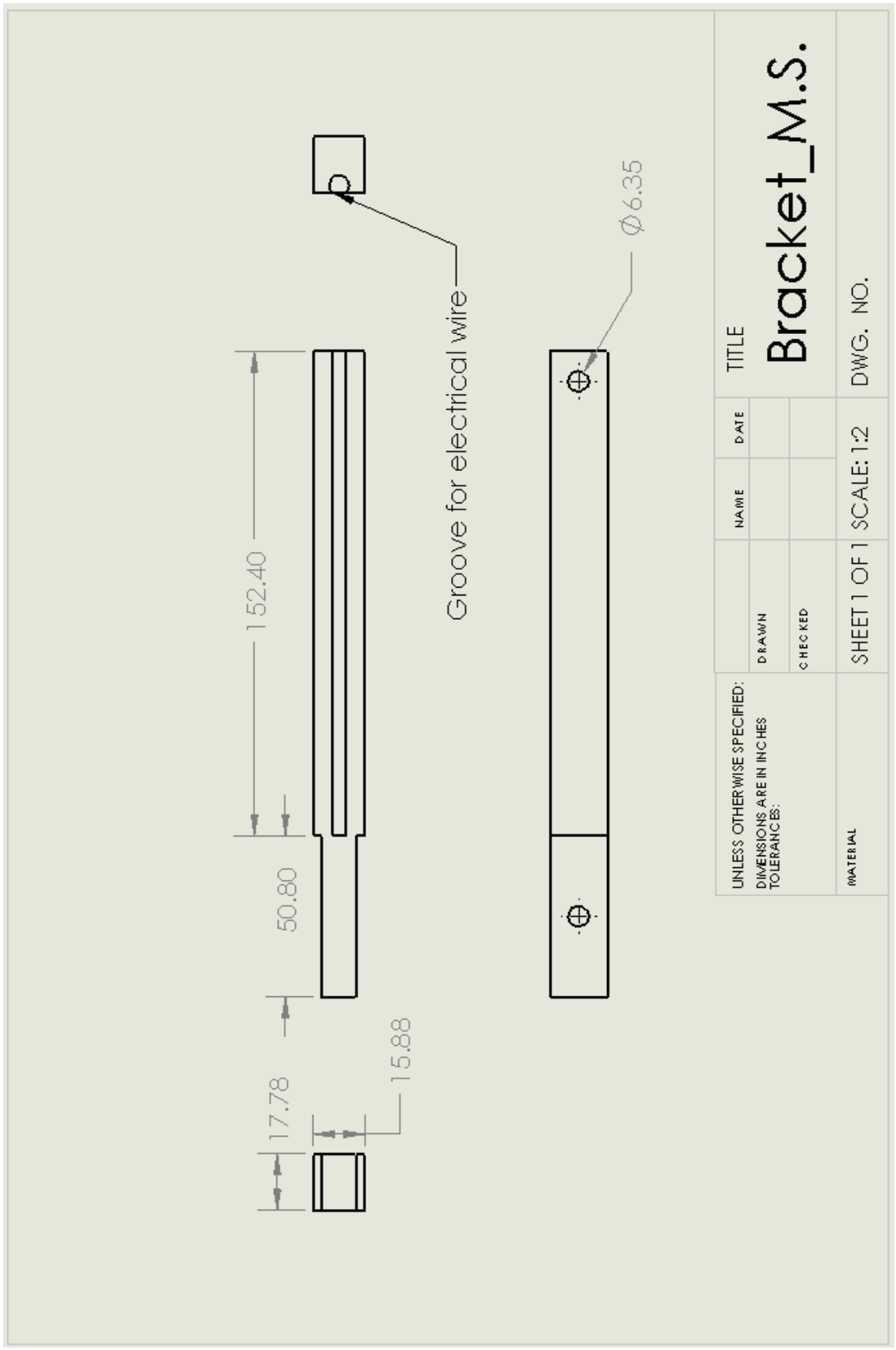
Groove for electrical wire
152.40
50.80
15.88
17.78
Ø6.35
UNLESS OTHERWISE SPECIFIED:
DIMENSIONS ARE IN INCHES
TOLERANCES:
DRAWN
CHECKED
NAME
DATE
TITLE
Bracket_M.S.
MATERIAL
SHEET 1 OF 1
SCALE: 1:2
DWG. NO.

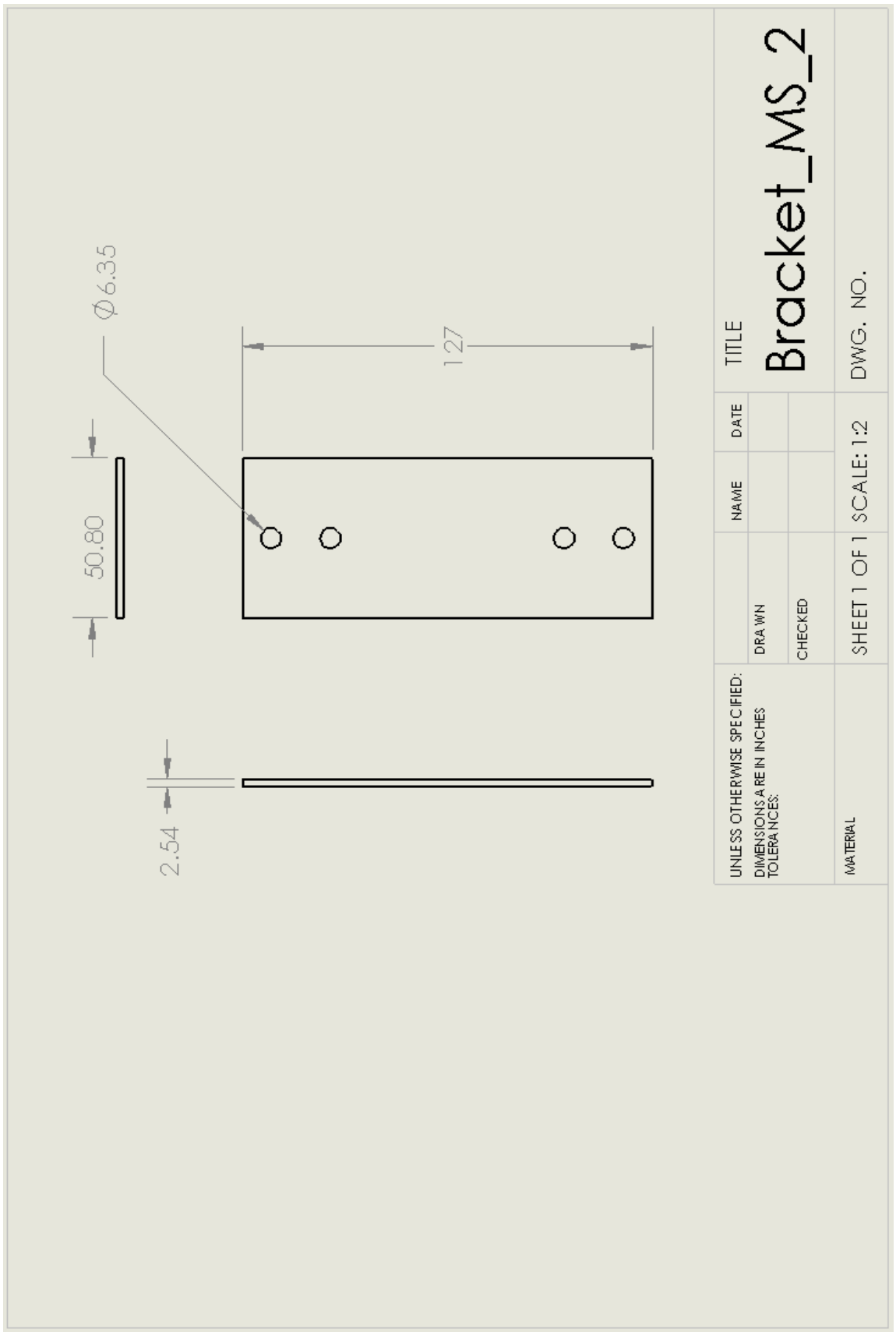
Ø6.35
50.80
127
2.54
UNLESS OTHERWISE SPECIFIED:
DIMENSIONS ARE IN INCHES
TOLERANCES:
DRAWN
CHECKED
NAME
DATE
TITLE
Bracket_MS_2
MATERIAL
SHEET 1 OF 1
SCALE: 1:2
DWG. NO.

APPENDIX B

Engineering drawings of bracket for optical sensor:

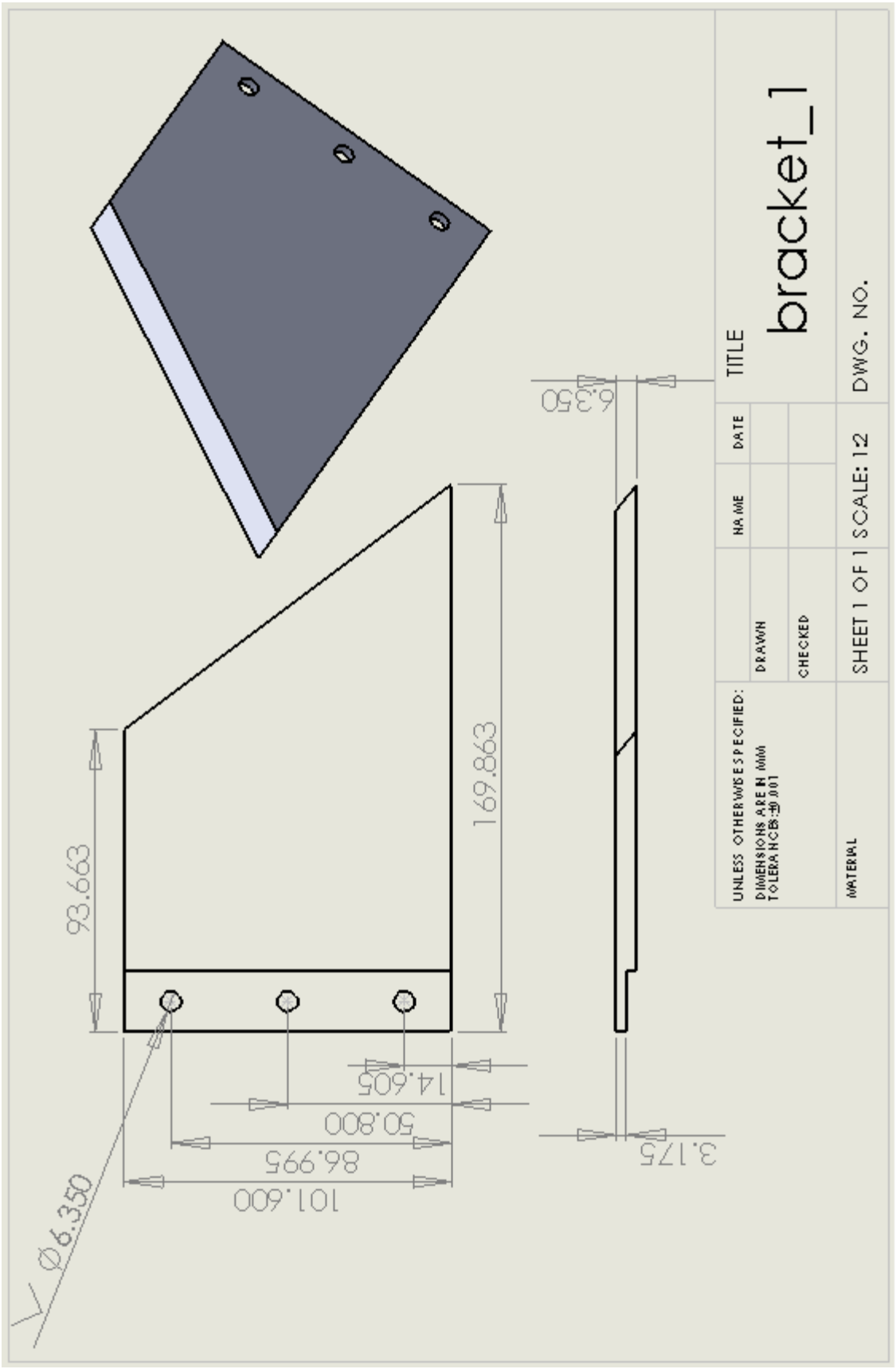
bracket_1
TITLE
DWG. NO.
SCALE: 1:2
SHEET 1 OF 1
MATERIAL
UNLESS OTHERWISE SPECIFIED:
DIMENSIONS ARE IN MM
TOLERANCES: ±0.001
DRAWN
CHECKED
NAME
DATE
93.663
169.863
6.350
14.605
50.800
86.995
101.600
Ø6.350
3.175

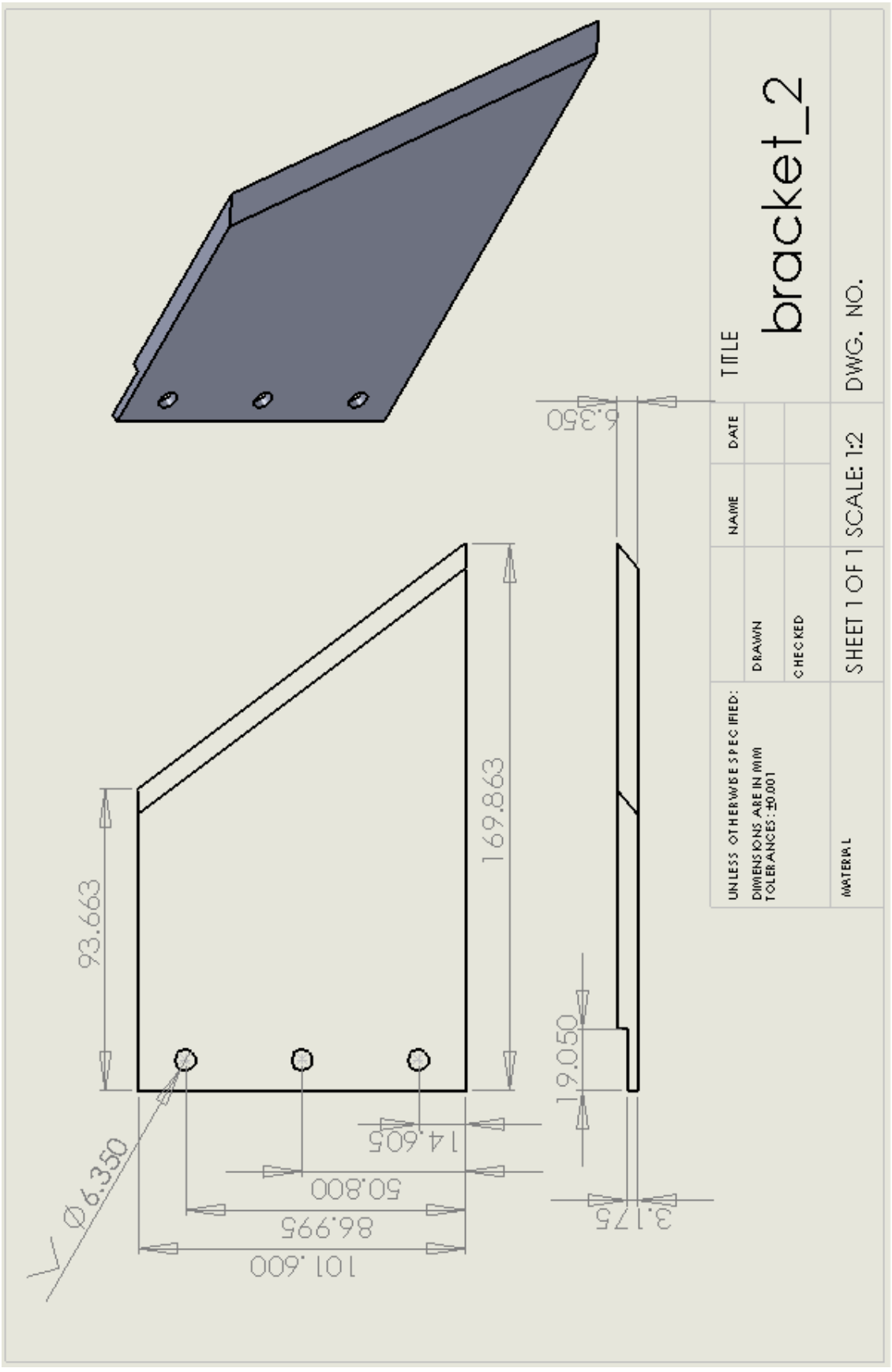
bracket_2
TITLE
DWG. NO.
SCALE: 1:2
SHEET 1 OF 1
MATERIAL
UNLESS OTHERWISE SPECIFIED:
DIMENSIONS ARE IN MM
TOLERANCES: ±0.001
DRAWN
CHECKED
NAME
DATE
93.663
169.863
6.350
19.050
3.175
14.605
50.800
86.995
101.600
Ø6.350

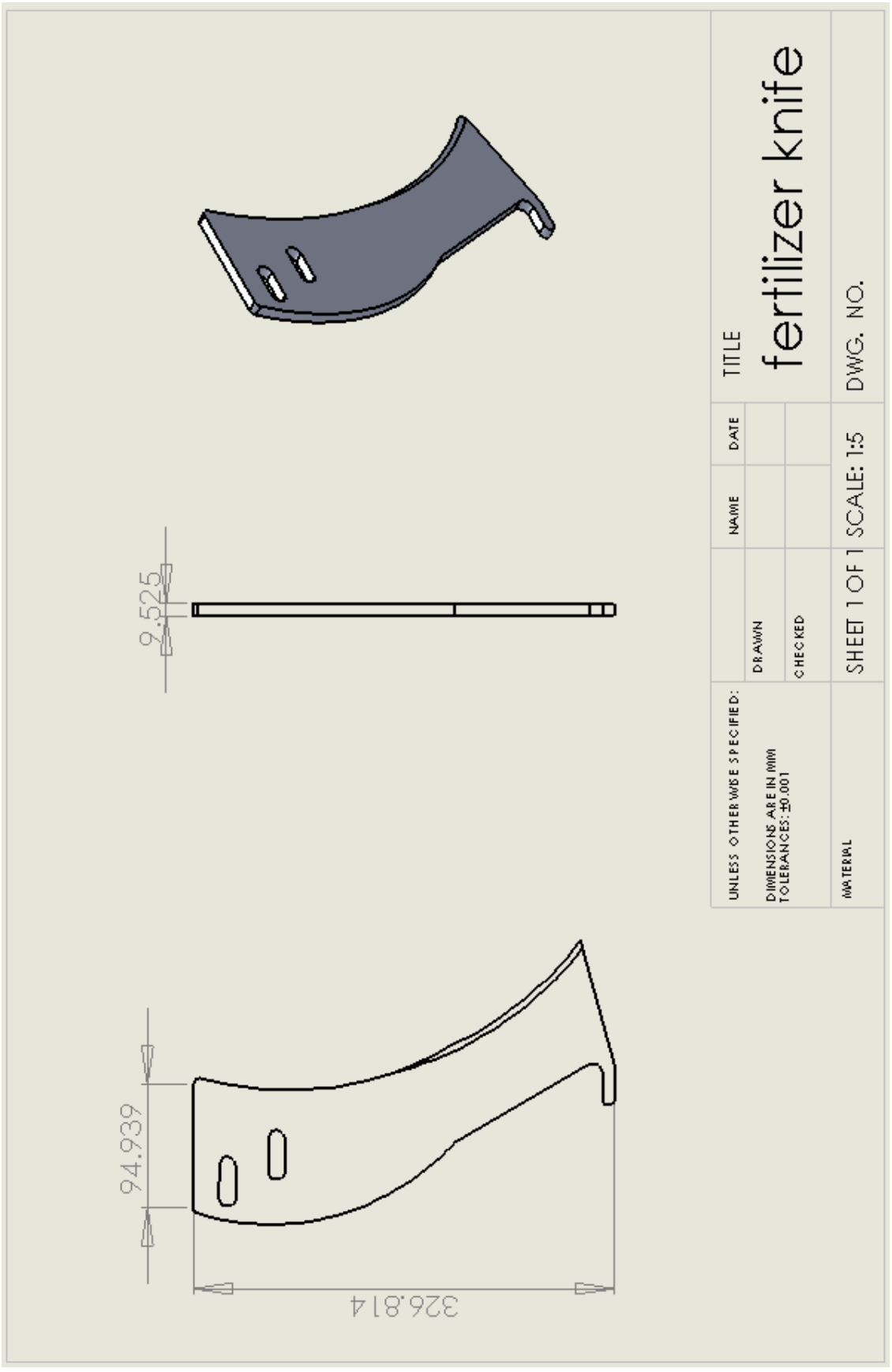
94.939
326.814
9.525
UNLESS OTHERWISE SPECIFIED:
DIMENSIONS ARE IN MM
TOLERANCES: ±0.001
MATERIAL
DRAWN
CHECKED
NAME
DATE
TITLE
fertilizer knife
SHEET 1 OF 1
SCALE: 1:5
DWG. NO.

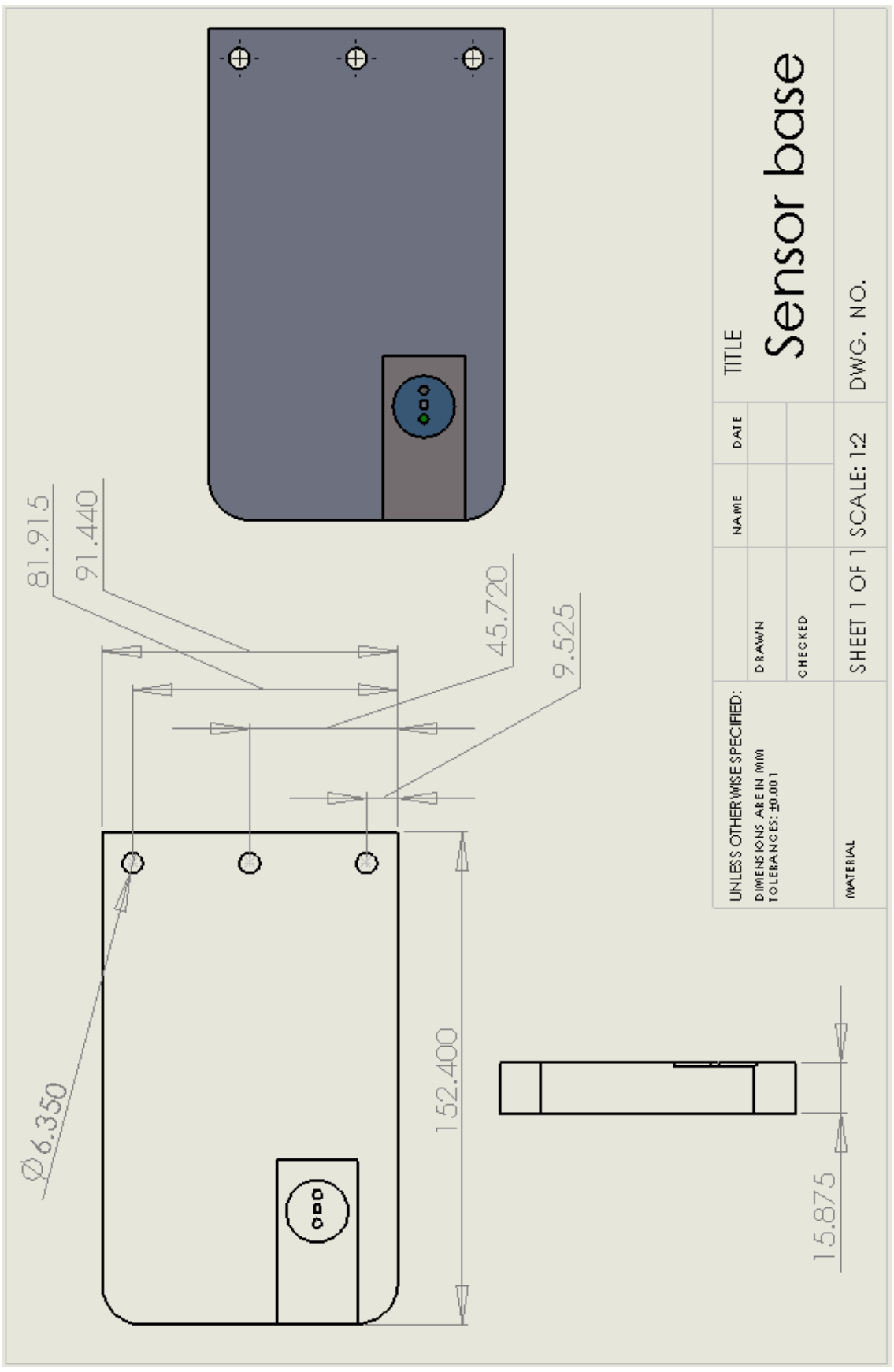
81.915
91.440
45.720
9.525
Ø6.350
152.400
15.875
UNLESS OTHERWISE SPECIFIED:
DIMENSIONS ARE IN MM
TOLERANCES: ±0.001
DRAWN
CHECKED
NAME
DATE
TITLE
Sensor base
MATERIAL
SHEET 1 OF 1
SCALE: 1:2
DWG. NO.

APPENDIX C

Engineering drawings of Two-side sensing capacitance based moisture sensor and Bracket designed to hold this sensor:

ITEM NO.	PART NUMBER	QTY.
1	teflon plate	1
2	electrode_2	2
3	electrode_1	1
4	teflon plate end	1
5	electrode support	1
6	plastic bolts	2

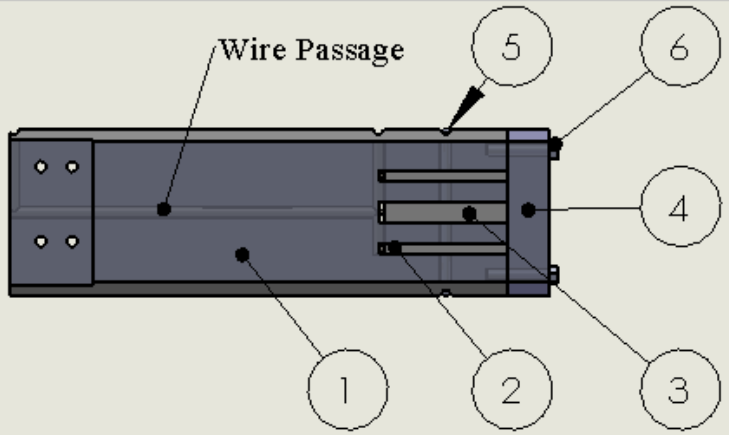

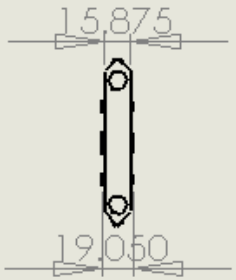

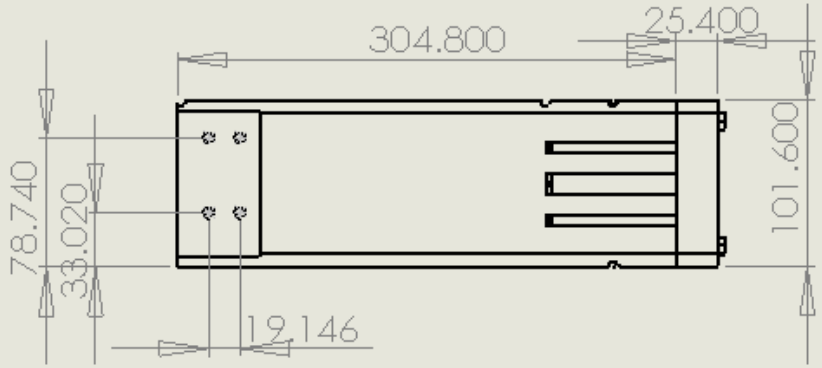

UNLESS OTHERWISE SPECIFIED:		NAME	DATE	TITLE
DIMENSIONS ARE IN MM TOLERANCES: ±0.001	DRAWN			capacitance based sensor
	CHECKED			
MATERIAL	SHEET 1 OF 1	SCALE: 1:5		DWG. NO.

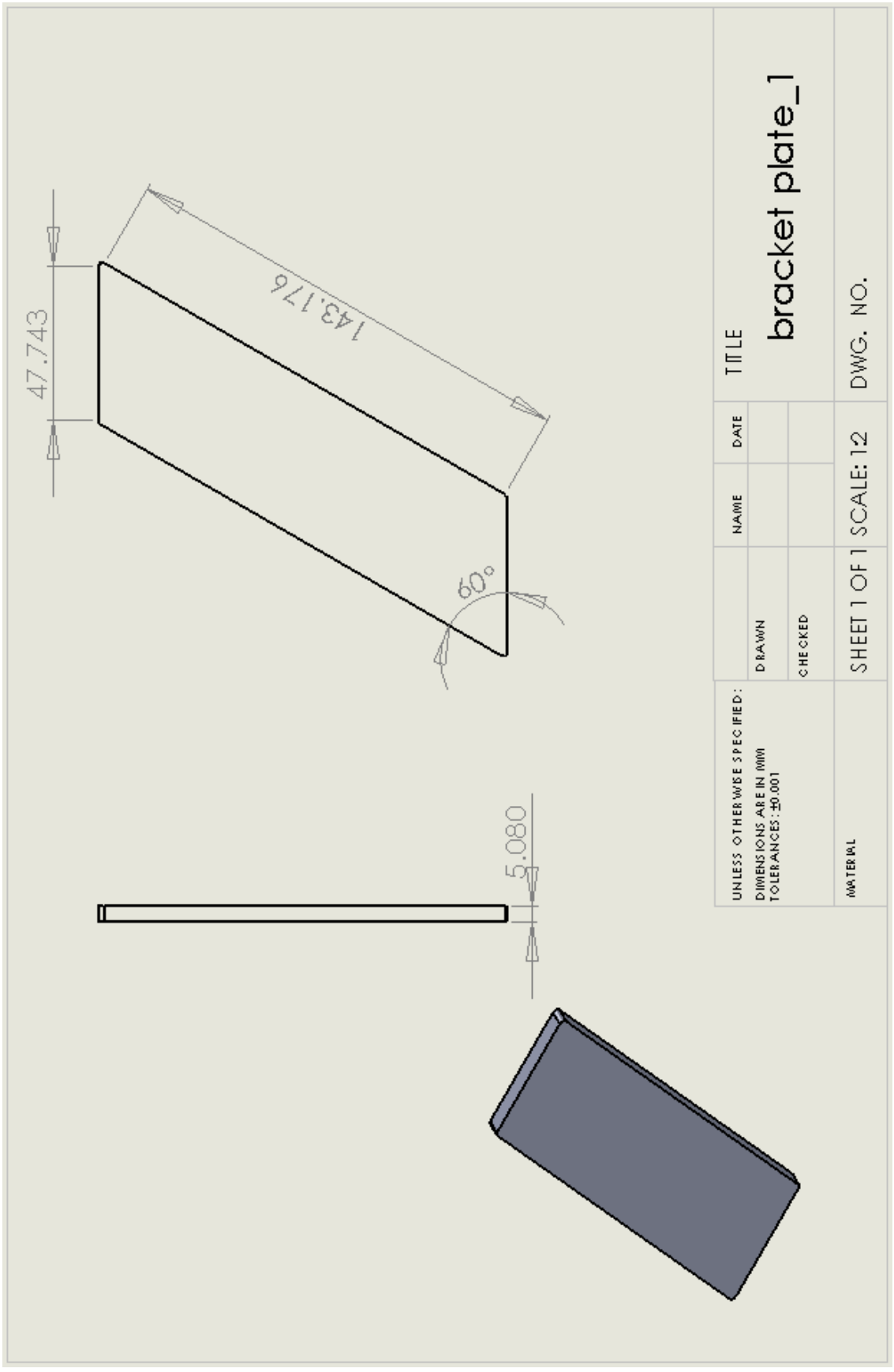
47.743
143.176
60°
5.080
UNLESS OTHER WISE SPECIFIED:
DIMENSIONS ARE IN mm
TOLERANCES: ±0.001
DRAWN
CHECKED
NAME
DATE
TITLE
bracket plate_1
MATERIAL
SHEET 1 OF 1
SCALE: 12
DWG. NO.

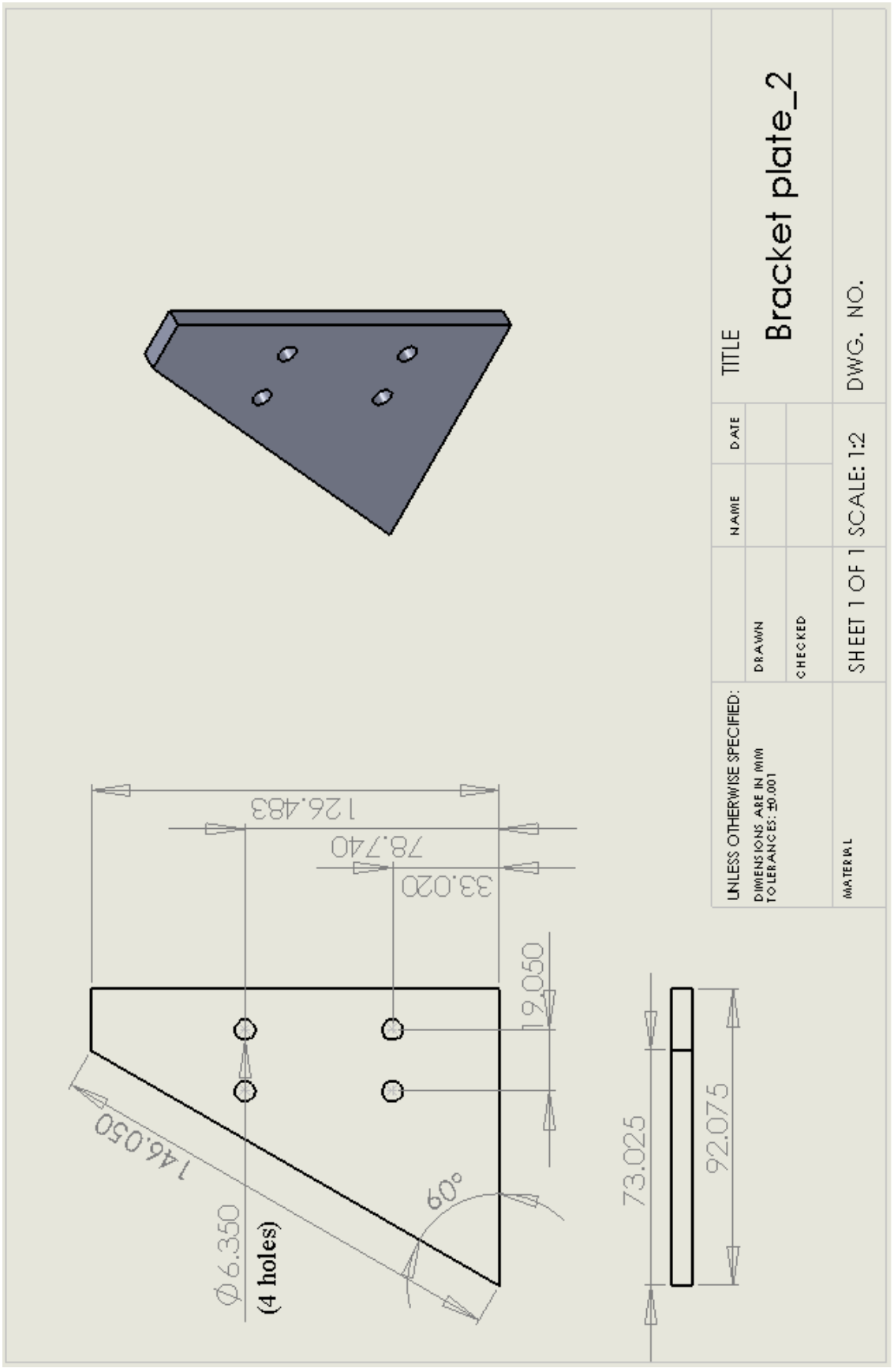
126.483
78.740
33.020
19.050
146.050
Ø6.350
(4 holes)
60°
73.025
92.075
UNLESS OTHERWISE SPECIFIED:
DIMENSIONS ARE IN mm
TOLERANCES: ±0.001
DRAWN
CHECKED
NAME
DATE
TITLE
Bracket plate_2
MATERIAL
SHEET 1 OF 1
SCALE: 1:2
DWG. NO.

ITEM NO.	PART NUMBER	QTY.
1	electrode_1	1
2	electrode_2	2

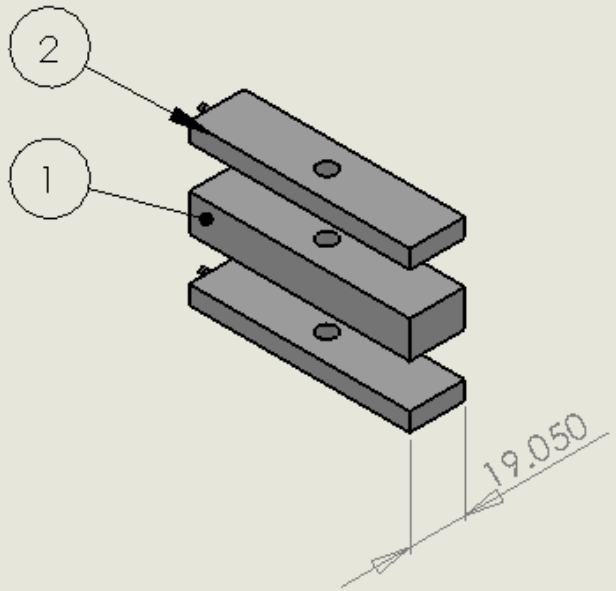

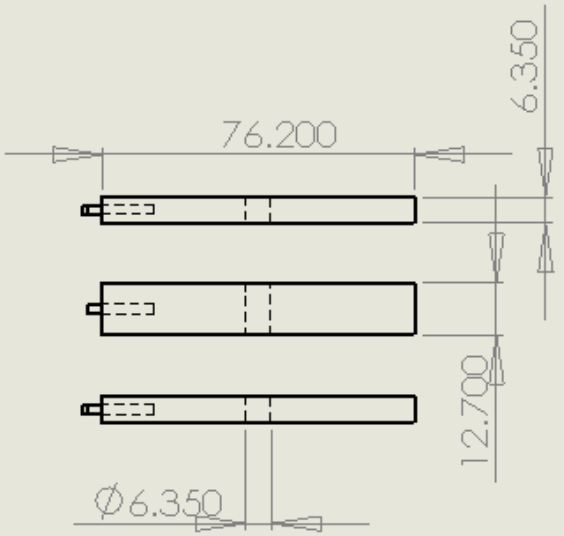

UNLESS OTHERWISE SPECIFIED: DIMENSIONS ARE IN MM TOLERANCES: ±0.001		NAME	DATE	TITLE electrodes
	DRAWN			
	CHECKED			
MATERIAL	SHEET 1 OF 1	SCALE: 1:2		DWG. NO.

APPENDIX D

Block diagram of data acquisition program

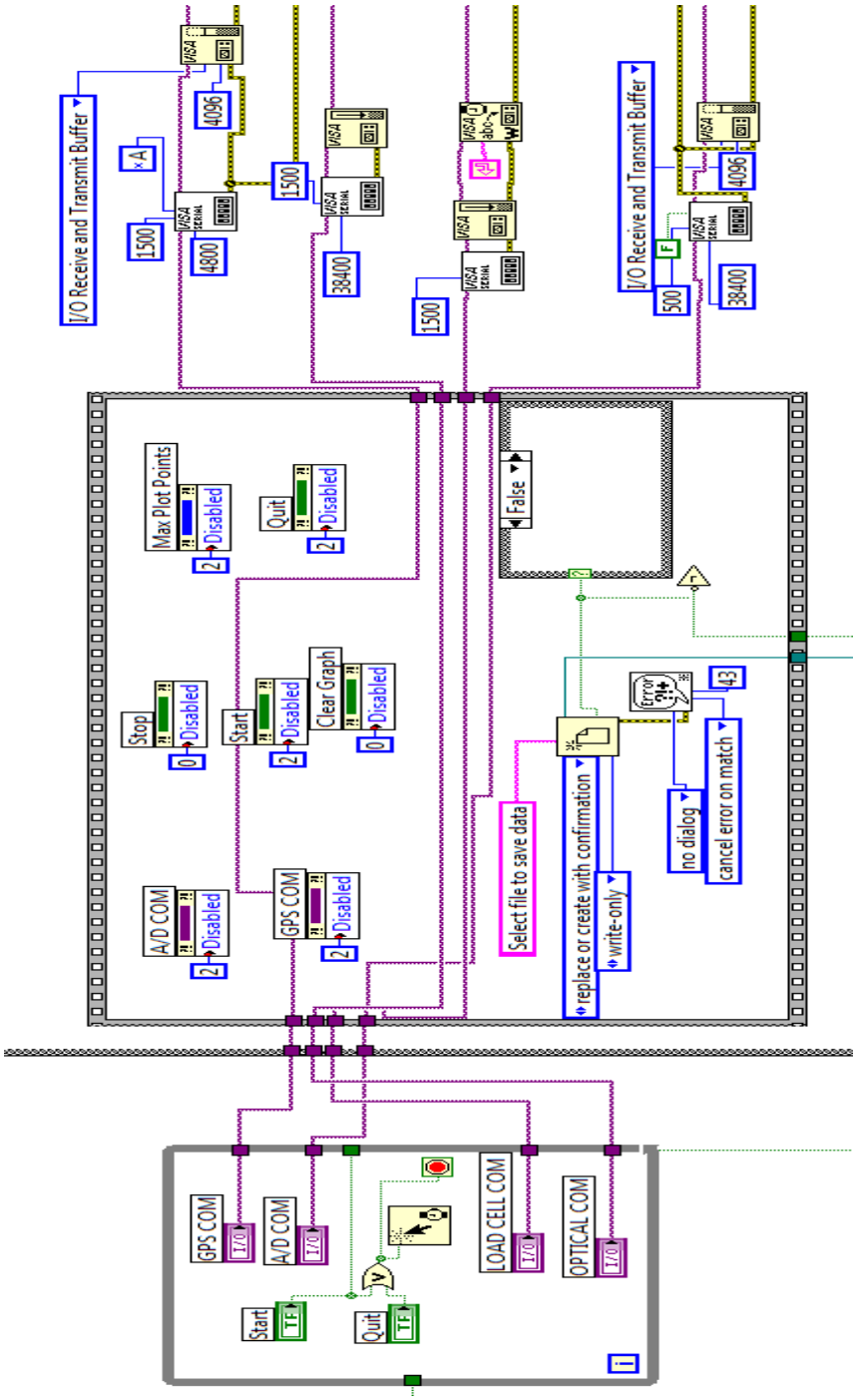

To read "sensor ports" and to "open file" for logging data

Column headers of log file

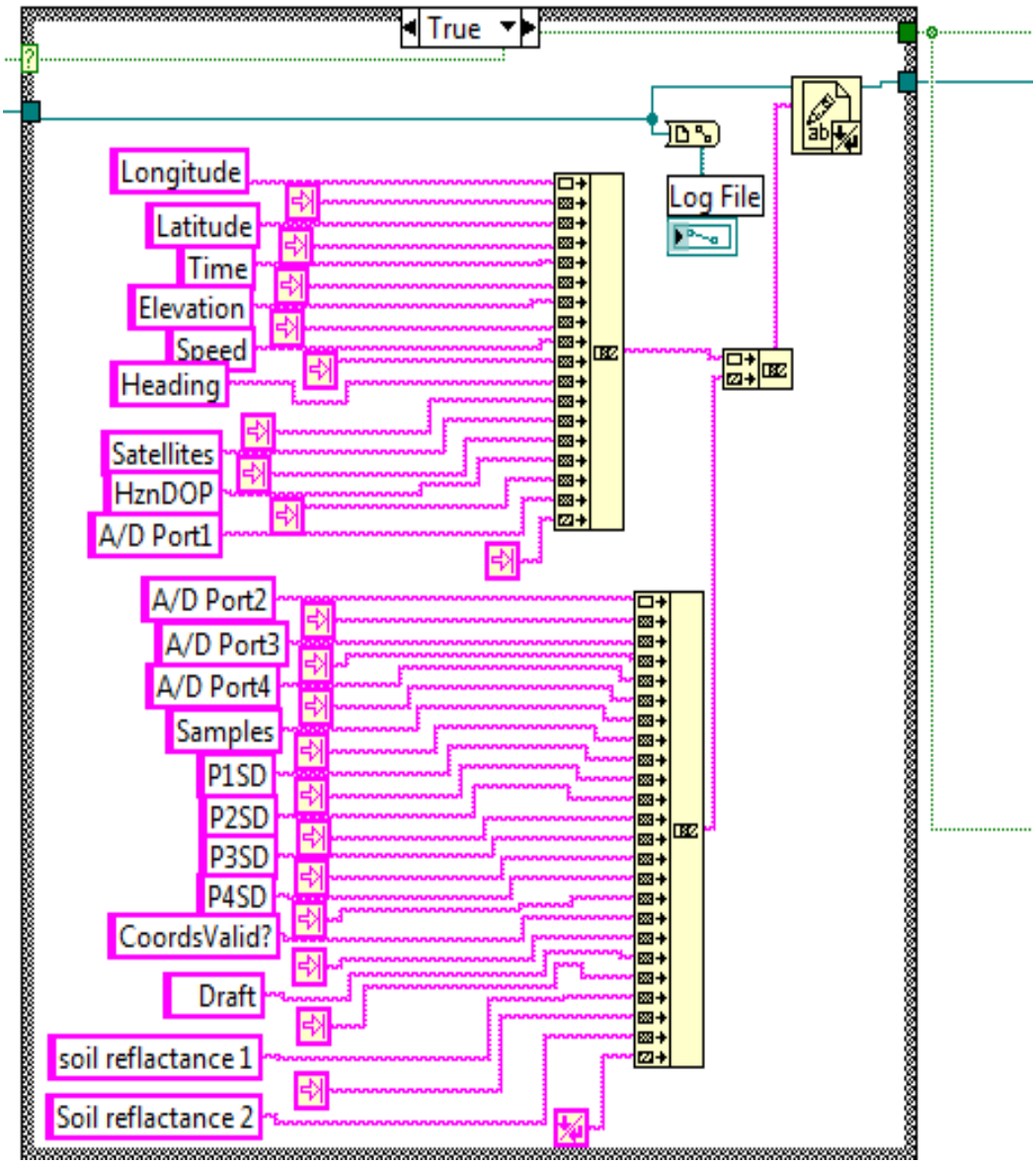

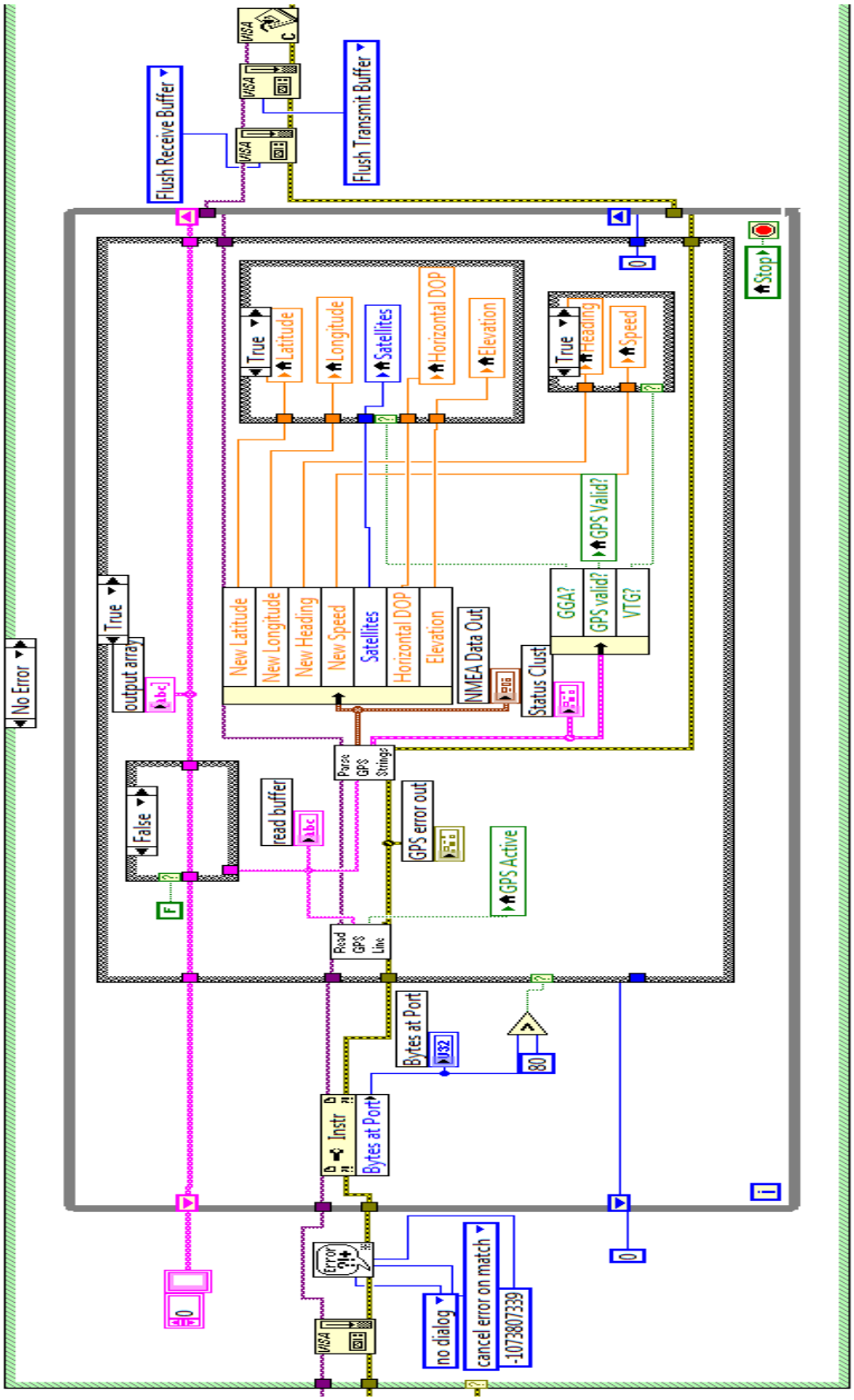

To read "GNSS receiver" data

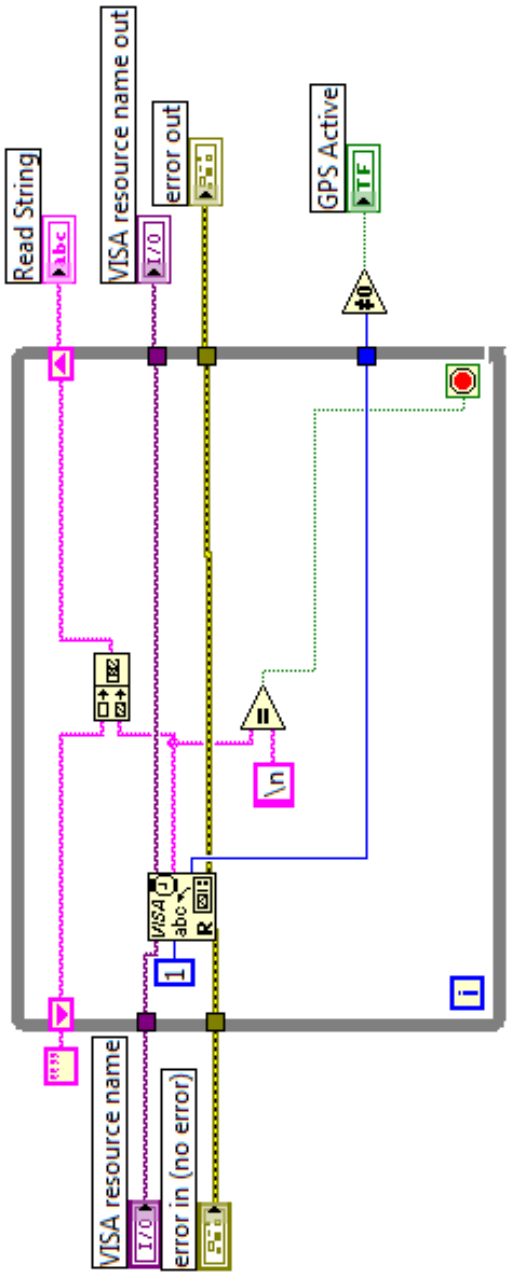

GPS sub.vi to read GPS line

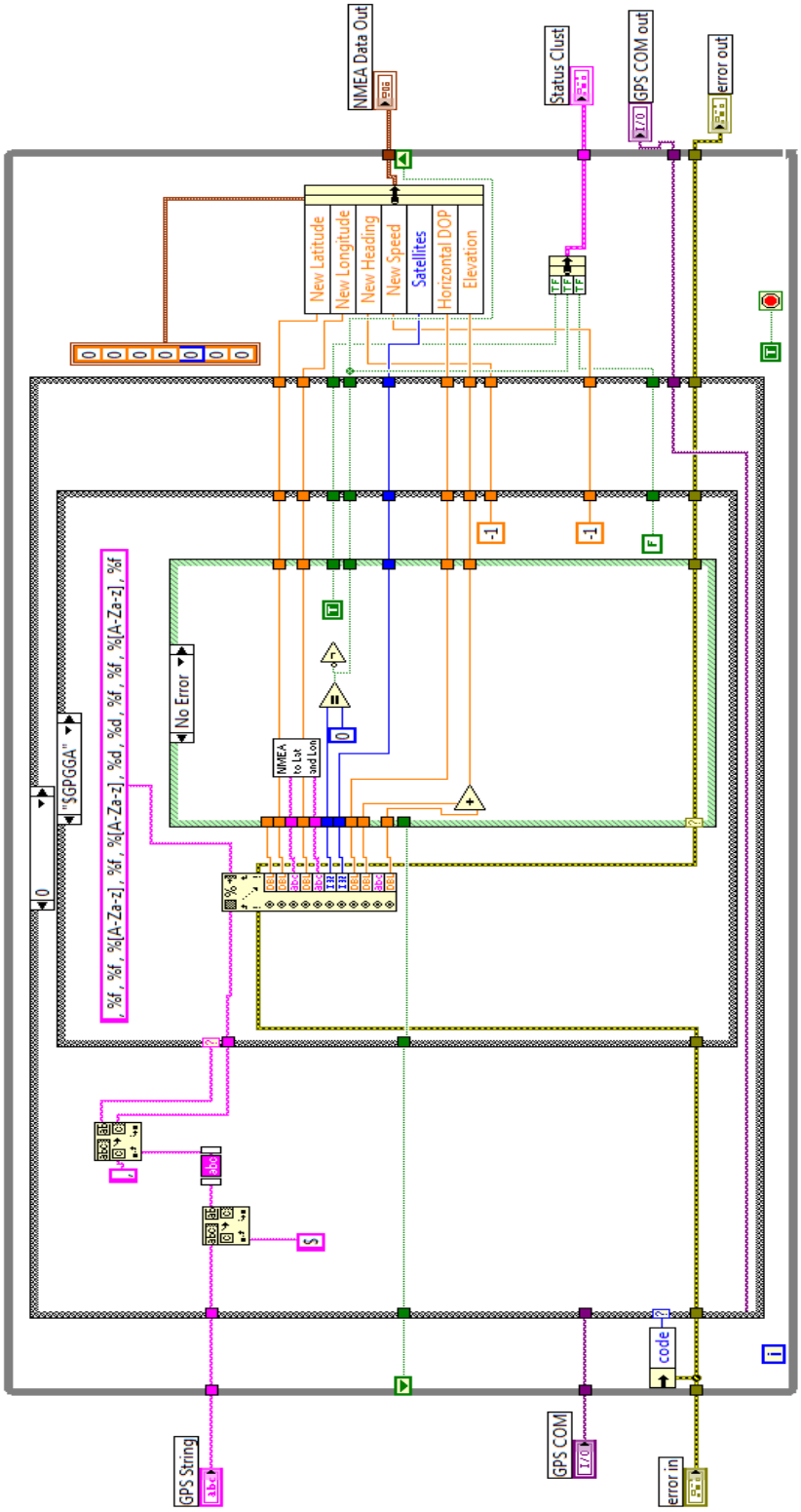

For "GPGGA" data

For “GPVTG” data

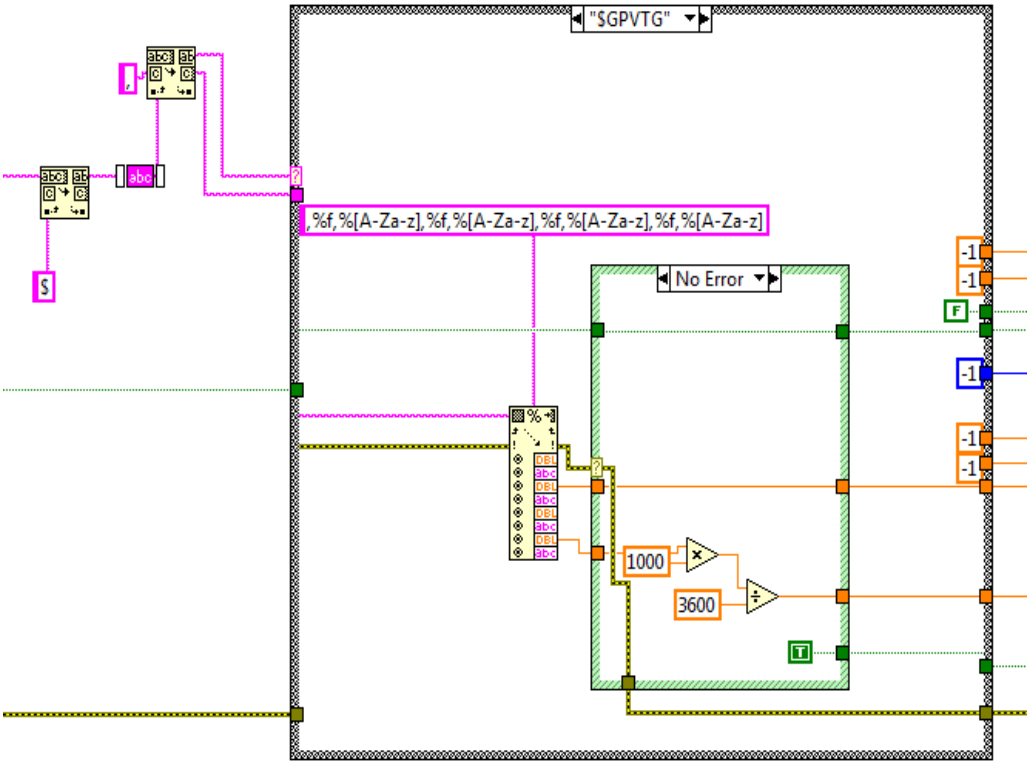

For “default” condition

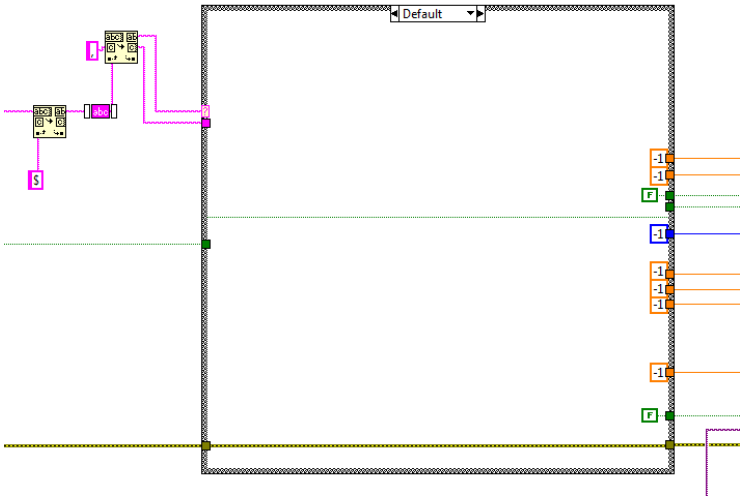

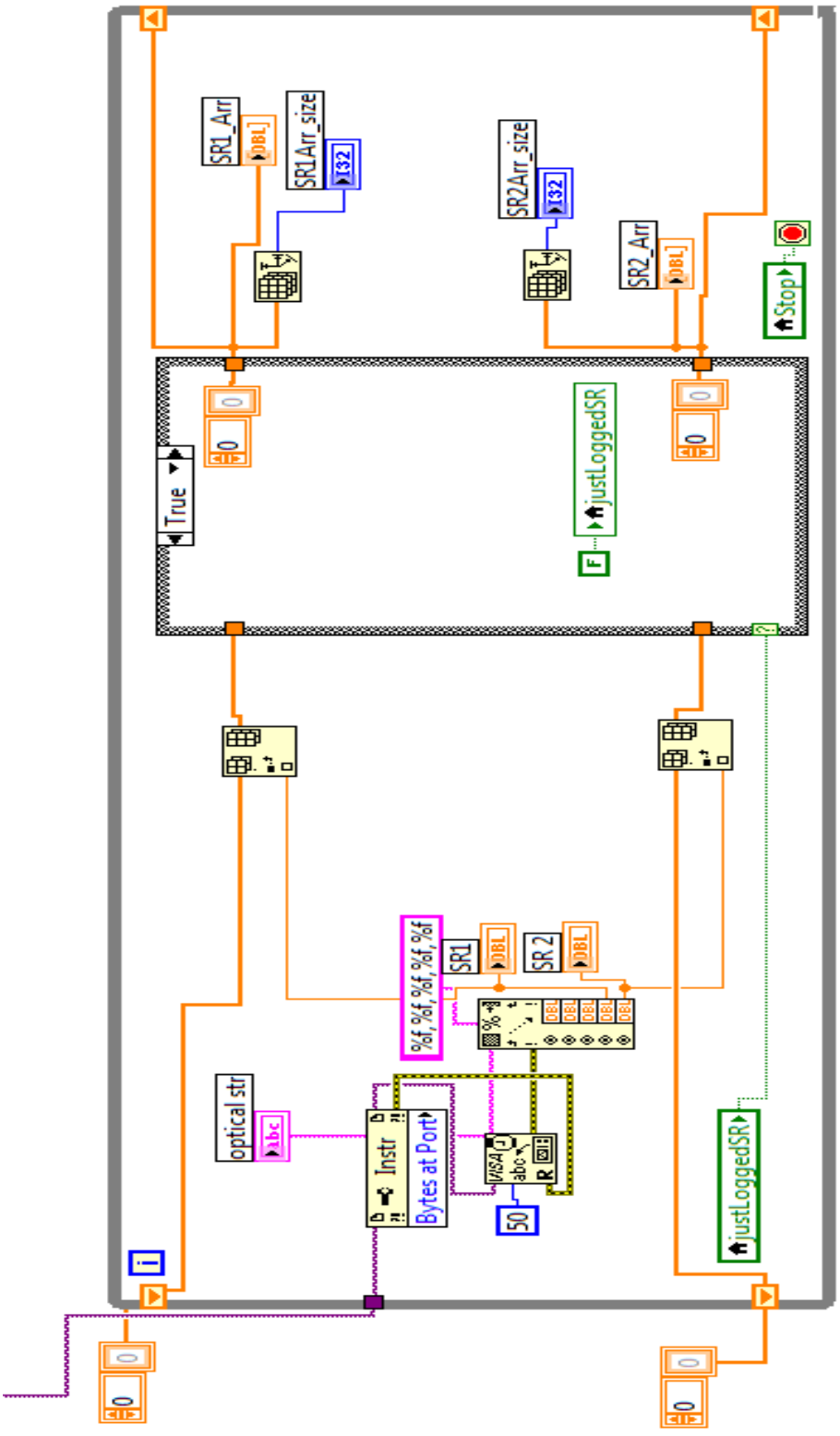

To read and average "optical sensor" data

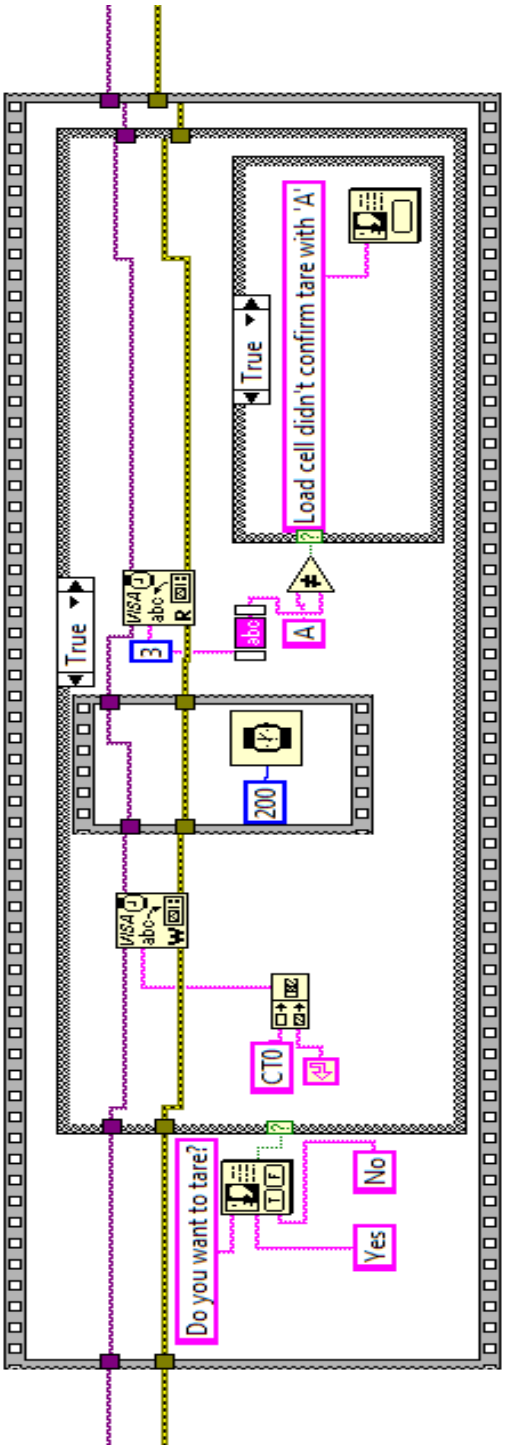

To tare "load cell" sensor

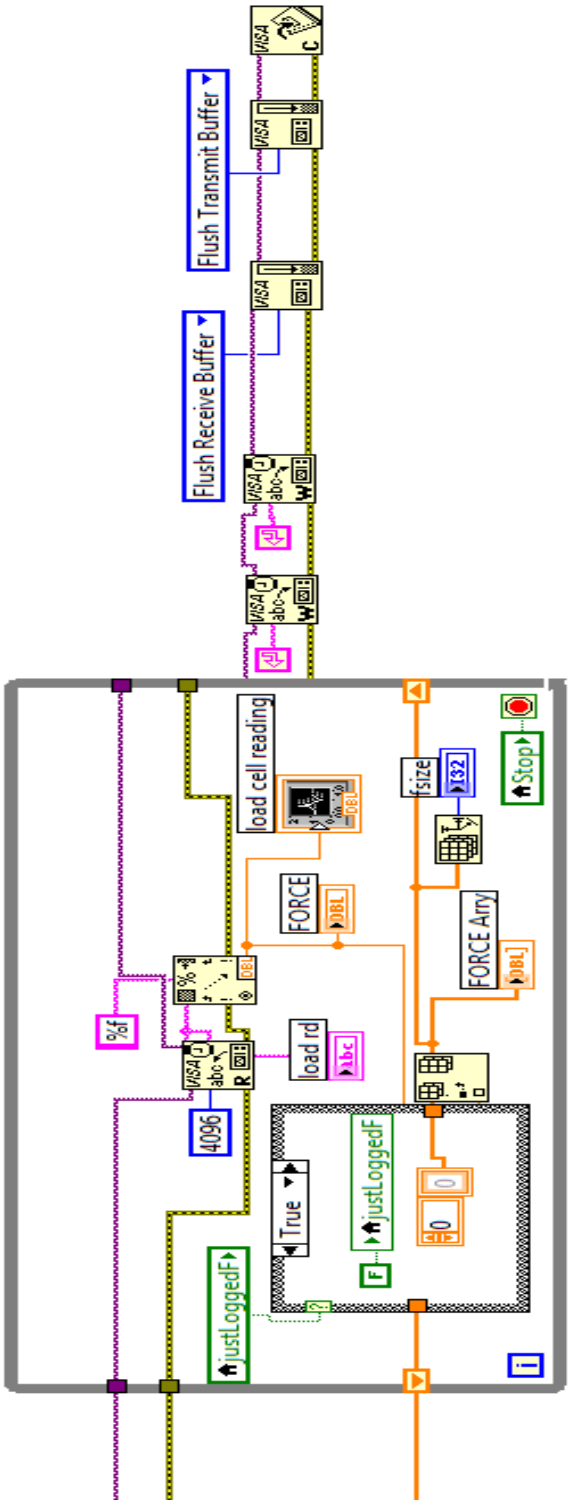

To read "load cell" sensor

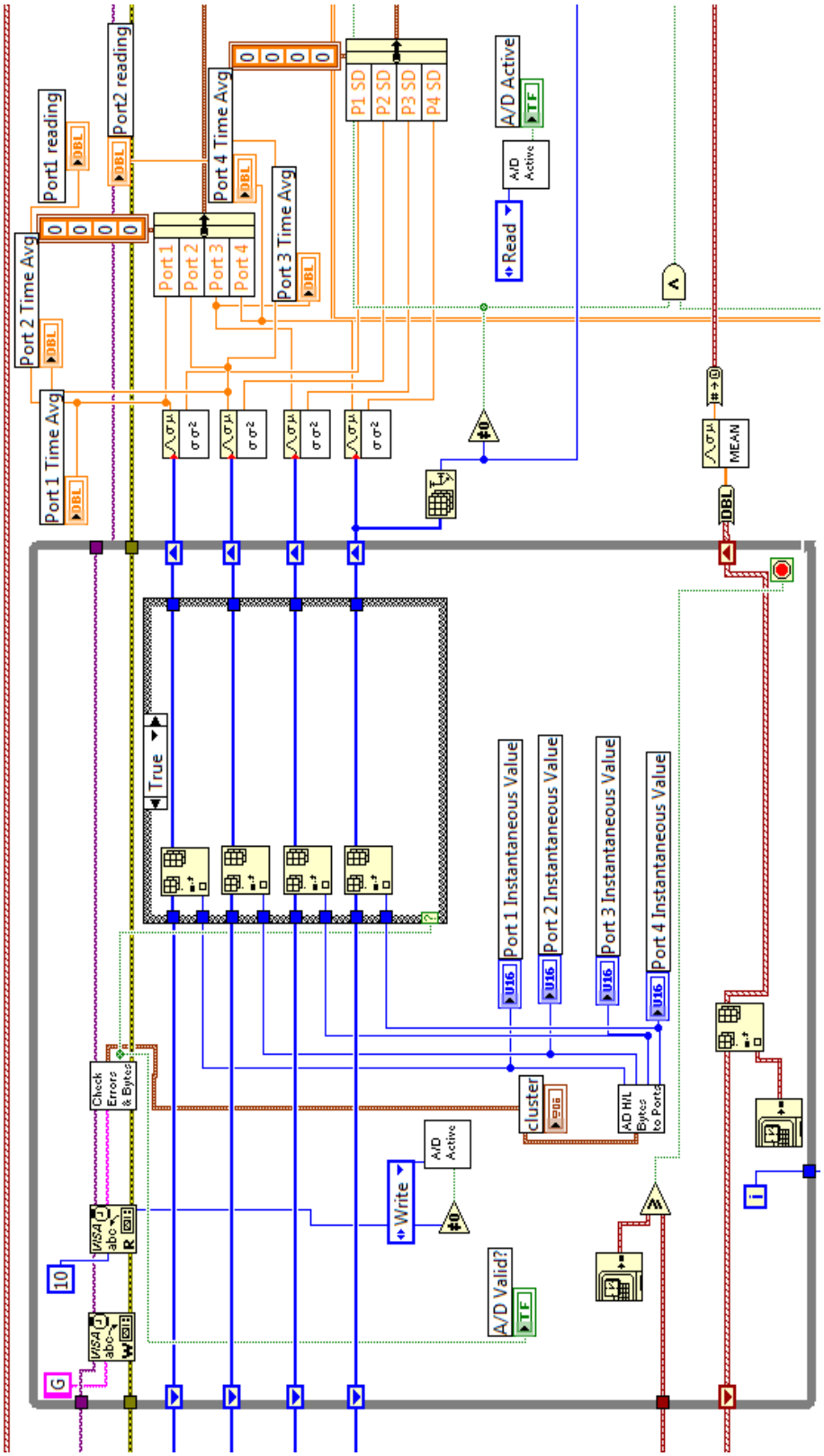

To read analog to digital convertor ports

Sub vi logging data from GNSS receiver, optical sensor, A/D convertor, load cell to text file

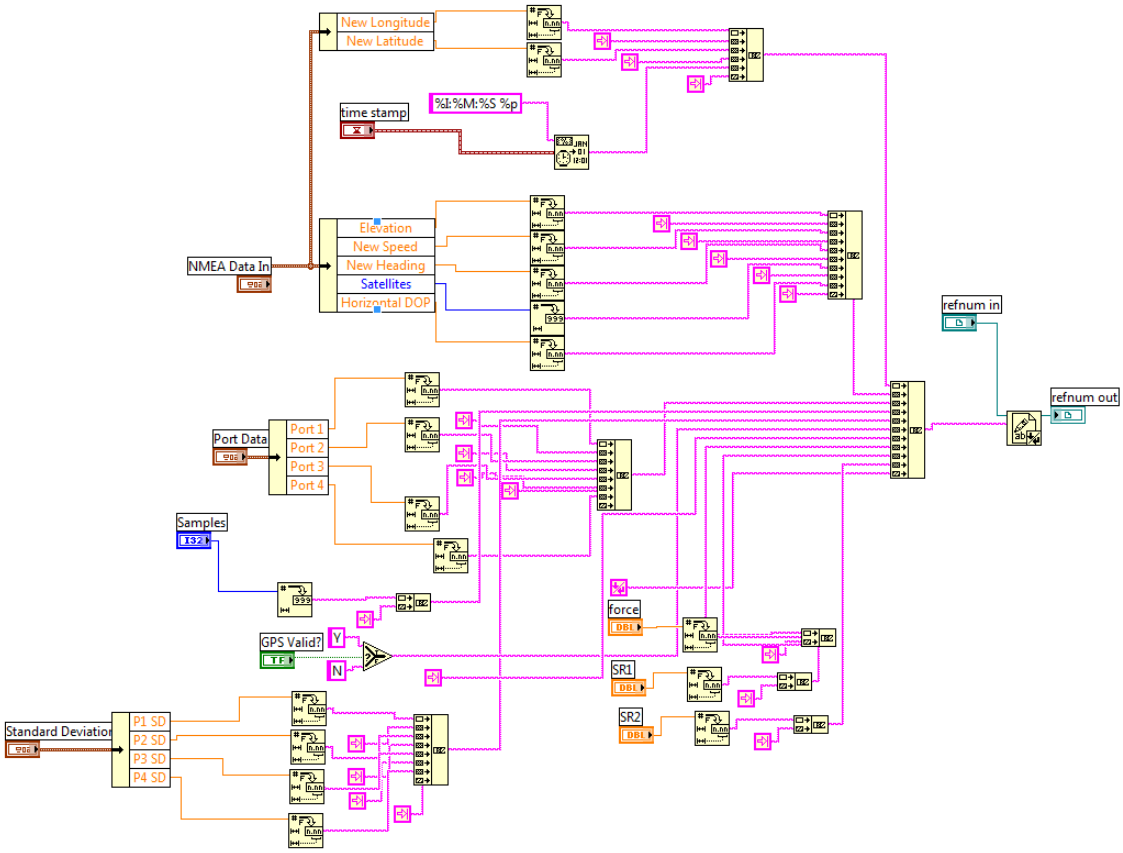

Flush buffer" and "close log file" functions

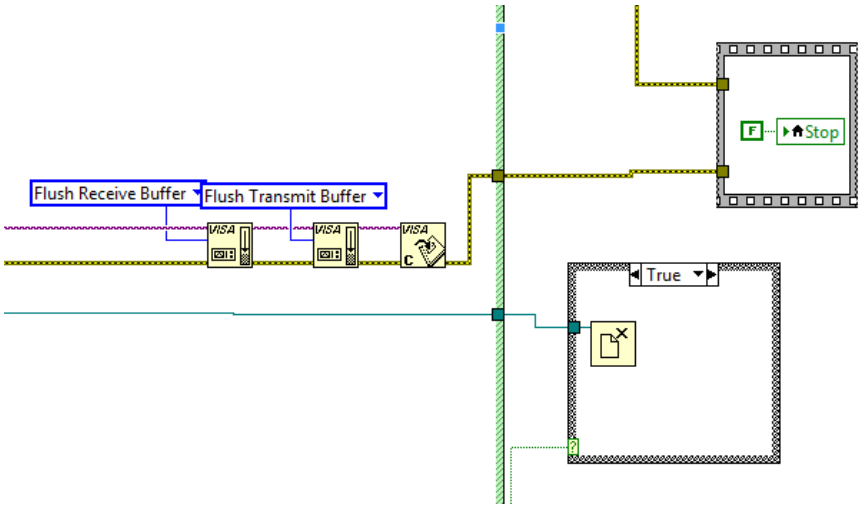

APPENDIX E

Laboratory experiment data

Table E-1: Laboratory calibration data of Capacitance based moisture sensors.

	Oven drying method			sensor output	
soil id	θm measured	θv measured	Bulk Density	Two-sided sensor	single-side sensor
	g/g	m3/m3	Mg/m3	mV	mV
1	0.09	0.13	1.37	2319.48	2847.78
1	0.20	0.22	1.09	1876.31	2656.44
1	0.03	0.05	1.51	2437.61	2885.35
1	0.26	0.34	1.32	1174.55	2232.86
2	0.04	0.06	1.40	2443.22	2903.37
2	0.22	0.35	1.56	1264.81	2546.05
2	0.08	0.10	1.26	2366.00	2894.61
2	0.16	0.20	1.22	1819.12	2729.19
2	0.03	0.04	1.39	2476.78	2916.92
2	0.24	0.41	1.68	1194.95	2389.49
3	0.17	0.21	1.27	1789.22	2763.04
3	0.22	0.32	1.45	1401.69	2638.86
3	0.10	0.13	1.30	2259.05	-
3	0.21	0.24	1.30	1601.21	2612.90
3	0.05	0.06	1.31	2425.14	2903.25
3	0.27	0.44	1.62	1157.99	1860.07
4	0.16	0.22	1.37	1765.29	2722.00
4	0.26	0.38	1.47	1186.16	2011.32
4	0.12	0.20	1.67	2163.83	2825.36
4	0.20	0.23	1.17	1629.60	2699.28
4	0.05	0.07	1.34	2437.18	2898.23
4	0.24	0.40	1.67	1210.77	2368.91
5	0.17	0.18	1.03	1730.83	2810.45
5	0.24	0.23	0.95	1240.05	2465.67
5	0.10	0.13	1.29	2305.24	2852.47
5	0.17	0.20	1.21	1981.70	2830.93
6	0.12	0.15	1.25	2209.83	2840.17
6	0.18	0.25	1.42	1585.14	2748.12
6	0.08	0.12	1.39	2356.47	2925.09
6	0.19	0.20	1.07	1768.42	2681.71
6	0.06	0.08	1.42	2436.20	2895.35
6	0.32	0.49	1.52	1157.16	1632.34
7	0.12	0.15	1.28	2273.01	2821.84
7	0.27	0.42	1.57	1176.46	2327.09

7	0.10	0.11	1.13	2346.75	2864.63
7	0.24	0.31	1.30	1510.27	2588.03
7	0.07	0.08	1.25	2414.93	2897.30
7	0.27	0.43	1.58	1177.10	2133.20
8	0.07	0.12	1.69	2253.57	2855.43
8	0.11	0.25	2.17	1519.48	2647.42
8	0.02	0.03	1.62	2458.95	2922.48
8	0.12	0.27	2.24	1713.59	2715.73
8	0.01	0.02	1.72	2480.19	2919.22
8	0.10	0.18	1.82	1856.17	2777.83
9	0.07	0.09	1.44	2290.99	2866.77
9	0.13	0.24	1.84	1592.44	2710.93
9	0.03	0.05	1.59	2443.06	2894.17
9	0.14	0.26	1.87	1819.91	2712.48
9	0.02	0.04	1.53	2487.53	2924.47
9	0.14	0.25	1.82	1417.95	2635.85
10	0.13	0.19	1.50	1970.25	-
10	0.19	0.36	1.93	1202.02	-
10	0.03	0.05	1.54	2452.24	2921.20
10	0.18	0.35	1.92	1195.85	2268.09
10	0.02	0.03	1.62	2484.33	2926.40
10	0.21	0.37	1.72	1196.91	2329.53
11	0.11	0.12	1.13	2159.18	2814.41
11	0.21	0.33	1.60	1370.06	2658.49
11	0.06	0.09	1.48	2393.14	2863.80
11	0.20	0.27	1.38	1557.52	2528.35
11	0.03	0.04	1.28	2464.64	2919.24
11	0.25	0.41	1.63	1183.83	2252.68
12	0.10	0.13	1.35	2241.84	2832.24
12	0.18	0.26	1.49	1653.23	2760.45
12	0.07	0.09	1.40	2360.11	2891.37
12	0.16	0.25	1.50	1794.38	2703.92
12	0.04	0.05	1.41	2450.73	2903.64
12	0.24	0.40	1.68	1178.11	2149.79
13	0.05	0.06	1.22	2400.58	2894.21
13	0.15	0.27	1.73	1688.65	2746.47
13	0.03	0.06	1.71	2442.44	2899.05
13	0.13	0.20	1.70	2002.70	2774.51
13	0.01	0.02	1.58	2493.66	2932.22
13	0.16	0.29	1.79	1495.71	2633.11
14	0.03	0.04	1.53	2439.58	2902.32
14	0.11	0.20	1.74	1501.72	2742.29
14	0.04	0.07	1.88	2368.95	2886.58
14	0.09	0.15	1.74	2180.74	2813.87
14	0.01	0.01	1.73	2489.88	2927.28
14	0.11	0.23	2.00	1673.40	2777.08

Table E-2: Load cell calibration data (lab experiment)

weight Applied	Trial 1	Trial 2	Trial 3
Lbs	mLbs	mLbs	mLbs
0	421.0	326.2	-645.4
50	43714.1	40910.4	51214.3
100	81491.6	79681.4	91972.5
150	124662.4	129049.0	142281.3
200	175497.9	173271.6	187953.1
250	218836.6	233849.1	237628.3
300	267304.2	262063.3	277794.2
350	323226.0	321761.3	322099.6
400	363862.9	350770.1	368190.9
450	405370.6	385921.8	422566.1
500	447490.6	466738.6	460868.0
550	490914.2	517067.4	502978.7
600	537060.6	553356.5	547730.7
650	585615.0	599546.9	606926.4
700	626489.8	625666.0	641477.2
750	712497.6	696544.8	701147.2
800	734503.2	717729.5	726404.3
850	777090.2	779481.7	777776.5
900	806962.1	801374.5	819026.8

Table E-3: Load cell calibration data (from manufacturer)

Applied weight	load cell output
lbs	lbs
0.0	-0.3
1245.9	1274.9
2498.9	2520.8
3752.3	3757.8
4998.3	5005.1
6251.2	6265.4
7498.8	7526.4
8750.2	8781.6
10000.9	10011.1

Table E-4: Laboratory calibration data of (NIR/Amber) optical sensor

			Trial 1	
soil id	Measured OM	Grav.WC(w)	NIR	Amber
	g/g	g/g		
1	1.70	0.17	0.56	0.14
2	1.90	0.21	0.59	0.15
3	2.60	0.25	0.45	0.13
4	2.90	0.24	0.40	0.12
5	1.30	0.15	0.75	0.15
6	1.00	0.10	0.97	0.20
7	3.00	0.23	0.50	0.14
8	2.10	0.23	0.55	0.14
9	1.60	0.19	0.50	0.12
10	3.10	0.28	0.55	0.15
11	0.80	0.06	0.97	0.23
12	0.90	0.08	0.96	0.23
13	1.40	0.17	0.42	0.12
14	3.20	0.26	0.43	0.14
15	1.20	0.14	0.68	0.15

Table E-4 (continues): Laboratory calibration data of VISNIR (NIR/Amber) optical sensor

Trial 2		Trial 3	
NIR	Amber	NIR	Amber
0.55	0.16	0.57	0.16
0.49	0.17	0.59	0.17
0.55	0.15	0.55	0.16
0.48	0.14	0.50	0.14
0.74	0.17	0.67	0.17
0.97	0.20	0.96	0.24
0.52	0.12	0.52	0.17
0.54	0.16	0.42	0.15
0.73	0.17	0.58	0.19
0.36	0.14	0.28	0.13
0.97	0.21	0.96	0.27
0.92	0.23	0.96	0.23
0.41	0.13	0.59	0.16
0.40	0.13	0.54	0.13
0.72	0.18	0.73	0.18

TableE-5: Laboratory calibration data of optical sensor with wavelengths in visible region (Red/Blue).

			trial 1		trial 2	
soil id	Grav.WC(w)	SOM	red	blue	red	blue
2a	0.01	2.77	0.599	0.193	0.631	0.366
2b	0.09	2.77	0.705	0.391	0.586	0.331
2c	0.17	2.77	0.365	0.193	0.392	0.236
3a	0.01	3.07	0.614	0.409	0.609	0.367
3b	0.09	3.07	0.687	0.37	0.702	0.377
3c	0.16	3.07	0.416	0.218	0.375	0.218
4a	0.01	2.97	0.791	0.464	0.602	0.37
4b	0.12	2.97	0.538	0.282	0.551	0.302
4c	0.22	2.97	0.349	0.204	0.318	0.184
5a	0.02	1.61	1.094	0.632	0.693	0.464
5b	0.13	1.61	0.786	0.415	0.737	0.374
5c	0.25	1.61	0.463	0.258	0.462	0.257
6a	0.02	2.61	0.591	0.352	0.541	0.304
6b	0.12	2.61	0.582	0.31	0.562	0.297
6c	0.22	2.61	0.328	0.173	0.305	0.171
7a	0.01	3.83	0.492	0.314	0.516	0.328
7b	0.08	3.83	0.597	0.341	0.534	0.301
7c	0.19	3.83	0.301	0.186	0.21	0.162
8a	0.00	1.33	0.809	0.472	1.081	0.61
8b	0.03	1.33	0.755	0.416	0.72	0.391
8c	0.07	1.33	0.444	0.254	0.47	0.261
9a	0.00	1.37	1.054	0.6	1.035	0.609
9b	0.05	1.37	0.691	0.369	0.695	0.377
9c	0.12	1.37	0.369	0.198	0.377	0.224
10a	0.01	2.97	0.577	0.361	0.762	0.432
10b	0.05	2.97	0.747	0.431	0.766	0.429
10c	0.12	2.97	0.323	0.188	0.333	0.188
12a	0.01	2.57	0.934	0.567	0.673	0.404
12b	0.08	2.57	0.661	0.36	0.69	0.393
12c	0.14	2.57	0.419	0.223	0.358	0.209
13a	0.01	2.48	0.636	0.344	0.545	0.318
13b	0.09	2.48	0.661	0.357	0.67	0.368
13c	0.19	2.48	0.36	0.218	0.331	0.191
14a	0.00	1.46	0.9553	0.556	0.96	0.548
14b	0.04	1.46	0.763	0.415	0.778	0.428
14c	0.11	1.46	0.445	0.235	0.434	0.227

15a	0.00	0.99	0.917	0.56	0.953	0.548
15b	0.04	0.99	0.618	0.336	0.594	0.314
15c	0.07	0.99	0.434	0.24	0.53	0.285

Table E-6: Locations and Moisture content measurement data by oven drying method from cores collected from field near Clay Center, NE

Longitude	Latitude	theta-m	theta -v
-98.12971	40.57910	0.18	0.22
-98.12973	40.57910	0.15	0.19
-98.12977	40.57910	0.18	0.22
-98.12971	40.57946	0.22	0.22
-98.12974	40.57946	0.20	0.25
-98.12977	40.57946	0.21	0.27
-98.12971	40.57979	0.23	0.30
-98.12974	40.57979	0.25	0.33
-98.12977	40.57979	0.24	0.29
-98.12971	40.58016	0.23	0.24
-98.12974	40.58016	0.22	0.28
-98.12977	40.58016	0.22	0.25
-98.12970	40.58056	0.26	0.26
-98.12973	40.58056	0.26	0.31
-98.12977	40.58056	0.24	0.31
-98.12970	40.58099	0.25	0.22
-98.12974	40.58100	0.23	0.31
-98.12977	40.58100	0.29	0.28
-98.12971	40.58155	0.21	0.29
-98.12974	40.58155	0.20	0.25
-98.12977	40.58155	0.21	0.27
-98.12970	40.58196	0.20	0.20
-98.12974	40.58195	0.18	0.23
-98.12978	40.58196	0.16	0.20

Table E-7: Three cone index measurements for each sampling location reported in table 6 and corresponding northing of each location

northing	cone index		northing	cone index
4492398.837	-		4492560.378	1825
4492398.837	6425		4492560.378	2485
4492398.837	3721		4492560.378	3215
4492398.923	3300		4492560.335	3405
4492398.923	4564		4492560.335	3581
4492398.923	5407		4492560.335	2808
4492399.052	4669		4492560.249	4213
4492399.052	4564		4492560.249	2563
4492399.052	4810		4492560.249	2422
4492439.158	3686		4492608.948	5424
4492439.158	2492		4492608.948	3511
4492439.158	2492		4492608.948	3756
4492439.072	4143		4492609.120	1966
4492439.072	4143		4492609.120	3792
4492439.072	2282		4492609.120	3792
4492439.244	2282		4492609.207	2492
4492439.244	2282		4492609.207	2282
4492439.244	4669		4492609.207	1650
4492475.903	4740		4492670.226	4002
4492475.903	3019		4492670.226	4002
4492475.903	3054		4492670.226	3440
4492475.86	3265		4492670.269	4072
4492475.86	3265		4492670.269	2598
4492475.86	3265		4492670.269	3335
4492475.86	3651		4492670.355	2212
4492475.86	4002		4492670.355	1931
4492475.86	3851		4492670.355	1966
4492516.318	2247		4492715.802	6284
4492516.318	1264		4492715.802	2844
4492516.318	4002		4492715.802	4775
4492516.297	1474		4492715.630	5968
4492516.297	2808		4492715.630	3932
4492516.297	1158		4492715.630	6214
4492516.267	3581		4492715.651	6039
4492516.267	1896		4492715.651	1264
4492516.267	1825		4492715.651	3220